İSTANBUL TEKNİK ÜNİVERSİTESİ ★ NÜKLEER ENERJİ ENSTİTÜSÜ

INVESTIGATION OF MASS TRANSFER AT NUCLEAR POWER REACTOR COOLING CHANNELS

YÜKSEK LİSANS TEZİ

Nük. En. Müh. ÖZKAN FEZA BİÇER

Tezin Enstitüye Verildiği Tarih : 12. Haziran. 1995

Tezin Savunulduğu Tarih 26. Haziran. 1995

Tezin Danışmanı : Prof. Dr. Şarman GENÇAY

Diğer Jüri Üyeleri Prof. Dr. Melih GEÇKİNLİ

Prof. Dr. Hasbi YAVUZ

HAZİRAN 1995

PREFACE

This study concerns the computer simulation of the mass transfer at nuclear reactor cooling channels by the method of subchannel analysis.

In the recent years a great deal of effort has been devoted to the subchannel type of computer codes which give more detailed information on the thermal-hydraulic behaviour of the rod bundle than the bundle average approach. In these codes, as their name indicates, the cross-sectional area of the rod bundle is divided into smaller sections called "subchannels". Using a lumped parameter approach the equations of mass, momentum, and energy written for each channel and solved numerically taking into account interchannel interactions such as mixing and diversion cross-flow. The end product is a map of pressures, mass flow rates, enthalpies, etc. throughout the bundle. Several subchannel codes have been quoted in the open literature. However only limited number are easily accessible. Once the subchannel codes are developed, they should be checked against experimental data.

With this work the subchannel code COBRA-IV-I is adapted into IBM PC compatibles as COBRA-PC4 at ITU Nuclear Energy Institute and using experimental data obtained from literature, the code is checked . Also some predictive experimental cases are simulated.

The main enforcement behind this study was the encouragements of my supervisor Prof. Dr. Şarman GENÇAY willing to use subchannel codes more effectively in our Institute's computers. I wish to express my special thanks to him giving me great support in both developing and preparing this study.

June 1995 Özkan Feza BİÇER

CONTENTS

NOMENCLATURE

A,a	=	Flow area (L^2)
C	=	Thermal conduction cefficient ($H/T\theta L$)
F_{ij}	=	Friction and form pressure loss due to cross flow
G	=	Mass flux (M/TL^2)
K	=	Spacer loss coefficient
K_{ij}	=	Cross-flow resistance coefficient
K_b	=	Irrecoverable pressure loss
d_h,D	=	Hydraulic diameter (L)
f	=	Friction factor
f_T	=	Turbulent momentum factor
g	=	Acceleration of gravity (L/T^2)
h	=	Enthalpy (H/M)
h^*	=	Enthalpy carried by diversion cross-flow (H/M)
l	=	Distance between subchannels (L)
m	=	Mass flow rate (M/T)
p	=	Pressure (F/L^2)
q'	=	Heat addition per unit length (H/LT)
s	=	Rod spacing or gap clearance (L)
t	=	Time (T)

T_i	=	Temperature (θ)
u	=	Axial velocity, effective enthalpy transport velocity (L/T)
u^*	=	Effective enthalpy transport velocity carried by diversion cross-flow (L/T)
υ	=	Transvers velocity (L/T)
v	=	Specific volume (L^3/M)
v'	=	Effective specific volume for momentum $(1-x)^2/\rho_f\,(1-\alpha)+x^2/\rho_g\,\alpha$ (L^3/M)
W	=	Diversion cross-flow (M/TL)
W'	=	Turbulnet cross-flow between adjacent subchannels (M/TL)
β	=	Turbulent mixing parameter
Δp_b	=	Irrecoverable pressure drop caused by the blockage (F/L^2)
$\Delta p_{friction}$	=	Pressure drop caused by friction (F/L^2)
Δp_{form}	=	Form pressure drop caused by the blockage (F/L^2)
Δx	=	Length of the control volume, $\Delta x = x_{i+1} - x_i$ (L)
ϕ	=	Two-phase friction multiplier
ρ	=	Specific mass (M/L^3)

SUBSCRIPTS

i,j	=	Indices for the subchannel control volumes
k	=	Indices for the control volumes which includes spacer or blocakge

LIST OF FIGURES

LIST OF TABLES

SUMMARY

In this study, mass transfer in the nuclear reactor cooling channels are simulated by the subchannel analysis code COBRA-PC4.

In order to perform this simulation, the COBRA-IV-I code should be adapted into available computer media. Original COBRA-IV-I code is obtained from OECD NEA Databank in the format compatible for IBM mainframe computers. Then the adaptation work is performed to obtain an IBM PC compatible COBRA-PC4 code.

After obtaining PC compatible code, simulation step is started for subchannels. Three kinds of experimental setup are simulated with fourteen different cases, and the results compared with the experimental data.

As the final stage of this work, predictive experimental cases are simulated in order to give the predictive data to the future experimental studies.

ÖZET

Bu çalışmada, nükleer reaktör soğutma kanallarındaki kütle transferi alt-kanal analiz programı olan COBRA-PC4 ile incelenmiştir.

Bu tür bir çalışma yapılabilmesi için, öncelikle, alt-kanal çözümlemesi yöntemi ile hesap yapan bir bilgisayar programı gerekmektedir. Altkanal çözümlemesi, bugüne dek en çok kullanılan yöntemdir. THI-3D, SABRE-1, HAMBO, THINC, ASSERT-4 ve COBRA-IV-I bu yöntemi kullanan programlardır. Bu programların en başarılılarından olan COBRA-IV-I bu çalışma için seçilmiştir.

COBRA- IV-I bilgisayar programı alt-kanal analizi metodu ile bir ya da daha çok alt-kanal üzerinde hesap yapabilme yeteneğine sahiptir. Programın bu yeteneğini kullanılarak nükleer reaktör soğutma kanallarındaki kütle transferi problemi modellenip benzetimi yapılabilmektedir.

Altkanal çözümlemesi, temel olarak, çubuk eksenlerine paralel hızların, çubuk eksenlerine dik (transvers) hızlara oranla çok büyük olduğu kabulüne dayanır. Bu kabulle, herbir altkanal için, komşu altkanallara kütle, momentum ve enerji alış-verişlerini de içinde bulunduran korunum denklemleri yazılır. Bir altkanal içinde transvers doğrultuda akışta ve fiziksel özelliklerde bir değişim olmadığı kabul edilir ve eksenel doğrultuda bütün kanal Δx sonlu aralıklara bölünerek sonlu fark denklemleri elde edilir.

Altkanal çözümlemesinde kullanılan bazı terimler:

Altkanal akış debisi: Altkanaldan eksenel yönde geçen debi. Bir altkanal içinde eksenel doğrultuda değişebilir.

Saptırılmış akış debisi: İki altkanalın sınırını geçen, transvers doğrultuda net akan kütlesel debi. Bu akış tek yönlüdür ve iki altkanal arasındaki basınç farkından veya altkanal içindeki saptırıcı kanatlardan meydana gelir. (COBRA programında bu büyüklüğün birim uzunluk başına olan miktarı kullanılmıştır).

Türbülans karışımı: Transvers doğrultuda debinin çalkanan bileşenidir. İki kanalın arayüzünde net olarak sıfırdır. Dolayısıyla kütlenin korumuna etki etmez, fakat momentum ve enerji alış-verişine etki eder.

COBRA-IV-I bigisayar programı, nükleer yakıt elemanları (yakıt çubuğu demetleri) içinde, sürekli ve geçici rejimde, entalpi ve debilerin değişimlerini ve dağılımları hesaplar. Bu programın özellikleri şunlardır:

•Altkanallar arasında türbülans karışımı ve sapatırılmış akış gözönüne alınır. Saptırılmış akış debsi, altkanal debisi yanında çok küçüktür.

•Herbir altkanalda iki fazlı, kayan akış gözönüne alınır ve tek boyutta (eksenel yönde, yani altkanal boyunca) çözüm yapılır.

•Fazların homojen karışmış ve termal dengede oldukları kabul edilmiştir. Entalpinin, altkanal debisinin, ısı akısının, basıncın, konumun ve zamanın fonksiyonu olan bir boşluk oranı tanımlanmıştır. Herbir fazın özellikleri altkanal içinde transvers doğrultuda üniform alınmıştır. Bilindiği gibi, halkasal akışta cidara komşu olan suyun hızı, buhar fazının içinde sürüklenmekte oaln su zerrelerinin hızıdan önemli ölçüde küçüktür.

•Geçici rejim hesaplamalarında alınan zaman aralıkları, ses dalgasının kanalı geçmesi için gereken süreden daha büyük alınarak, ses dalgasının yayılma etkisi hesaba katılmamıştır.

•Kullanılan çözüm yöntemiyle bir sınır değer probleminin çözümü yapılır. Sınır şartları, girişteki altkanal debisi ve çapraz akış debisi, çıkıştaki basınçtır.

•Konum ve zaman adımlarının seçiminde, çözümün kararlılığının sağlanması için gereken hiç bir sınırlama yoktur.

•Probleme uygun olarak programın boyutları değiştitirilebilir.

•Akış önündeki kısmi engeller, yön değiştirici kanatlar ve çubukların etrafına sarılmış olan tel sargılar hesaba katılabilir.

•Güç yoğunluğunun belirlenmesi durumunda, yakıt ve zarf sıcaklıkları, yakıt çubuğu için seçilmiş olan bir modelle hasaplanır.

•Komşu altkanallar arasında bir türbülans karışımı gözönüne alınır. Net türbülans karışımı sıfırdır ve saptırılmış akışa ilave bir etki yapar. Sonuçta bu iki çapraz süperpoze edilebilirler.

•Denklemlerın çözümünde bazı ampirik bağıntılar kullanılmaktadır. Programın yazıldığı zamana kadar yapılmış olan deneyler ve elde edilen ampirik bağıntılar yeterli olmadığından bazı kabuller yapılmıştır. Kullanılan ampirik bağıntılar ve yapılan kabuller bir hata içerdiğinden, çözüm üzerine etkileri tartışmalıdır.

•Programda kullanılan ampirik bağıntılar; sürtüme katsayısı korelasyonu, aşırı soğuk sıvı kaynama boşluk oranı korelasyonu, iki faz sürtme çarpanı korelasyonu, iki faz boşluk oranı korelasyonu, tek faz karışım korelasyonu, iki faz karışım korelasyonu, konumlandırıcılar için basınç kaybı korelasyonları, ısı transferi korelasyonları, konumlandırıcılarda meydana gelen saptırılmış akış, saptırılmış akış direnç katsayısıdır.

•Enerji ve momentum korunumu denklemlerinde görülen h^* ve u^*, çapraz akışta hakim olan kanalın, entalpisi ve hızı olarak alınmaktadır.

İTÜ Nükleer Enerji Enstitüsü bilgisayarlarında, çalışan bir COBRA-IV-I programı bulunmadığından, program OECD NEA Databank'ından alınarak uygun bilgisayar ortamına aktarılmış ve çalıştırılmıştır.

Orijinal program IBM mainframe bilgisayarlarına uygun olarak hazırlanmış şekli ile Databank'tan alındığından, IBM PC uyumlu bilgisayarlarda çalışabilmesi için uyarlanması gerekmiştir.

Bu işlem yerine getirilirken COBRA-PC4 programı oluşturulmuştur. Bu program PC üzerindeki DOS, WINDOWS ve OS/2 işletim sistemlerinde denenmiş ve en uygun ortamın WINDOWS ortamı olguğuna karar verilmiştir. Windows ortamı DOS ortamı gibi aktif bellek kullanımını 640 KB ile sınırlamadığından COBRA-PC4 programı istenilen giriş koşullarında çalıştırılabilmiştir.

Bu aşamadan sonra, deneysel sonuçlarla COBRA-PC4 programının doğruluğunun kontrolüne başlandı. Bunun için ondört ayrı durum kullanılmıştır. Bu durumlar aşağıda gösterilmiştir:

•Tek fazlı deneysel verilerin elde edildiği düzeneğin geomerisi şu şekildedir: 0.847 m uzunluğunda birbirine bağlantılı iki düşey kanal, bağlantı aralığı 1.52 mm genişliğinde ve 3.17 mm kalınlığında, kanalların hidrolik çapları 12.6 ve 12.5 mm, kesit alanları 166.2 ve 165 mm^2, tıkanmanın yeri birinci kanalda kanal girişinden 0.327 m içerde.

•Tek fazlı akış için, plaka tipi tıkanmada değişik akış hızlarına sahip iki, %29.8 oranında tıkanma ve bir, %59.2 oranında tıkanma durumu incelenmiş, sonuçlar deney verileri ve COBRA-IIIC sonuçları ile karşılaştırılmıştır.

•Tek fazlı akış için, eğimli tipteki tıkanmada bir, %58.6 tıakanma oranında tek parçalı tıkanma ve iki, %64.2 tıkanma oranında iki parçalı tıkanma incelenmiştir.

•İki fazlı deneysel verilerin elde edildiği düzeneğin geomerisi de şu şekildedir: 1.129 m uzunluğunda birbirine bağlantılı iki düşey kanal, bağlantı aralığı 1.52 mm genişliğinde ve 3.17 mm kalınlığında, kanalların hidrolik çapları 12.43 ve 12.55 mm, kesit alanları 162.4 ve 165.5 mm^2, tıkanmanın yeri birinci kanalda kanal girişinden 0.272 m içerde.

•İki fazlı akış için, üç adet değişik boşluk oranlarına sahip durum incelenmiştir. Bu incelemede boşluk sürüklenmesinin

COBRA-PC4 tarafından ne kadar benzetilebildiğine dikkat edilmiştir.

•İki fazlı akış için, plaka tipi tıkanmada değişik akış hızlarına sahip üç %31.9 oranında tıkanma ve bir, %61 oranında tıkanma durumu incelenmiş, sonuçlar deney verileri ve COBRA-IIIC sonuçları ile karşılaştırılmıştır.

COBRA-PC4 programı ile esas olarak kontrol çalışmaları yapıldıktan sonra, bilgisayar üzerinde deney adı verilebilecek çalışmalara başlandı. Bu aşamada dokuz değişik durum için bilgisayar deneyi yapıldı.

Bu deneyler şunlardır:

•Geometri olarak iki fazlı akış deneylerinde kullanılan geometri seçilmiştir.

•İki fazlı akış, tıkanmasız üç değişik akış şartı için COBRA-PC4 ile inceleme yapılmıştır

•İki fazlı akış, plakalı %31.9 oranında tıkanma ve altı değişik akış şartı için inceleme yapılmıştır

Bu çalışmadan ileride yapılacak deneylere kaynak olacak sonuçlara ulaşılmıştır.

Ayrıca, deney setinin oniki altkanallı bir benzetimi yapılarak soğutucu kanalları incelenmiştir. Bu deney setindeki akış kanalı altı, ısıtıcı çubuk çevresindeki hacimden oluşmaktadır. Elde edilen sonuçlarla, ASSERT programının sonuçları karşılaştırılarak sonuçların uyumlu olduğu görülmüştür.

CHAPTER 1

INTRODUCTION

The thermal-hydraulic design of a power reactor core depends on the expected performance of the core, like core life, fuel burn-up, power load follow characteristics etc. This information is used to obtain heat removal capacity of the core considering "critical heat flux" (CHF) which is one of the most important quantity in reactor design.

Thus, thermal-hydraulic analysis of the nuclear fuel assemblies used in power reactors requires detailed information on coolant parameters such as pressure, flow rate, quality, void fraction, enthalpy etc. throughout these assemblies. Because of these parameters are used for the determination of limitation to the rate at which heat can be removed from a nuclear fuel bundle.

Therefore, experiments in fuel assemblies of complex geometry are important for the determination of the local conditions. Unfortunately, obtaining experimental results aimed at having detailed information on mass flow, enthalpy, void fraction and pressure distribution throughout the fuel rod bundle are very difficult if not impossible.

Another thermal-hydraulically important subject is to investigate consequences of coolant flow area blockages in fuel assemblies. In pressurised water reactors during the refilling and reflooding phases of a hypothetical loss-of-coolant-accident, the temperature of the zirconium fuel cladding could reach peak values. These peak temperatures couples with high internal pressure of fission product gases may result a ductile or brittle failure of cladding. This failure could result in a swelling of the fuel rod. In this case the flow area of a subchannel or a group of subchannels could be reduced. The grid spacers and especially in CANDU reactors, the end plates may also perturb the emergency core cooling fluid flow significantly.

Most of the experiments done on flow area blockages had a simple geometry in order to gain a good insight into the thermal-hydraulic aspects and to obtain detailed information on the variation of the key parameters; liquid and gas flow rates, void fractions and pressures in the blocked and unblocked channels. Obviously complex geometry experiments are more desirable, but due to measurement difficulties in rod bundles the determination of above parameters, at present, very difficult.

To overcome these experimental difficulties, another approach to the problems which consist of more sophisticated analysis techniques has been employed [1-3]. In these techniques, the complex geometry of the fuel assemblies is divided into small cells called "subchannels". Using lumped parameter approach the one dimensional conservation equations of mass, momentum and energy are derived for each subchannel and solved numerically while taking into account inter channel interactions.

The solution is a map of mass flow rates, enthalpies, void fractions etc. throughout the rod bundle. Using these data either experimentally determined critical heat flux is then correlated to the above local conditions or consequences of flow area blockage could be determined for rod bundles.

The purposes of this work are the followings.

- Adapting the subchannel analysis computer code COBRA-IV-I into IBM PC computers as COBRA-PC-4 at ITU Nuclear Energy Institute.

- Altering executable binary code type in order overcome computer core storage limitations.

- Comparing the results of COBRA-PC-4 with the results of COBRA-IIIC and experiments which are found in the literature. The experiments in two interconnected parallel subchannels with or without blockage are chosen for the comparison.

- Making computer experiments and produce results for the fictitious experimental cases in interconnected parallel subchannels.

CHAPTER 2

COMPUTATIONAL SUBCHANNEL ANALYSIS [4-7]

Subchannel analysis, stands on the assumption of order of magnitude of the axial flow rates are higher than transverse flow rates. With this assumption, subchannels are divided axially into small control volumes and the conservation equations for axial flow are written while taking into account the exchange of mass, momentum, and energy between adjacent subchannels. The transverse equations are used to ensure the coupling of the subchannels axial equations.

2.1 Definitions of some terms

Axial mass flow rate (m_i): This term represents the predominant axial flow rate of the selected subchannel control volume, i.

Transverse mass flow rate per unit length (W_{ij} and $W_{ij}'^{D}$): Two mechanisms create transverse mass flows; transverse pressure gradients that drive diversion cross-flow and turbulent fluctuations in the axial flow that drive turbulent mass exchanges.

Diversion cross-flow rate (W_{ij}): Net transverse mass flow rate between the boundary of adjacent subchannels. It is a directed flow and is a result of pressure gradients between two adjacent subchannels or diversion effects of flow blockages, fuel rod bowing in subchannel.

Turbulent interchange ($W_{ij}'^{D}$): This exchange is postulated to involve equal volumes of eddies which cross a transverse subchannel boundary. If these eddies are also of equal density, as they effectively are for single-phase flow conditions, then no net mass exchange results, but both momentum and energy are exchanged between subchannels.

2.2 Specifications of COBRA-IV-I computer code

COBRA-IV computer code is an extended version of the COBRA-IIIC subchannel code which computes the flow and enthalpy distributions in nuclear fuel rod bundles or cores for both steady state and transient conditions.

Specifications of this computer code are given as the followings.

a) Turbulent mixing and diversion cross-flow rates are considered between adjacent subchannels. Diversion cross-flow rate is assumed as smaller than axial flow rate.

b) At each subchannel, it is assumed that two phase fluid, slip flow conditions are valid and one dimensional (axial direction) solution is computed.

c) Homogenous equilibrium model is assumed. Void fraction defined as a function of enthalpy, subchannel flow rate, heat flux, pressure, location and time. Properties of each phase are uniform at transverse direction in subchannel. As well known, in annular flow liquid flow rates close to boundary smaller then the flow rates of the liquid droplets in gaseous phase.

d) Time steps used in transient computations, taken as bigger than time required to the propagation of sound waves along the channel, so effect of propagation of sound waves is not considered.

e) A boundary value problem is solved by selected solving method. These boundary conditions are inlet subchannel mass flux, cross-flow flow rate and exit pressure.

f) There is no stability restriction while choosing either space or time steps.

g) Maximum number of subchannels around a fuel rod is 6, maximum number of adjacent subchannels to one subchannel is 4.

h) Along the flow direction, separator blades, grid spacers and wire wraps could be considered in computation.

i) For determination of power density, fuel and cladding temperatures are computed by the model chosen for fuel rod.

j) Only between adjacent subchannels, turbulent mixing is considered. Since equal mass exchange model is assumed, net turbulent mixing is zero but it has additional effect on diversion cross-flow rates. So these two cross-flows could be superposed.

2.3 Conservation equations used in COBRA

Mass Balance

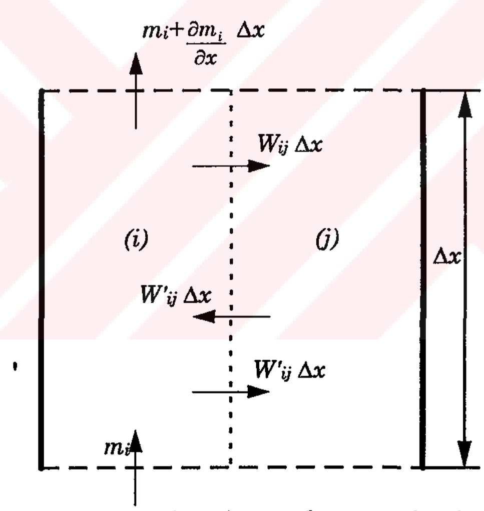

Figure 2.1 Control volume for continuity equation

Applying continuity equation only ith subchannel adjacent to jth subchannel following equation is obtained

$$\frac{\partial}{\partial t}\rho_i A_i \Delta x = m_i - m_i - \frac{\partial m_i}{\partial x}\Delta x - W_{ij}\Delta x + W'_{ji}\,\Delta x - W'_{ij}\,\Delta x \,. \tag{2.1}$$

In this equation two phase density is defined as

$$\rho_i = \rho_g \alpha + \rho_f (1-\alpha)\,. \tag{2.2}$$

Assuming there is no change in cross-section area with time and $W'_{ij} = W'_{ji}$ equation (2.1) is reduced to

$$A_i \frac{\partial}{\partial t} \rho_i \Delta x + \frac{\partial m_i}{\partial x} \Delta x + W_{ij} \Delta x = 0 \tag{2.3}$$

or obtained as

$$A_i \frac{\partial}{\partial t} \rho_i + \frac{\partial m_i}{\partial x} + W_{ij} = 0. \tag{2.4}$$

If i^{th} subchannel adjacent to more than one subchannel continuity equation is

$$A_i \frac{\partial \rho_i}{\partial t} + \frac{\partial m_i}{\partial x} = -\sum_j (W_{ij}) \tag{2.5}$$

Energy Balance

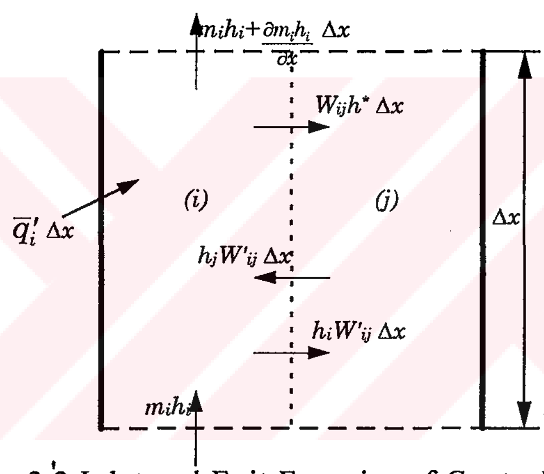

Figure 2.2 Inlet and Exit Energies of Control Volume

Internal Energy of control volume is

$$\rho_g u_g \alpha A_i \Delta x + \rho_f u_f (1-\alpha) A_i \Delta x \tag{2.6}$$

Since gaseous and liquid phases are in thermal equilibrium, $p_g = p_f = p$ and using relationship $h = u + \frac{p}{\rho}$ and definition

$$\rho_i'' = \frac{\rho_g h_g \alpha + \rho_f h_f (1-\alpha)}{h_i} \tag{2.7}$$

Internal Energy is reduced to

$$\rho_i'' u_i A_i \Delta x \tag{2.8}$$

Energy balance equation :

$$\frac{\partial}{\partial t}\rho_i'' u_i A_i \Delta x = m_i h_i - m_i h_i - \frac{\partial m_i h_i}{\partial x}\Delta x + \overline{q}_i' \Delta x$$
$$- W_{ij} h^* \Delta x + W'_{ji} h_j \Delta x - W'_{ij} h_i \Delta x \tag{2.9}$$

Considering no change in channel cross-section area in time, and performing required reductions equation 2.9 is

$$A_i \frac{\partial}{\partial t}\rho_i'' u_i + \frac{\partial m_i h_i}{\partial x} = \overline{q}_i' - W_{ij} h^* + W'_{ij}(h_j - h_i). \tag{2.10}$$

First term of LHS of this equation expanded as

$$A_i \frac{\partial}{\partial t}\rho_i'' u_i = A_i \frac{\partial}{\partial t}(\rho_i'' h_i - \rho_i'' \frac{p_i}{\rho_i''}) = A_i \frac{\partial}{\partial t}(\rho_i'' h_i) - A_i \frac{\partial p_i}{\partial t} \tag{2.11}$$

and then substituted into equation 2.10 following equation is obtained

$$A_i \frac{\partial}{\partial t}\rho_i'' h_i + \frac{\partial m_i h_i}{\partial x} = \overline{q}_i' - W_{ij} h^* + W'_{ij}(h_j - h_i) + A_i \frac{\partial p_i}{\partial t} \tag{2.11}$$

In order to prepare this equation to numerical solution, it is needed to expand multipication terms under derivation sign. First term of equation 2.11 using the equation 2.7 could be expanded as

$$\begin{aligned} \rho_i'' h_i &= \rho_g h_g \alpha + \rho_f h_f (1-\alpha) \\ &= \rho_g \alpha [h_i - (1-x) h_{fg}] + \rho_f (1-\alpha)(h_i - x h_{fg}) \\ &= [\alpha \rho_g' + (1-\alpha)\rho_f] h_i - [\alpha(1-x)\rho_g + x(1-\alpha)\rho_f] h_{fg} \end{aligned} \tag{2.12}$$

Expression in second parenthesis

$$\psi = \alpha(1-x)\rho_g + x(1-\alpha)\rho_f \tag{2.13}$$

is named slip correction term. Using this definition $\rho_i'' h_i$ term turns to

$$\rho_i'' h_i = \rho_i h_i - \psi h_{fg}. \tag{2.14}$$

Derivation of this term with respect to time could be expanded as

$$\frac{\partial}{\partial t}\rho_i'' h_i = \frac{\partial}{\partial h_i}(\rho_i h_i - \psi h_{fg}) \cdot \frac{\partial h_i}{\partial t} = (\rho_i - h_{fg}\frac{\partial \psi}{\partial h_i}) \cdot \frac{\partial h_i}{\partial t} \tag{2.15}$$

Second term of equation 2.11 expanded as

$$\frac{\partial m_i h_i}{\partial x} = m_i \frac{\partial h_i}{\partial x} + h_i \frac{\partial m_i}{\partial x} = m_i \frac{\partial h_i}{\partial x} - W_{ij} h_i . \qquad (2.16)$$

Last term of equation 2.11 could be disregarded. This assumption and substituting equations 2.15 and 2.16 into equation 2.11 energy balance is

$$A_i[\rho_i - h_{fg} \frac{\partial \psi}{\partial h_i}] \frac{\partial h_i}{\partial t} + m_i \frac{\partial h_i}{\partial x} = \bar{q}_i' - W'_{ij}(h_i - h_j) + W_{ij}(h_i - h^*) \qquad (2.17)$$

or for the case of more than one adjacent subchannel

$$A_i[\rho_i - h_{fg} \frac{\partial \psi}{\partial h_i}] \frac{\partial h_i}{\partial t} + m_i \frac{\partial h_i}{\partial x} = \bar{q}_i' - \sum_j W'_{ij}(h_i - h_j) + \sum_j W_{ij}(h_i - h^*) \qquad (2.18)$$

is obtained.

Heat transfer term $\bar{q}_i'$ could be divided into two terms. First term is heat transfer from fuel rod to the subchannel. Second term $\bar{q}_{i2}'$ is heat transfer between subchannels. It is assumed that transferred heat is proportional to the temperature difference between subchannels and coefficient is depend on channel geometry and fluid heat conduction coefficient. With these assumptions $\bar{q}_i'$ term is shown as

$$\bar{q}_i' = q_i' - \sum_{j=1}^{N'} C_{ij}(T_i - T_j) . \qquad (2.19)$$

Using this definition of $\bar{q}_i'$ and effective enthapy flow rate $u_i'' = \frac{m_i}{A_i(\rho_i - h_{fg} \frac{\partial \psi}{\partial h_i})}$ modifying equation 2.18, energy balance equation is

$$\frac{1}{u_i''} \frac{\partial h_i}{\partial t} + \frac{\partial h_i}{\partial x} = q_i' - \sum_j (T_i - T_j) \frac{C_{ij}}{m_i} - \sum_j (h_i - h_j) \frac{W'_{ij}}{m_i} + \sum_j (h_i - h^*) \frac{W_{ij}}{m_i} \qquad (2.21)$$

First and second terms on the RHS of equation (2.2), represents only the net heat addition to the channel i. Third term refers to enthalpy exchange by turbulent mixing between channels. W'_{ij} calculated from an empirical relation. Last term refers to transferred energy by diversion cross-flow.

Axial Momentum Balance

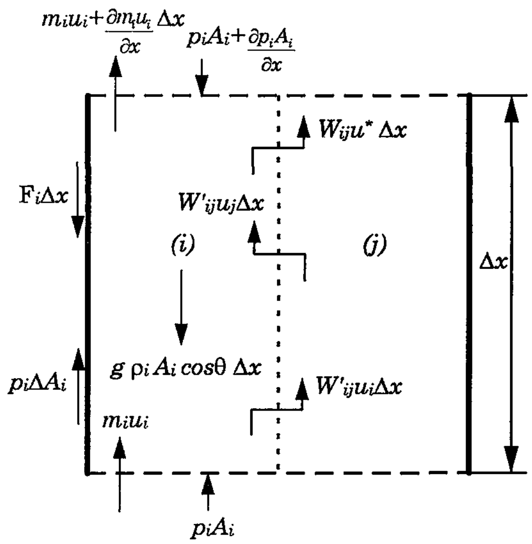

Figure 2.3 Inlet and Exit Momentun from Control Volume

Genaral form of momentum balance is shown as

$$\begin{Bmatrix} \text{rate of momentum} \\ \text{accumulation} \end{Bmatrix} = \begin{Bmatrix} \text{momentum} \\ \text{inlet rate} \end{Bmatrix} - \begin{Bmatrix} \text{momentum} \\ \text{exit rate} \end{Bmatrix} + \begin{Bmatrix} \text{external} \\ \text{forces} \end{Bmatrix}.$$

Considering ith subchannel and adjacent jth subchannel writing terms using figure 2.3

$$\frac{\partial}{\partial t} m_i \Delta x = m_i u_i + W'_{ji} u_j \Delta x - m_i u_i - \frac{\partial m_i u_i}{\partial x}\Delta x - W'_{ij} u_i \Delta x$$
$$- W_{ij} u^* \Delta x - g A_i \rho_i \cos\theta \Delta x - F_i \Delta x - A_i \frac{\partial p_i}{\partial x} \tag{2.22}$$

Since $W'_{ij} = W'_{ji}$, axial momuntum balance is reduced to

$$\frac{\partial}{\partial t} m_i = W'_{ij}(u_j - u_i) - W_{ij} u^* - \frac{\partial m_i u_i}{\partial x} - g A_i \rho_i \cos\theta - F_i - A_i \frac{\partial p_i}{\partial x}. \tag{2.23}$$

While obtaining this equation only one flow rate is used. This flow rate, which is defined as

$$u_i = \frac{m_i \nu_i'}{A_i} \tag{2.24}$$

is effective momentum flow rate. ν_i' in this definition is effective momentum specific volume and defined as

$$\nu_i' = \frac{x^2}{\alpha}\nu_g + \frac{(1-x)^2}{1-\alpha}\nu_f \tag{2.25}$$

Frictional force $F_i\Delta x$ that in axial momentum equation has two source. First is continuous viscous losses and second is local losses. Local losses originated from spacer and blockage in subchannel. Frictional force acting on the unit length of control volume due to local and continuous losses is

$$F_i = \frac{A_i f_i \phi_i \nu_i}{2D_i}\left(\frac{m_i}{A_i}\right)^2 + \frac{A_i K_i \nu_i}{2\Delta x}\left(\frac{m_i}{A_i}\right)^2 \tag{2.26}$$

In equation 2.24 there is a multipicated derivation term. It is needed to expand this term. Using continuity equation and u_i definition

$$\frac{\partial m_i u_i}{\partial x} = 2u_i\left(-W_{ij} - A_i\frac{\partial \rho_i}{\partial t}\right) + m_i^2\frac{\partial}{\partial x}\left(\frac{\nu_i}{A_i}\right) \tag{2.27}$$

is obtained. Expressions 2.26 and 2.27 are substituted into equation 2.23 then axial momentum equation is

$$\frac{1}{A_i}\frac{\partial}{\partial t}m_i - 2u_i\frac{\partial \rho_i}{\partial t} + \frac{\partial p_i}{\partial x} = \left(\frac{m_i}{A_i}\right)^2\left[\frac{K_i\nu_i}{2}G(x) + A_i\frac{\partial}{\partial x}\left(\frac{\nu_i}{A_i}\right) + \frac{\nu_i f_i \phi_i}{2D_i}\right] - f_T\sum_j (u_i - u_j)\frac{W_{ij}'}{A_i} + \sum_j (2u_i - u^*)\frac{W_{ij}}{A_i} - g\rho\cos\theta \tag{2.28}$$

for N adjacent subchannel. Here

$$G(x) = \begin{cases} \dfrac{1}{\Delta x} & ;\ x_k < x < x_{k+1} \\ 0 & ;\ x < x_k,\ x_{k+1} < x \end{cases}$$

Transverse Momentum Balance

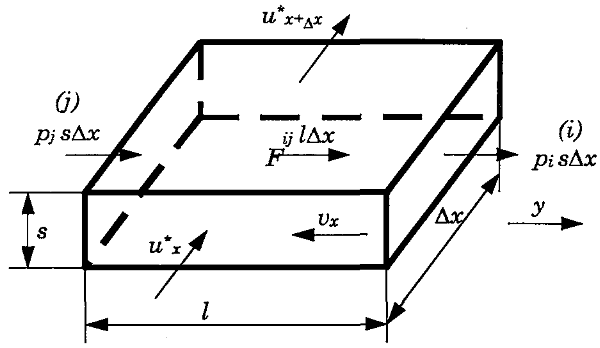

Figure 2.4 Inlet and Exit Momentum in Transvers Direction

According to figure 2.4 transvers momentum balance is

$$-F_{ij}\Delta x l - p_j s\Delta x + p_i s\Delta x = \frac{\partial \rho^*}{\partial t} sl\Delta x \upsilon_x - (\rho^* slu^* \upsilon_x)_x + (\rho^* slu^* \upsilon_x)_{x+\Delta x} \tag{2.29}$$

After each term reduced by $l\Delta x$

$$-F_{ij} + (p_i - p_j)\frac{s}{l} = \frac{\partial \rho^*}{\partial t} s\upsilon_x + \frac{(\rho^* slu^* \upsilon_x)_{x+\Delta x} - (\rho^* slu^* \upsilon_x)_x}{\Delta x} \tag{2.30}$$

is obtained. Last term in $\Delta x \to 0$ limit turns to $\partial[\rho^* su^*]/\partial x; W_{ij} = \upsilon_x s\rho^*$ substituted into equation 2.30. Then transvers momentum balance is

$$-F_{ij} + (p_i - p_j)\frac{s}{l} = \frac{\partial W_{ij}}{\partial t} + \frac{\partial [u^* W_{ij}]}{\partial x} \tag{2.31}$$

In this equation ρ*

$$\rho^* = \begin{cases} \rho_i; W_{ij} > 0 \\ \rho_j; W_{ij} < 0 \end{cases} \tag{2.32}$$

In steady-state condition $\left(p_i - p_j = K_{ij}\frac{\rho^* \upsilon^2}{2}\left(\frac{s}{l}\right)\right.$ and $\left.\upsilon = \frac{W}{\rho^* s}\right)$ friction and form pressure loss due to cross flow is

$$F_{ij} = \frac{K_{ij}|W_{ij}|W_{ij}}{2s^2\rho^*}\left(\frac{s}{l}\right) \tag{2.33}$$

Modifying equation 2.31

$$\frac{\partial W_{ij}}{\partial t}+\frac{\partial[u^{*}W_{ij}]}{\partial x}+\left(\frac{s}{l}\right)\frac{K_{ij}|W_{ij}|}{2s^{2}\rho^{*}}W_{ij}=(p_{i}-p_{j})\frac{s}{l} \qquad (2.34)$$

Irrecoverable Pressure Loss, K_b, **Spacer Loss Coefficient,** K, **Diversion Cross-Flow Resistance,** K_{ij} [8]

The irrecoverable pressure loss defined as

$$K_{b}=\frac{\Delta p_{b}}{\frac{1}{2}\rho_{i}v^{2}} \qquad (2.5)$$

where v is the average velocity of the undisturbed flow.

The spacer loss coefficient is defined as

$$K=\frac{\Delta p_{form}}{\frac{1}{2}\nu\left(\frac{m}{A}\right)^{2}}. \qquad (2.6)$$

Assuming linear pressure drop within distance Δx_i $K_i=K/\Delta x_i$ is used for spacer loss coefficient.

The diversion cross-flow resistance defined as

$$K_{ij}=\frac{p_{i}-p_{j}}{\frac{1}{2}|W_{ij}|W_{ij}}s^{2}\rho\frac{s}{l} \qquad (2.7)$$

2.4 COBRA PC-4 Code

Original FORTRAN listings of COBRA-IV-I computer code is obtained from OECD NEA Data-bank which is tested for IBM 3084 mainframe computers. This form of code is not suitable for execution on PC computers and Workstation. Since available computers in our institute are PC compatibles COBRA-IV-I code should be adapted into these computers in order to be executed. Original flow chart of COBRA-IV-I code shown at Fig. 2.1

Some enhancements and modifications are required for this kind of adaptation. In order to obtain suitable executable code following enhancements are performed.

-Input and output files are arranged at utility SPECSET.

-Incompatible CSPECS utility is replaced by SCISS.

-Input/output and include files are arranged at COBRA-IV-I master file.

-In order to have a modular structure, which is more easy to maintain and to generate executable binary, COBRA-IV-I master file divided into its subprograms.

-All of the subprograms are compiled in library form with the help of the modular form.

-Several compiler dependent syntax and runtime errors which occurred at test stage of executable binary are fixed in COBRA-PC-4

-For executable binary, MS-FORTRAN 5.1 compiler is used for obtaining DOS, WINDOWS and OS/2 executables.

2.5 Changes made on COBRA-IV-I computer code

Important modifications that are performed on COBRA-IV-I are shown below.

Master COBRA-IV-I FORTRAN source file chopped into the files for each routine, since the compiler is not suitable for compiling a single master file

Two IBM3084 system dependent assembler routine replaced with compiler dependent routines to check date and time; IDAY.FOR, ICLOCK.FOR

Input/Output files are arranged in COBRA.FOR main routine so an option for input file could be made.

Compiler errors from preinitialization statements are fixed.

A timer added in code to indicate total running time for further benchmark purposes

The initalizer routine CLEAR.FOR is discarded, since variables are already initialised to zero by compiler, also DUMP.FOR option is disabled.

In AREA.FOR routine variable preinitalization statements are separated from the definition statements due to compiler error.

Format statement is changed due to consistency with the output list at routine CARDG2.FOR

In CARDG4.FOR routine read statements are reorganised to the proper input format.

At CARDG7.FOR routine several CALL LOADL statements are modified to CALL LOADL1, CALL LOADL2 statements due to compiler error about inconsistency of parameter list.

Read statements are reorganised to the documented input format at routine CARDG8.FOR

If block is modified due to compiler error in routine CARDGC.FOR

Variable definition statements are separated and placed before the initialisation statements in routine CHF1.FOR

At the printout stage of RESULT.FOR, subcahnnel length data converted from inch to mm, pressure data converted form psi to N/m^2, mass flow rate data converted form lb/sec to kg/h. Also output format specifications are corrected due to compiler warning.

All routines, but main routine COBRA.FOR, are compiled and routine library is built by these routines. Using this library form is very modular while obtaining the executable binary of COBRA. Main routine also compiled and linked with the routine library then executable is obtained. Final flow chart of COBRA-PC4 is shown at Fig. 2.2

This procedure of obtaining executable is performed at several different operating systems, DOS, OS/2, WINDOWS. DOS operating system is restricted with the maximum core memory which is an upper limit on the executable size of 640 KB, however other operating systems OS/2 and WINDOWS have not such software based core restrictions. While the array sizes in COBRA code are grown, the executable size would be bigger than 640 KB in DOS operating system. This problem let us to use OS/2 or WINDOWS environments for running the code. Current COBRA-PC-4 executable binary is in form of WINDOWS one.

After the completion of these work, original test cases of COBRA-IV-I are tested on COBRA-PC-4 and exactly the same results are obtained.

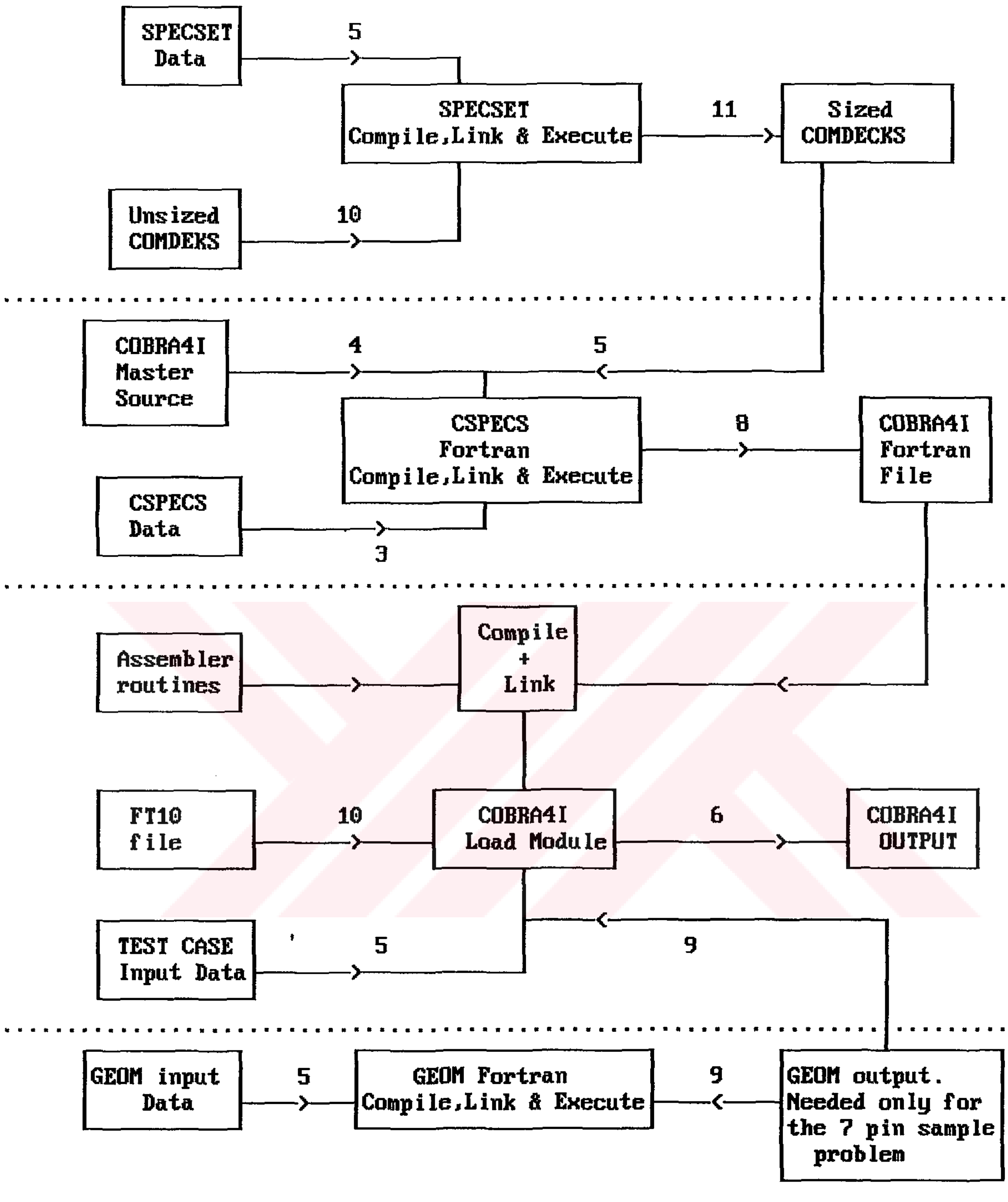

Figure 2.5 COBRA-IV-I FLOW CHART [4]

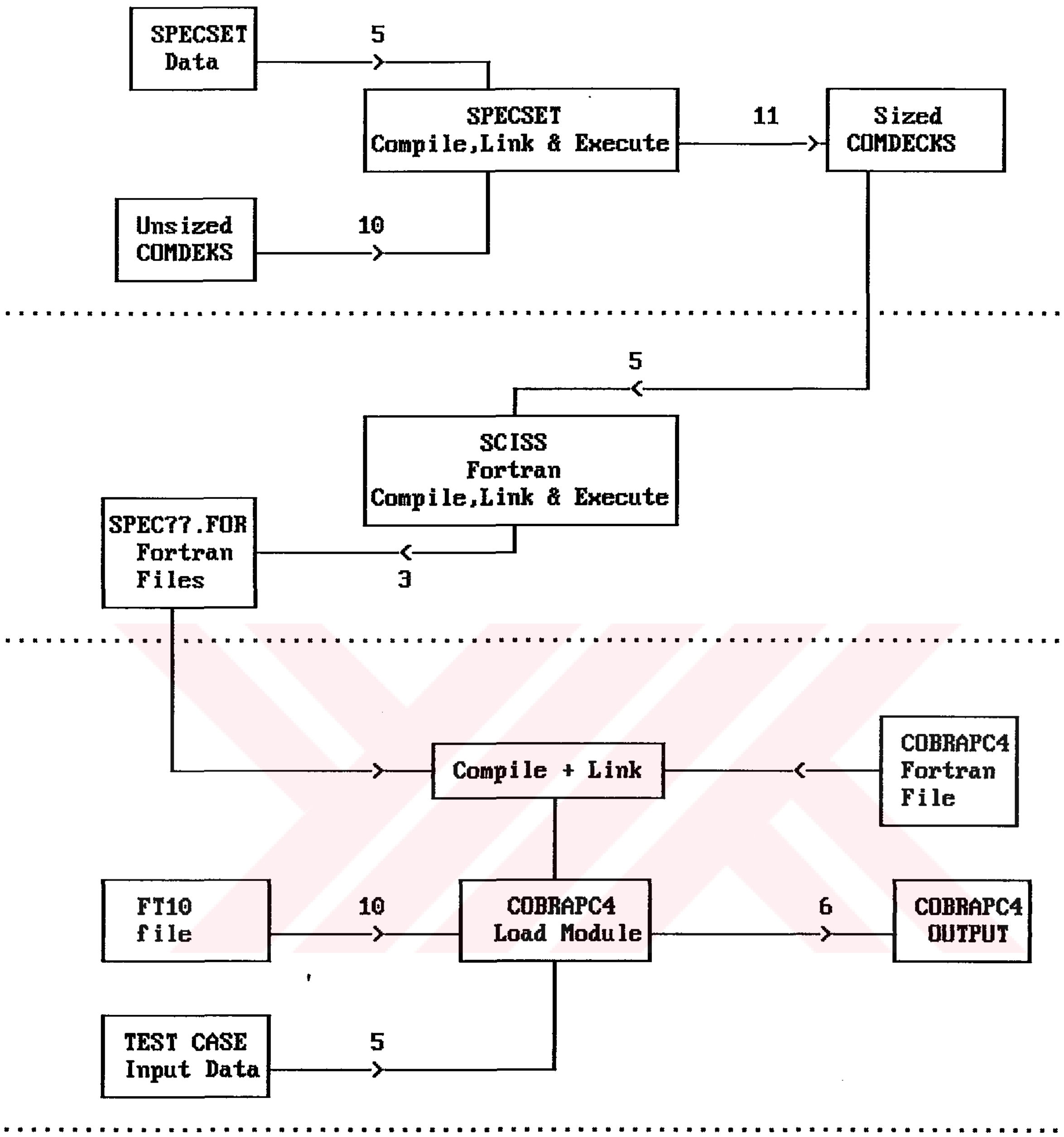

Figure 2.6 COBRA-PC4 FLOW CHART

CHAPTER 3

VERIFICATION OF COBRA-PC-4 RESULTS

3.1 Experimental Data - Overview

Three groups of sample experimental data are chosen from literature. These are the followings.

1. Single phase with subchannel blockage.
2. Two phase.
3. Two phase with subchannel blockage.

The experiments are performed on a test section consist of two parallel subchannels. List of the experimental geometry and set-up is given in the Fig. 3.1 and the Tables 3.1, and 3.2.

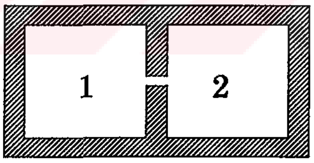

Figure 3.1 Geometry of Test Sections [1]

Table 3.1 Single phase with subchannel blockage Experimental Data [1]

Square Channel			
Gap Clearance		*1.52 mm*	*0.06 in.*
Gap Thickness		*3.17 mm*	*0.12 in.*
Hydraulic diameter	*CH1*	*12.6 mm*	*0.496 in.*
	CH2	*12.5 mm*	*0.492 in.*
Hydraulic perimeter	*CH1*	*52.762 mm*	*2.07724 in.*
	CH2	*52.8 mm*	*2.07874 in.*
Area	*CH1*	*166.2 mm*^{2}	*0.258 in.*^{2}
	CH2	*165.0 mm*^{2}	*0.256 in.*^{2}
Interconnection length		*847.0 mm*	*33.35 in.*
Blockage Location	*CH1*	*327.7 mm*	*12.90 in.*

Table 3.1 Continue

	Blockage Type	Area Reduction	Flow Rate (kg/h)		Flow Fractions		Total Mass Flux
			CH1	CH2	CH1	CH2	(Mlb/h-ft^2)
Run#10	Plate	29.8%	1854	1717	.5192	.4808	2.2087
Run#11	Plate	29.8%	2633	2393	.5116	.4884	3.1086
Run#8	Plate	29.8%	1859	1761	.5239	.4761	2.238
Run#18	Smooth	58.6%	1816	1862	.4937	.5063	2.2750
Run#19	Smooth	58.6%	2640	2665	.4976	.5024	3.2812
Run#20	Smooth x 2	64.2%	1816	1798	.5025	.4975	2.2353
Run#21	Smooth x 2	64.2%	2635	2634	.5001	.4999	3.2589

Table 3.2 Two phase with and without subchannel blockage, Experimental Data [2,3]

Square Channel			
Gap Clearance		1.52 mm	0.06 in
Gap Thickness		3.17 mm	0.12 in
Hydraulic diameter	CH1	12.43 mm	0.4894 in
	CH2	12.55 mm	0.4941 in
Hydraulic perimeter	CH1	52.26 mm	2.058 in
	CH2	52.75 mm	2.077 in
Area	CH1	162.4 mm^2	0.2517 in^2
	CH2	165.5 mm^2	0.2565 in^2
Interconnection length		1129.6 mm	44.47 in
Blockage Location	CH1	272 mm	10.71 in
Centroit Distance		155.88 mm	0.6252 in

	Blockage Type	Area Reduction	Liq. Mass Flux (kg/sqm-s)		Void Mass Flux (kg/sqm-s)		Flow Fractions	
		CH1	CH1	CH2	CH1	CH2	CH1	CH2
Run V-1	-	0%	3175	3089	13.47	0.	0.60	0.
Run V-6	-	0%	3125	3065	8045	0.	0.51	0.
Run V-9	-	0%	3113	3075	14.86	1.20	0.59	0.17
Run#1	Plate	31.9%	2006	1969	10.4	10.5	0.589	0.60
Run#2	Plate	31.9%	2022	1994	9.7	0.0	0.595	0.
Run#3	Plate	31.9%	2008	1964	0.	9.8	0.	0.602
Run#4	Plate	61%	2016	1983	11.8	10.9	0.597	0.612

Using experimental set-up and data, a proper input data were prepared for execution of COBRA-PC4 code. The results corresponding to the input cases are shown in the following figures.

It is concluded that COBRA-PC4 code is capable of simulating the flow in subchannels.

3.2 Single Phase With Subchannel Blockage

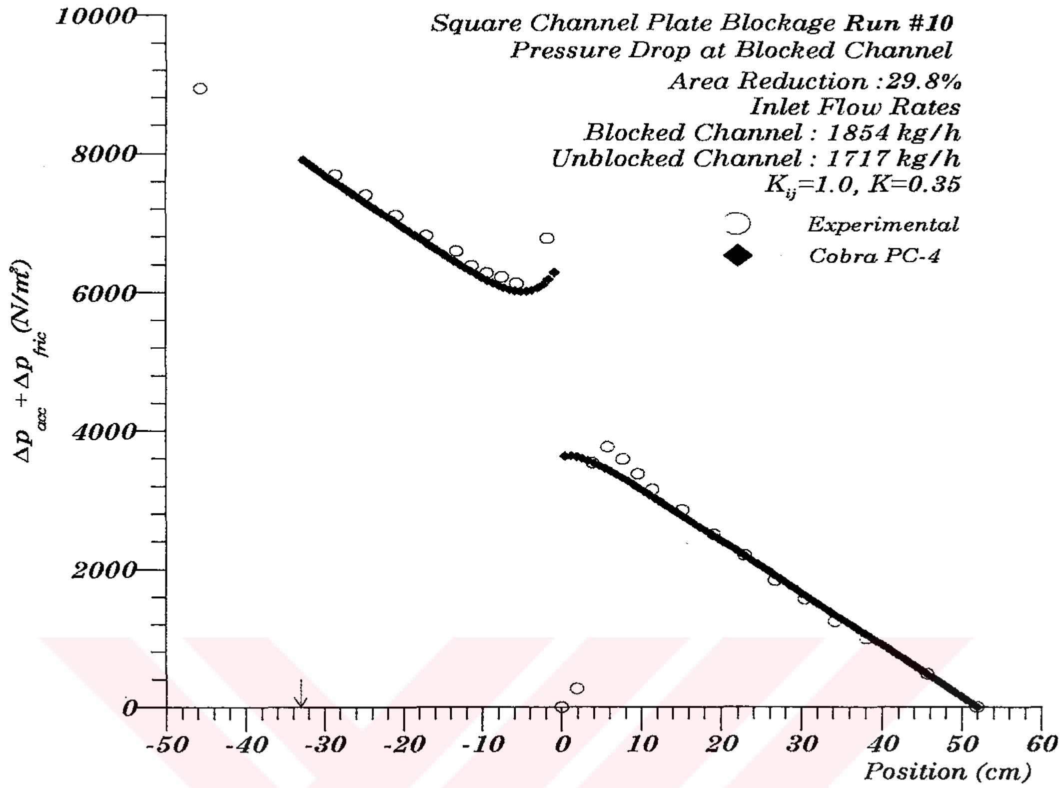

Figure 3.2 Comparison of COBRA-PC4 Predictions with Experimental Data

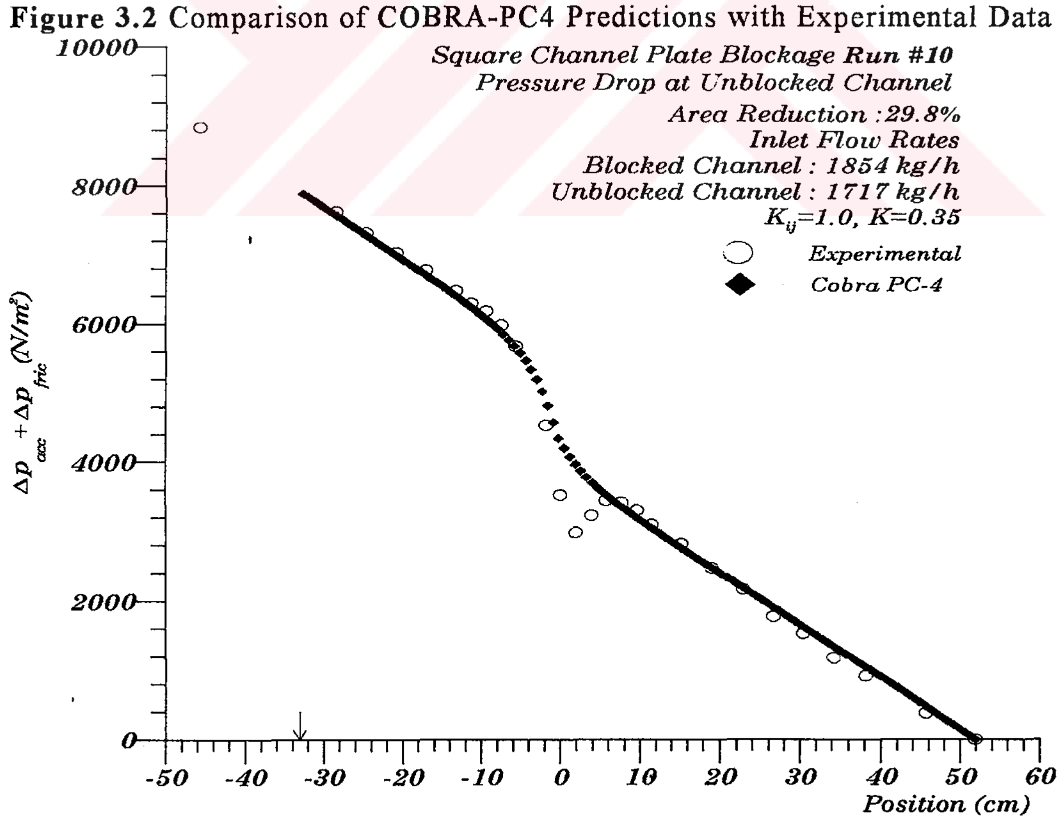

Figure 3.3 Comparison of COBRA-PC4 Predictions with Experimental Data

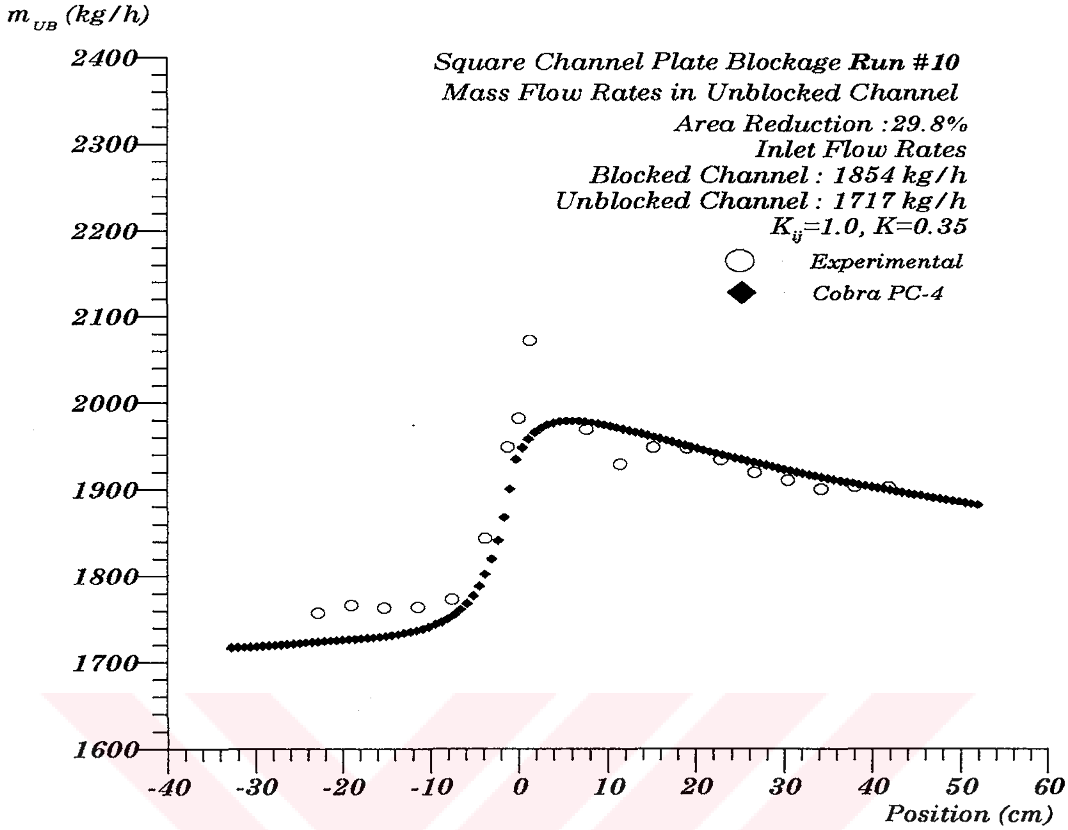

Figure 3.4 Comparison of COBRA-PC4 Predictions with Experimental Data

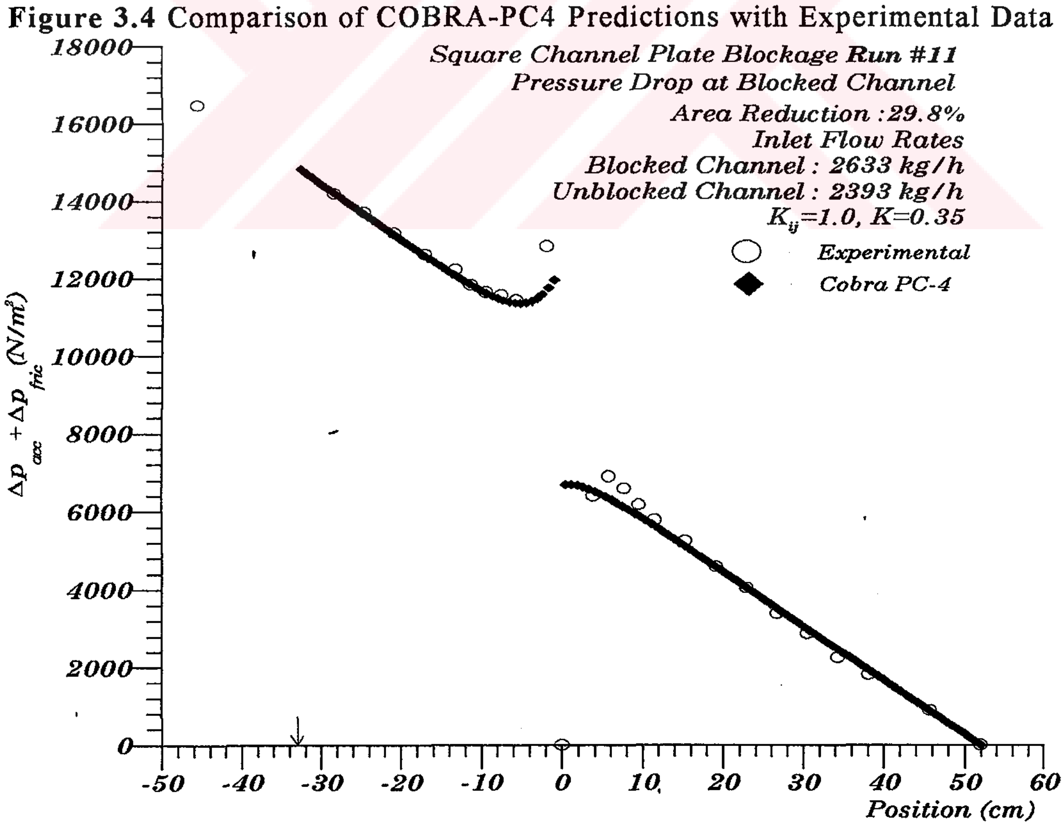

Figure 3.5 Comparison of COBRA-PC4 Predictions with Experimental Data

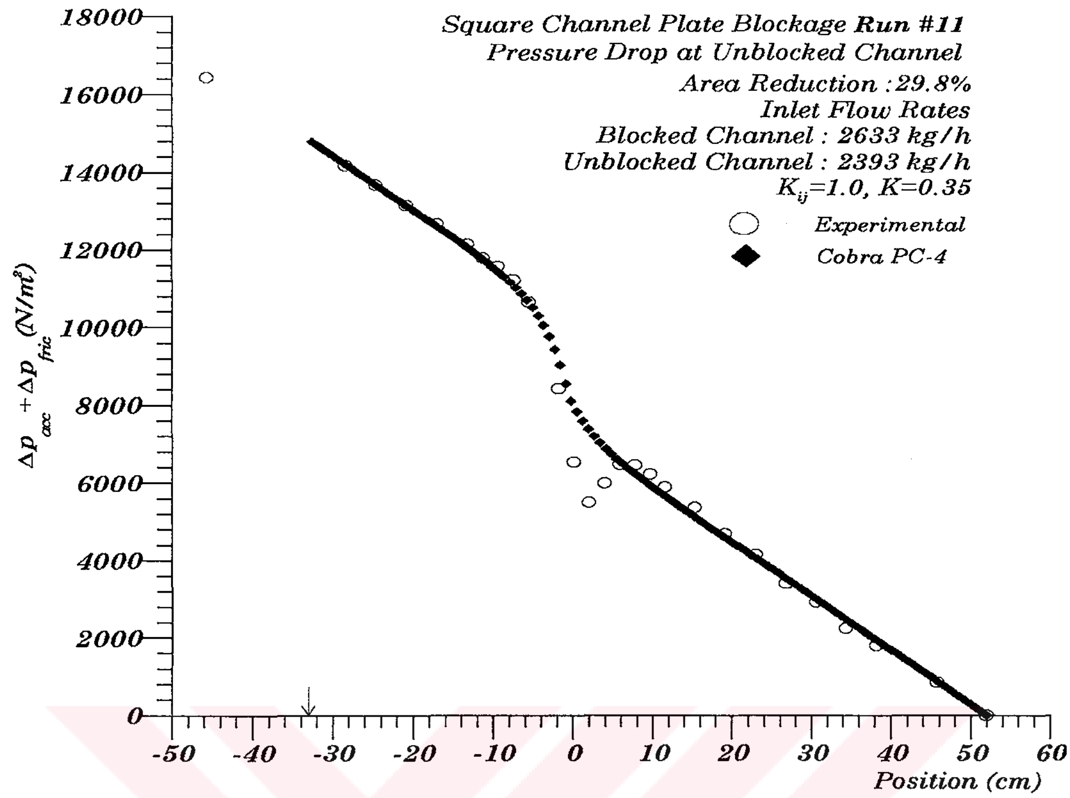

Figure 3.6 Comparison of COBRA-PC4 Predictions with Experimental Data

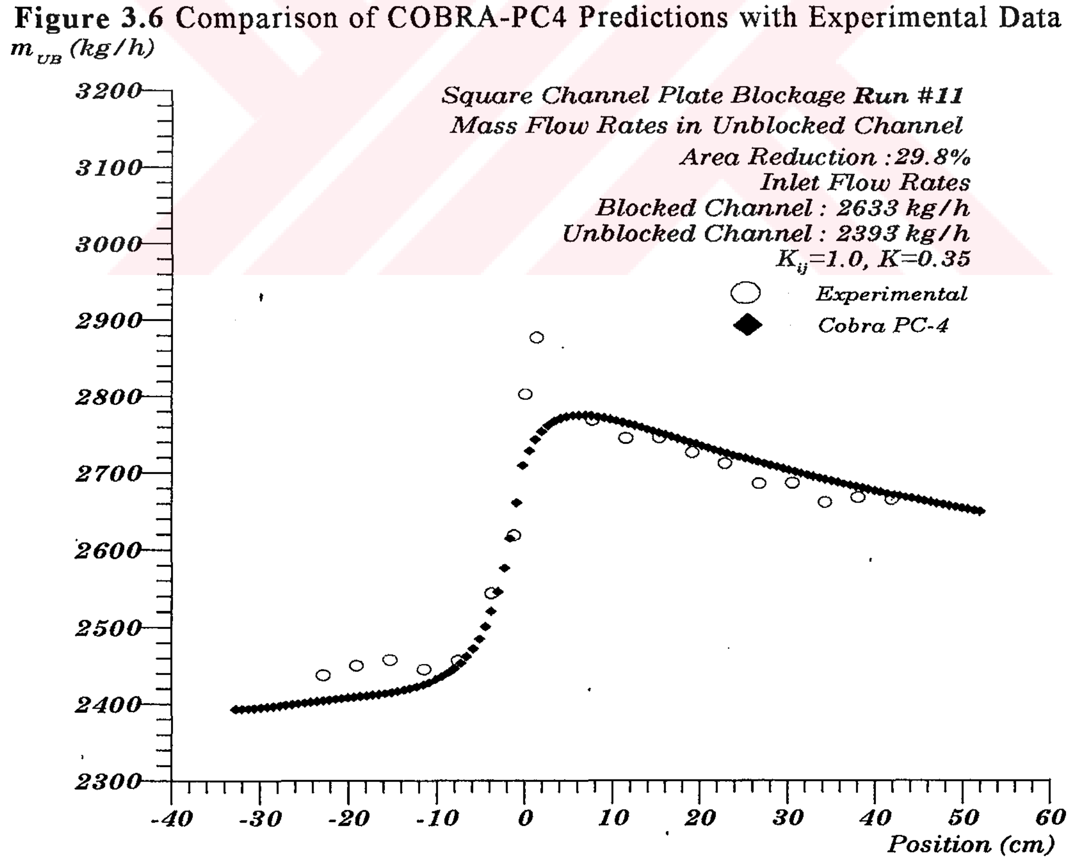

Figure 3.7 Comparison of COBRA-PC4 Predictions with Experimental Data

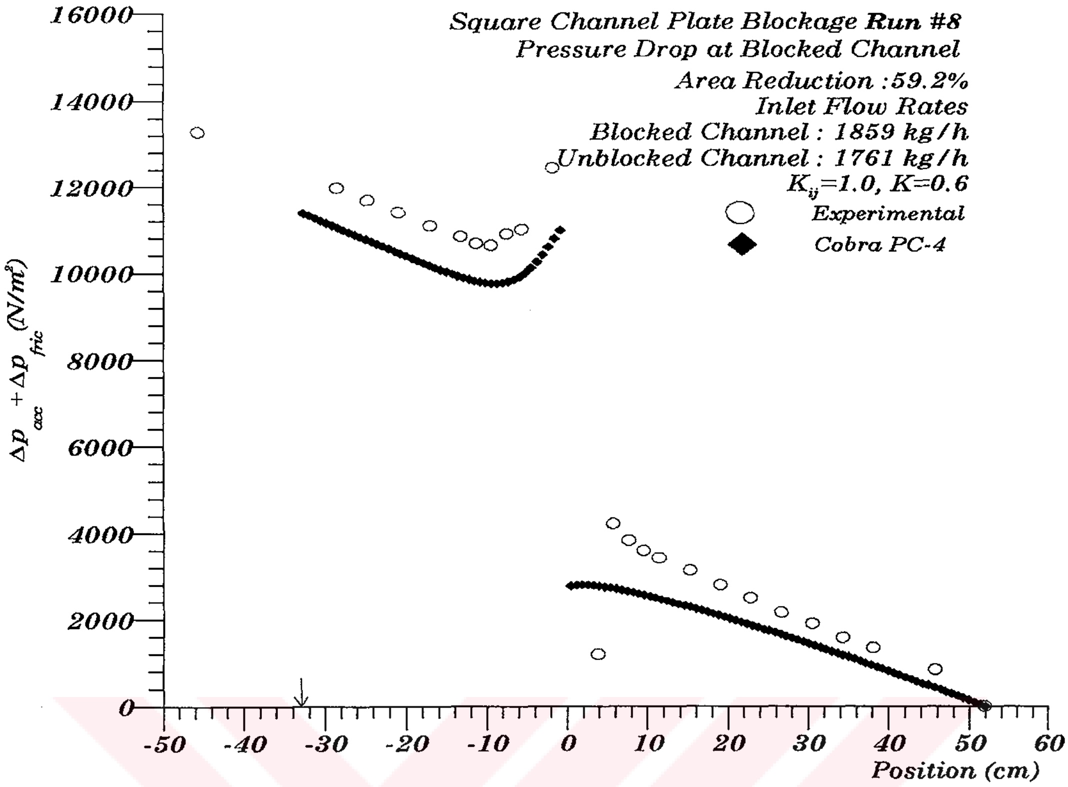

Figure 3.8 Comparison of COBRA-PC4 Predictions with Experimental Data

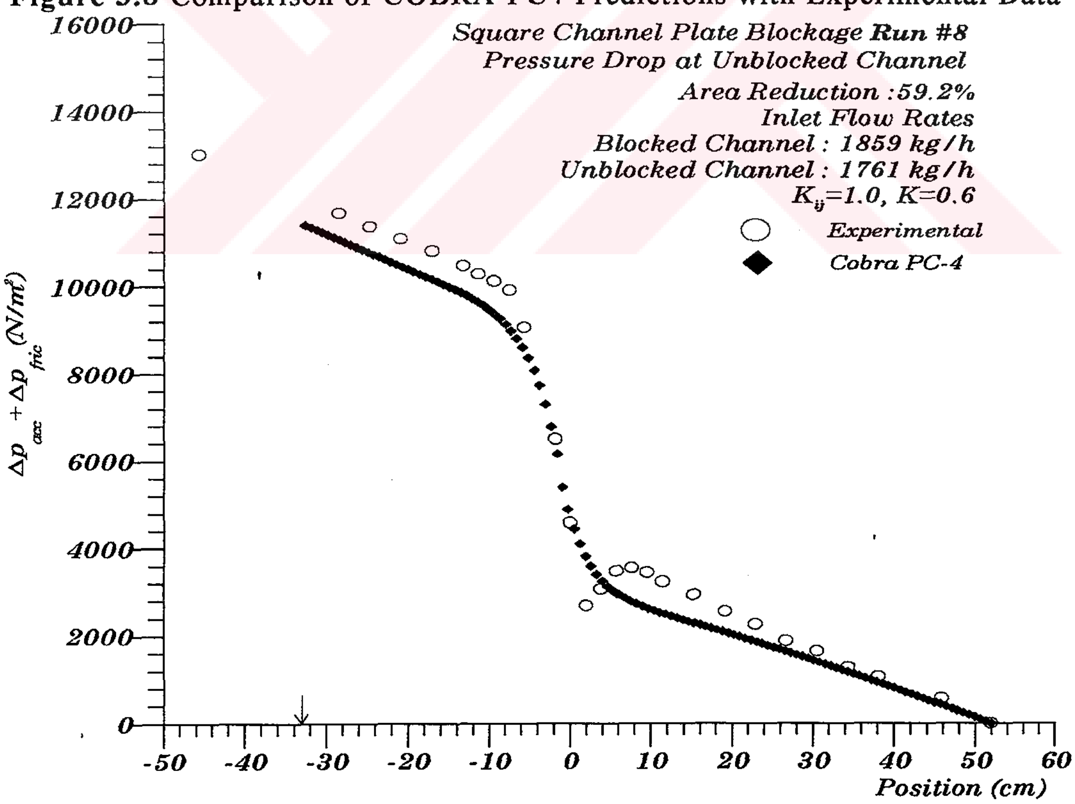

Figure 3.9 Comparison of COBRA-PC4 Predictions with Experimental Data

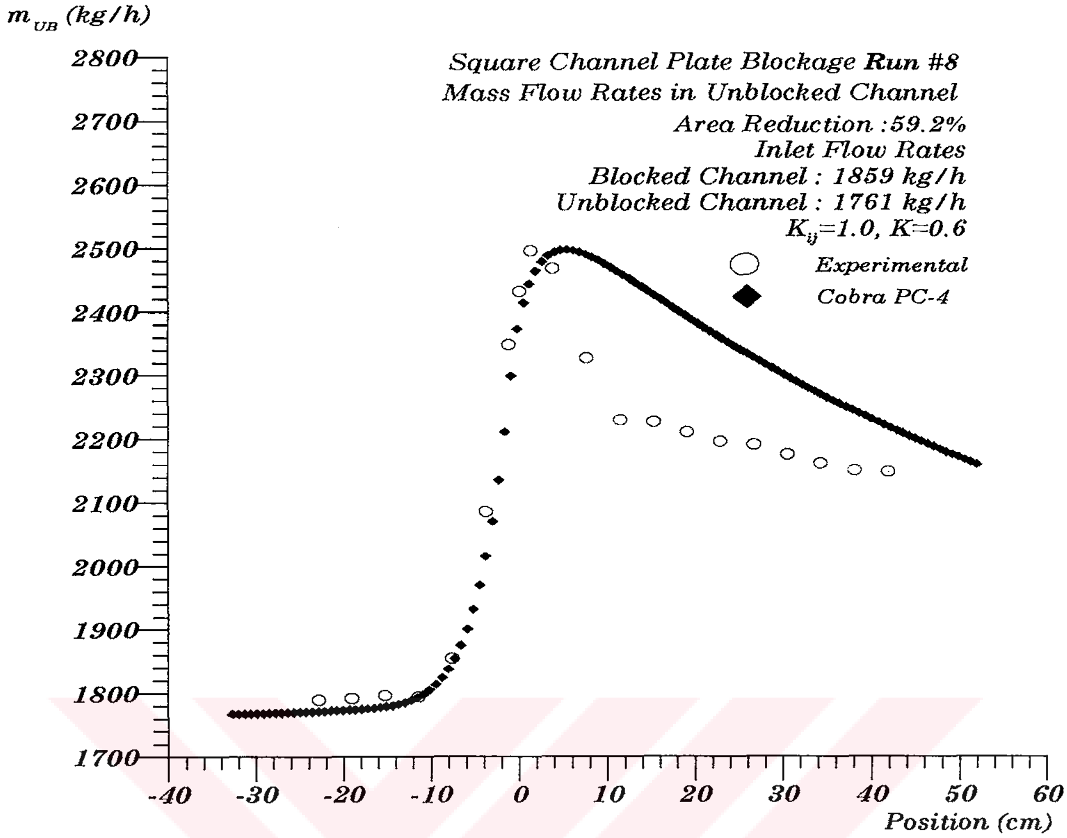

Figure 3.10 Comparison of COBRA-PC4 Predictions with Experimental Data

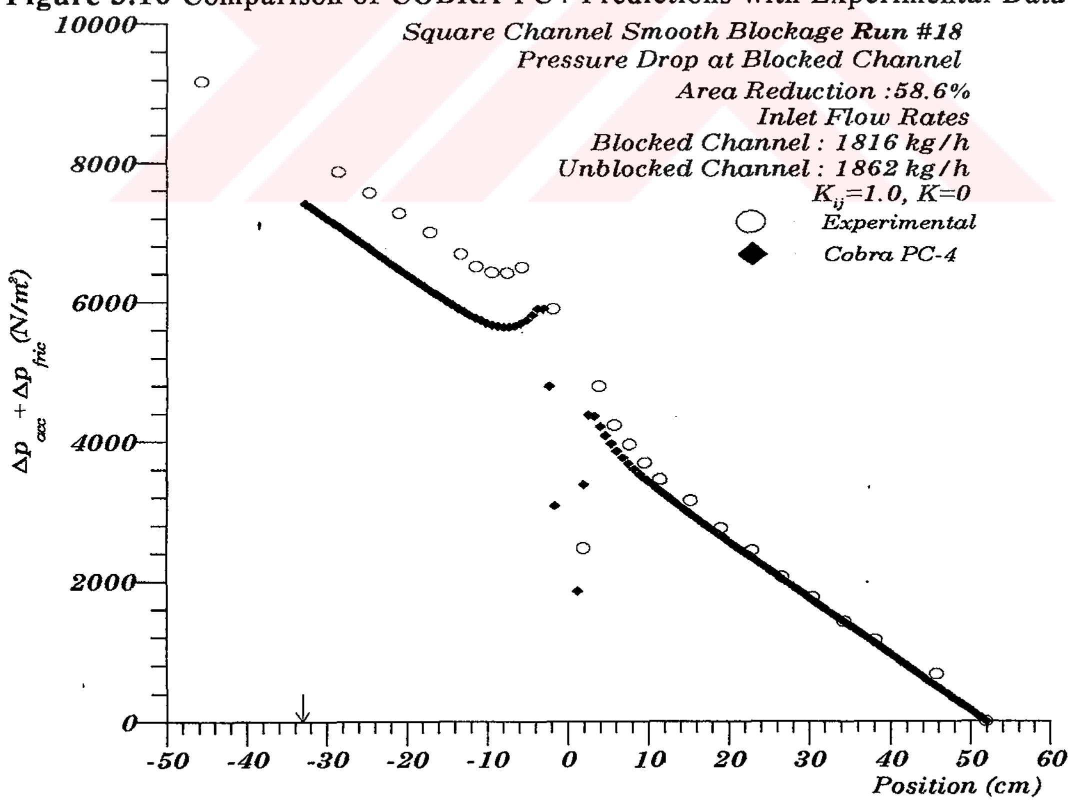

Figure 3.11 Comparison of COBRA-PC4 Predictions with Experimental Data

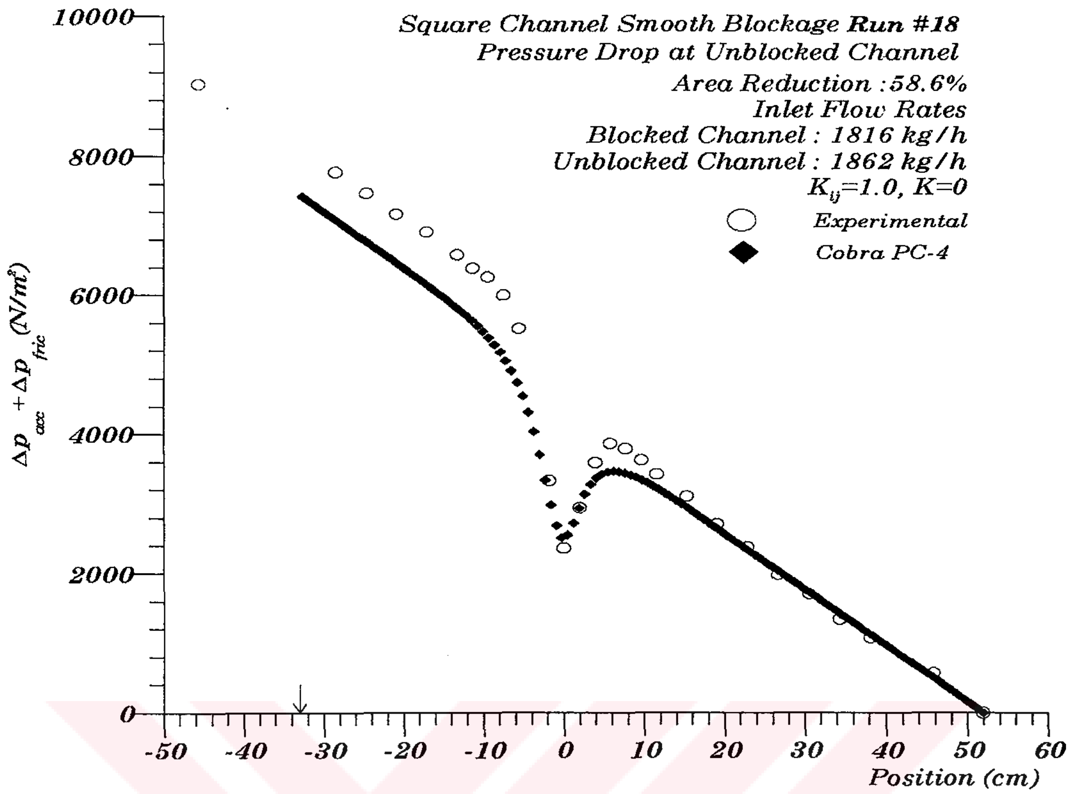

Figure 3.12 Comparison of COBRA-PC4 Predictions with Experimental Data

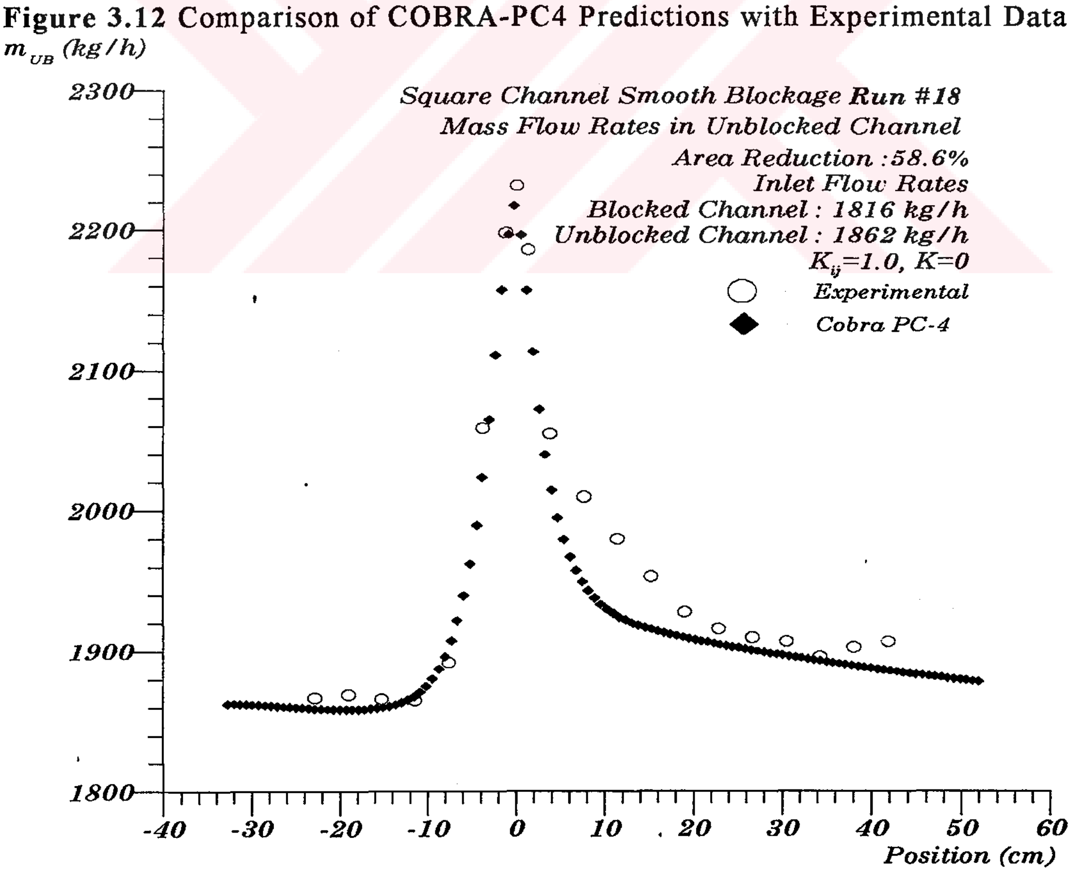

Figure 3.13 Comparison of COBRA-PC4 Predictions with Experimental Data

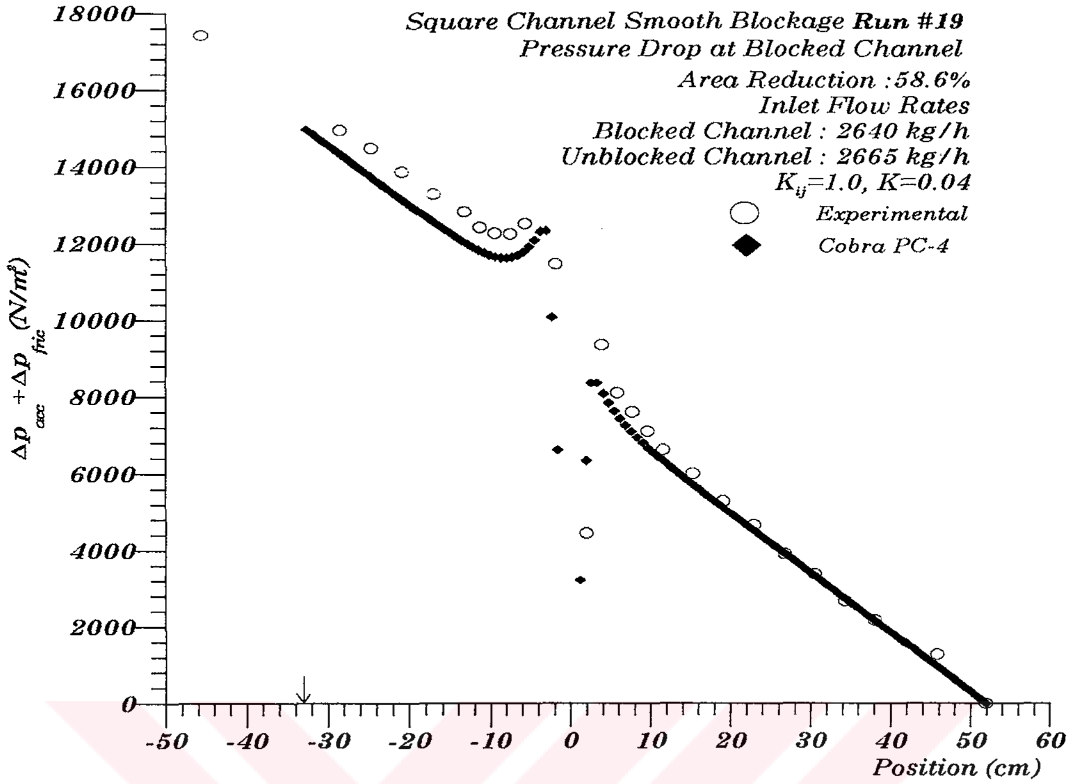

Figure 3.14 Comparison of COBRA-PC4 Predictions with Experimental Data

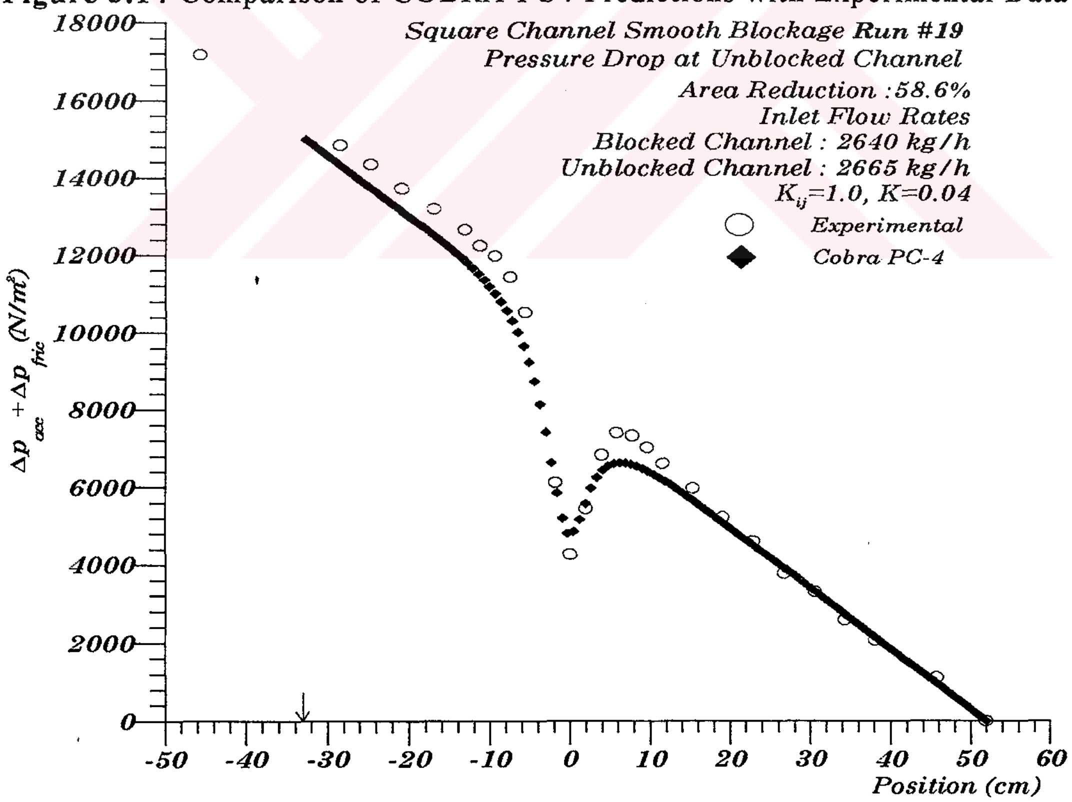

Figure 3.15 Comparison of COBRA-PC4 Predictions with Experimental Data

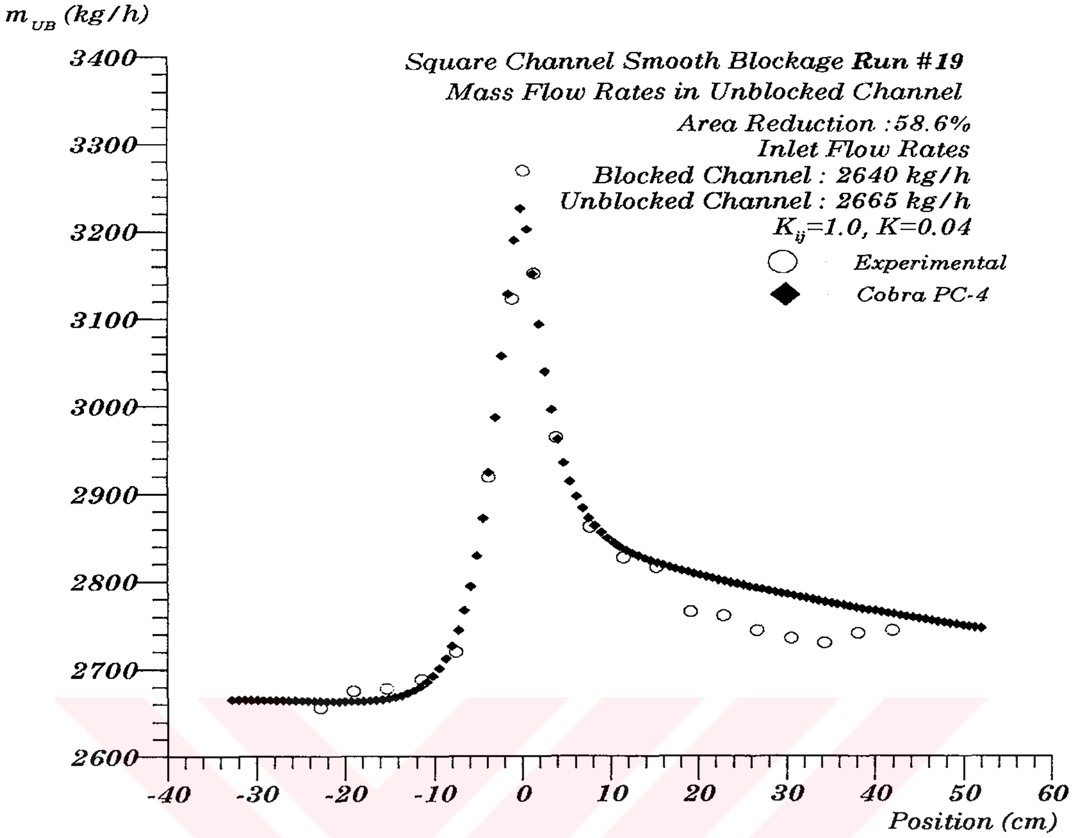

Figure 3.16 Comparison of COBRA-PC4 Predictions with Experimental Data

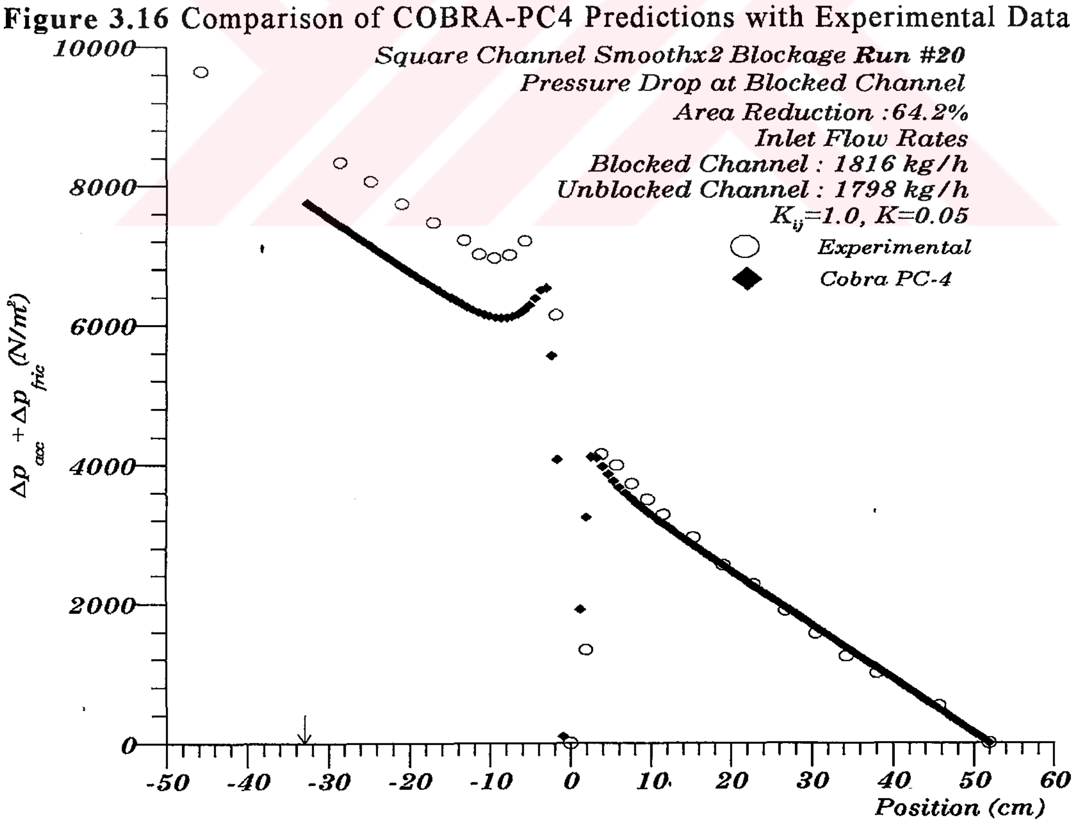

Figure 3.17 Comparison of COBRA-PC4 Predictions with Experimental Data

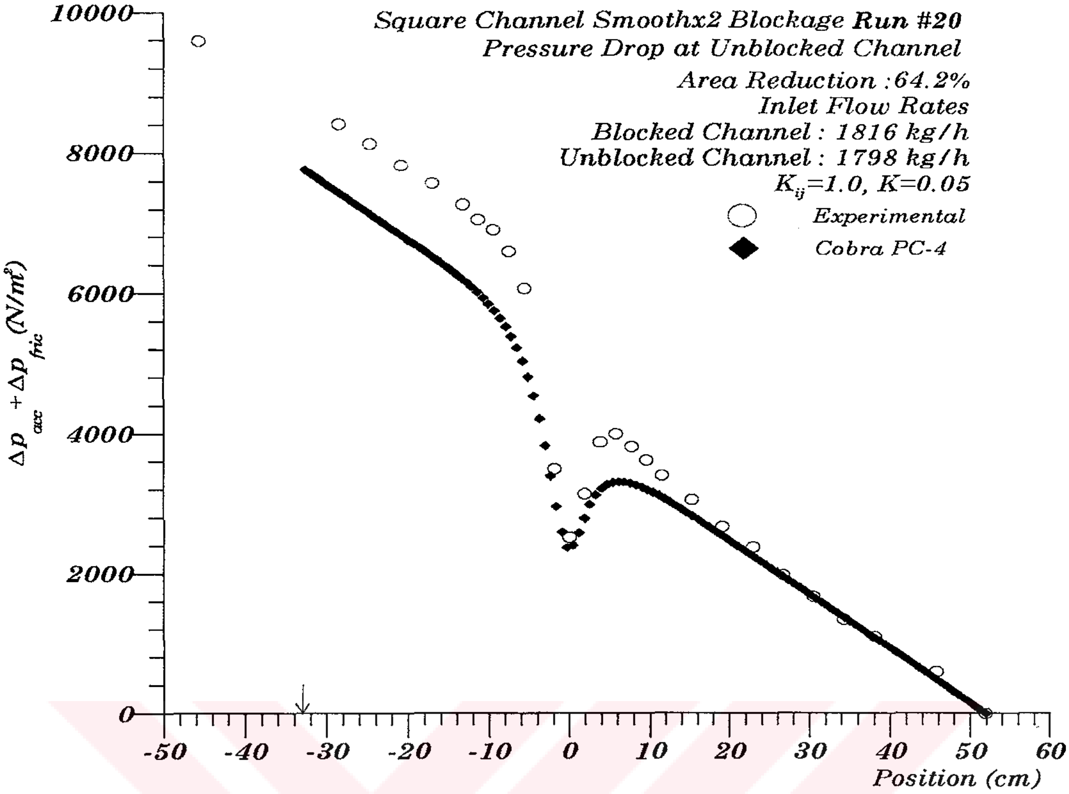

Figure 3.18 Comparison of COBRA-PC4 Predictions with Experimental Data

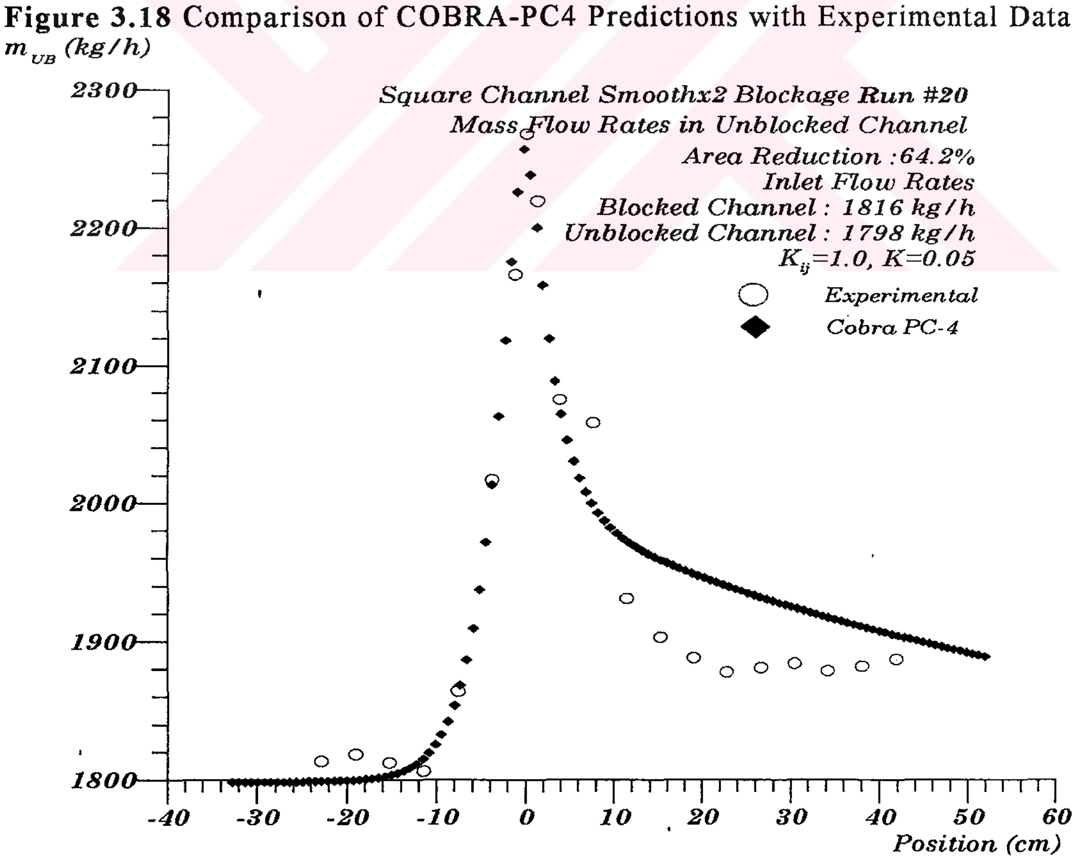

Figure 3.19 Comparison of COBRA-PC4 Predictions with Experimental Data

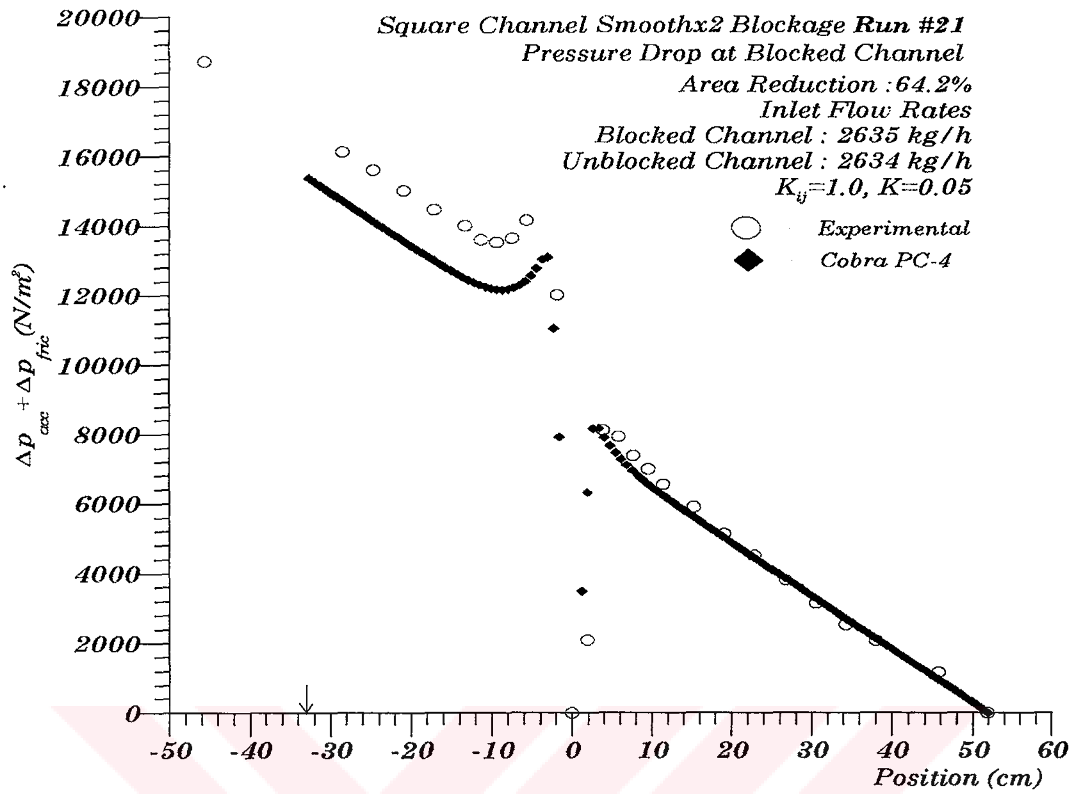

Figure 3.20 Comparison of COBRA-PC4 Predictions with Experimental Data

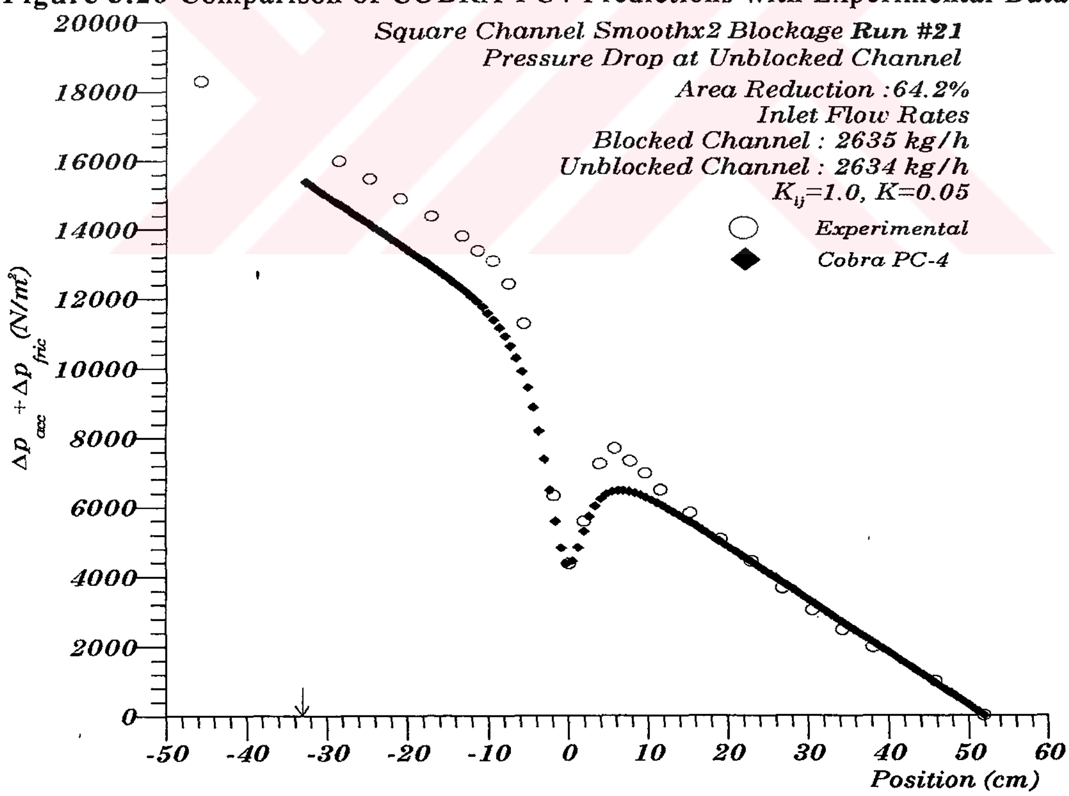

Figure 3.21 Comparison of COBRA-PC4 Prediotions with Experimental Data

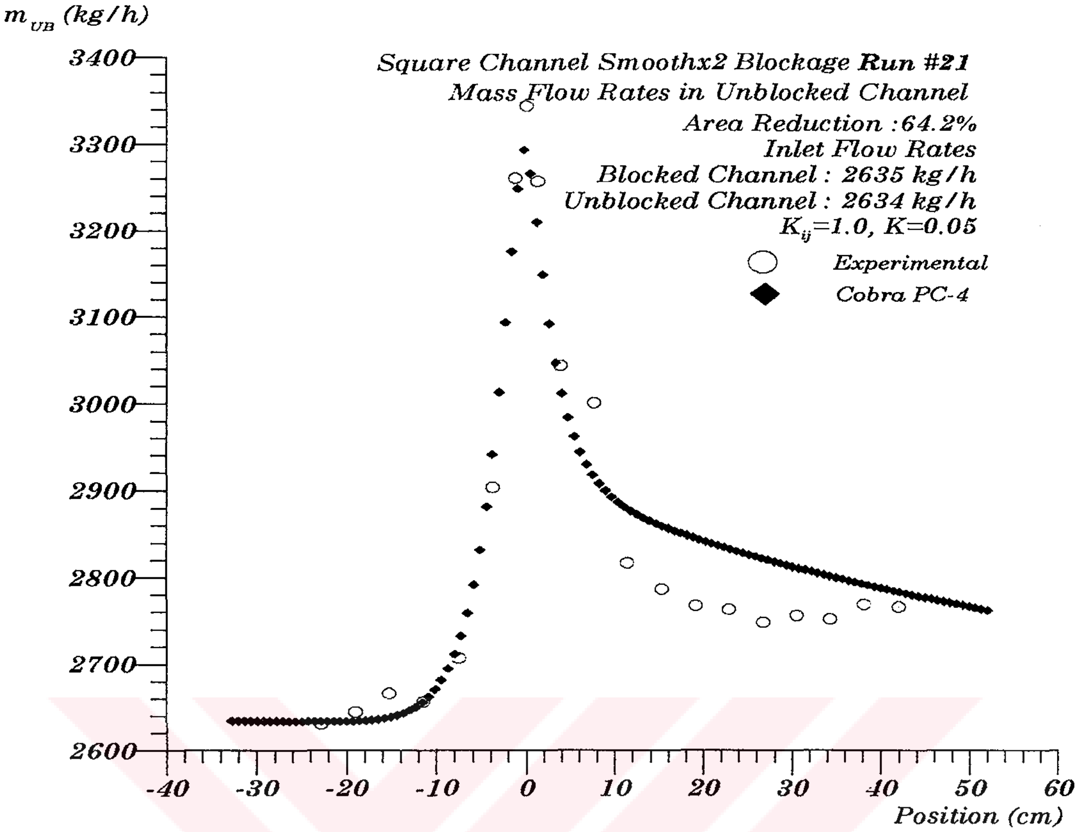

Figure 3.22 Comparison of COBRA-PC4 Predictions with Experimental Data

3.3 Two Phase Flow Without Blockage

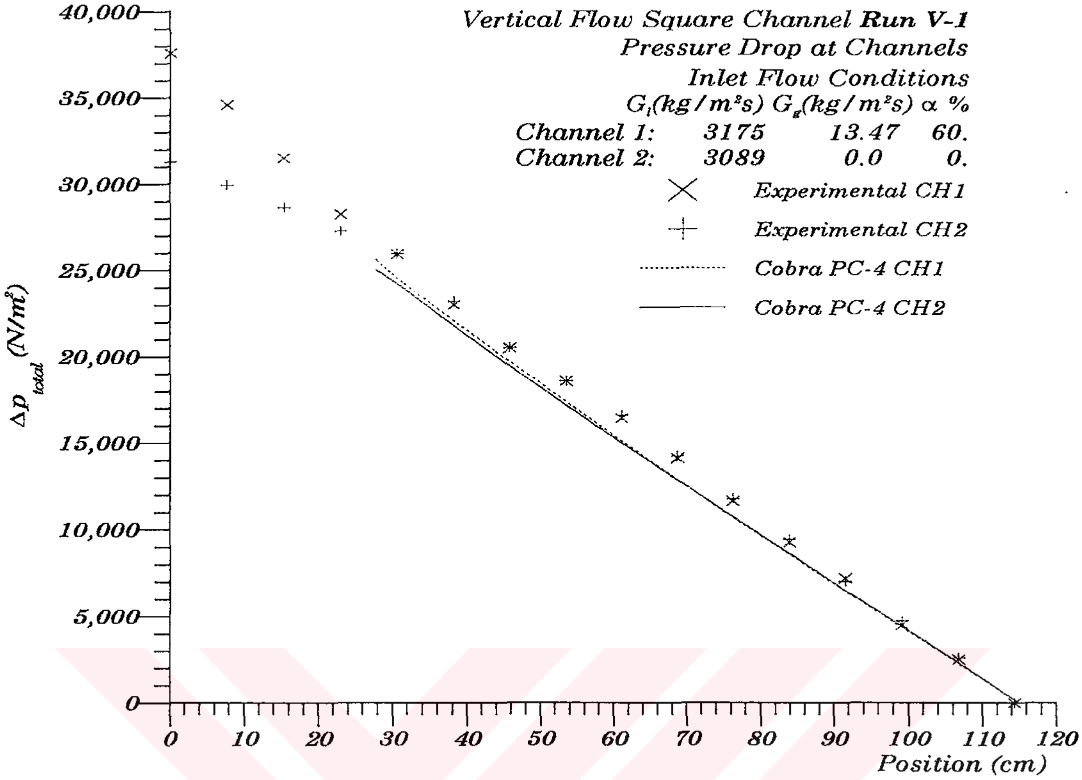

Figure 3.23 Comparison of COBRA-PC4 Predictions with Experimental Data

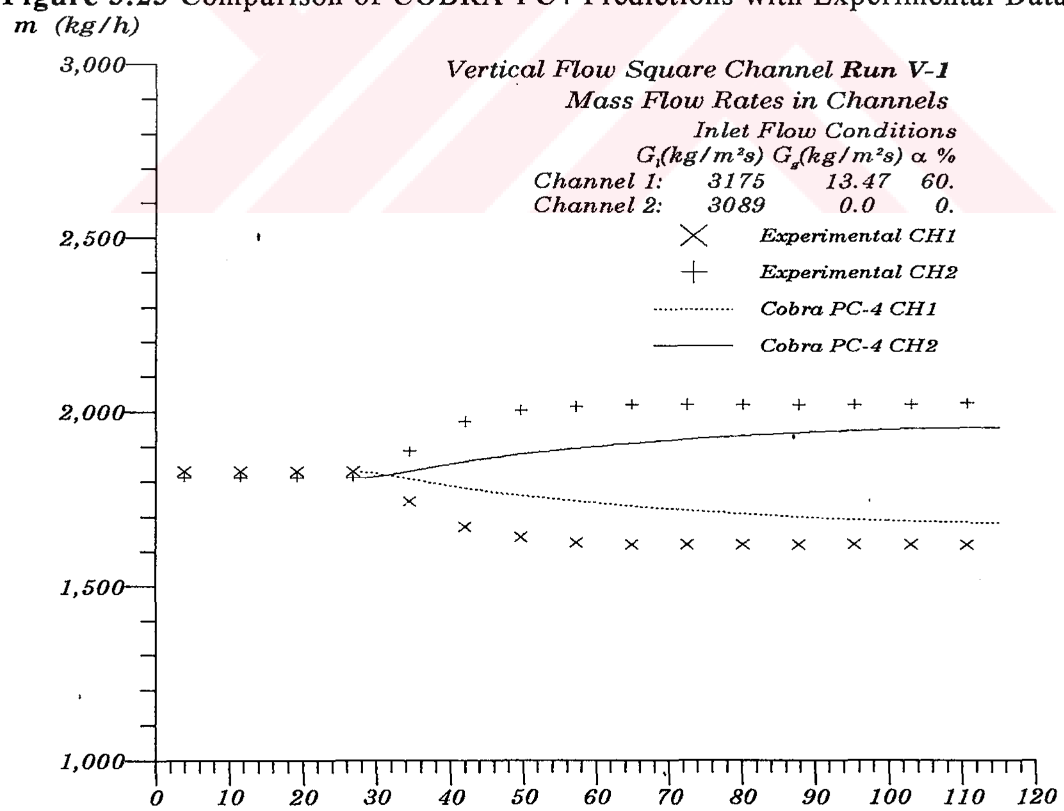

Figure 3.24 Comparison of COBRA-PC4 Predictions with Experimental Data

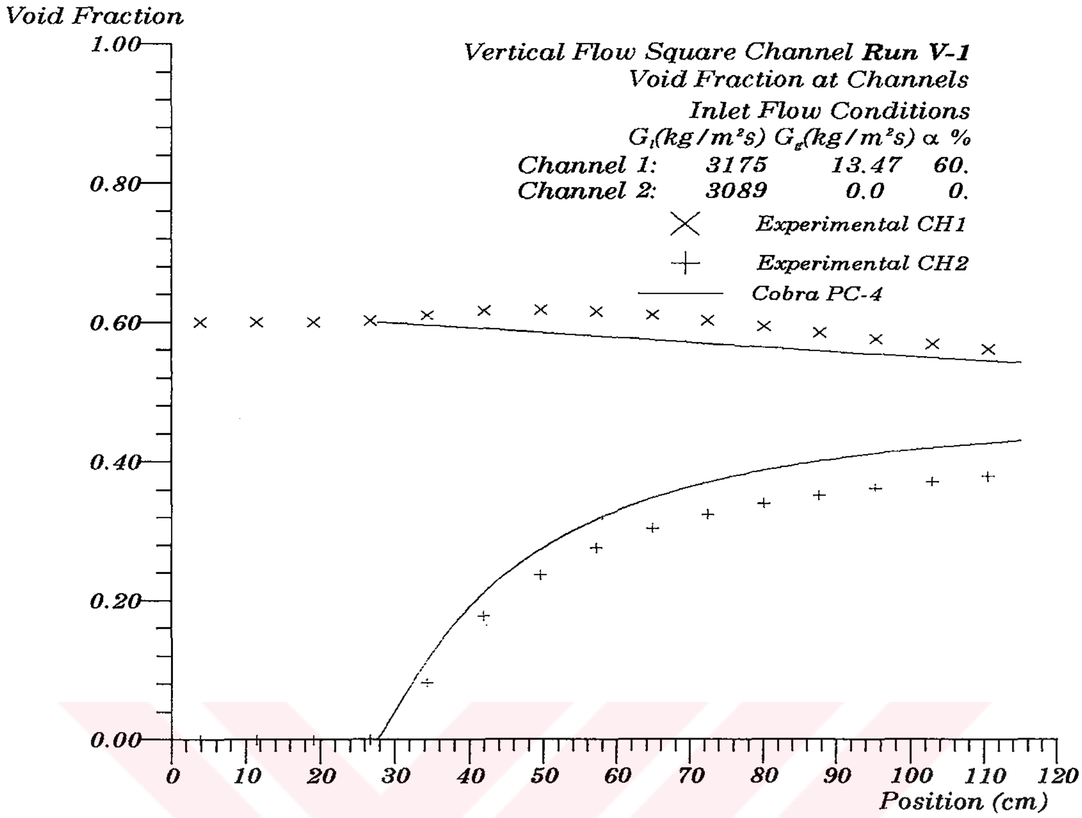

Figure 3.25 Comparison of COBRA-PC4 Predictions with Experimental Data

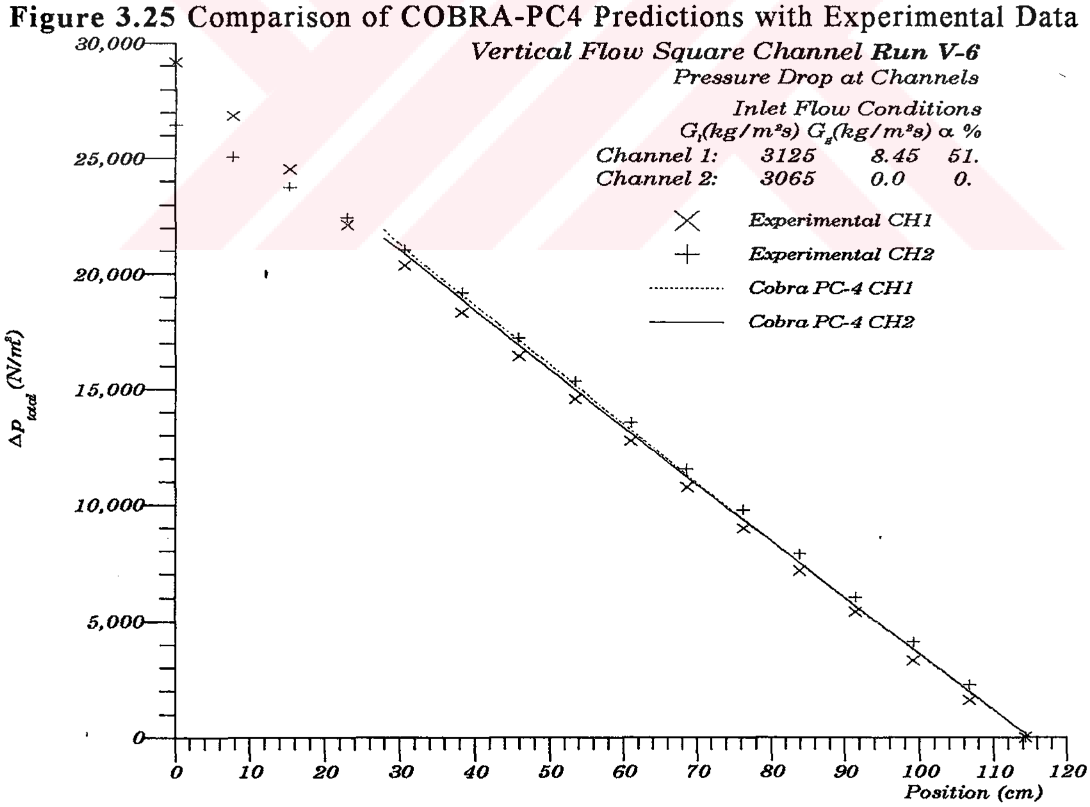

Figure 3.26 Comparison of COBRA-PC4 Predictions with Experimental Data

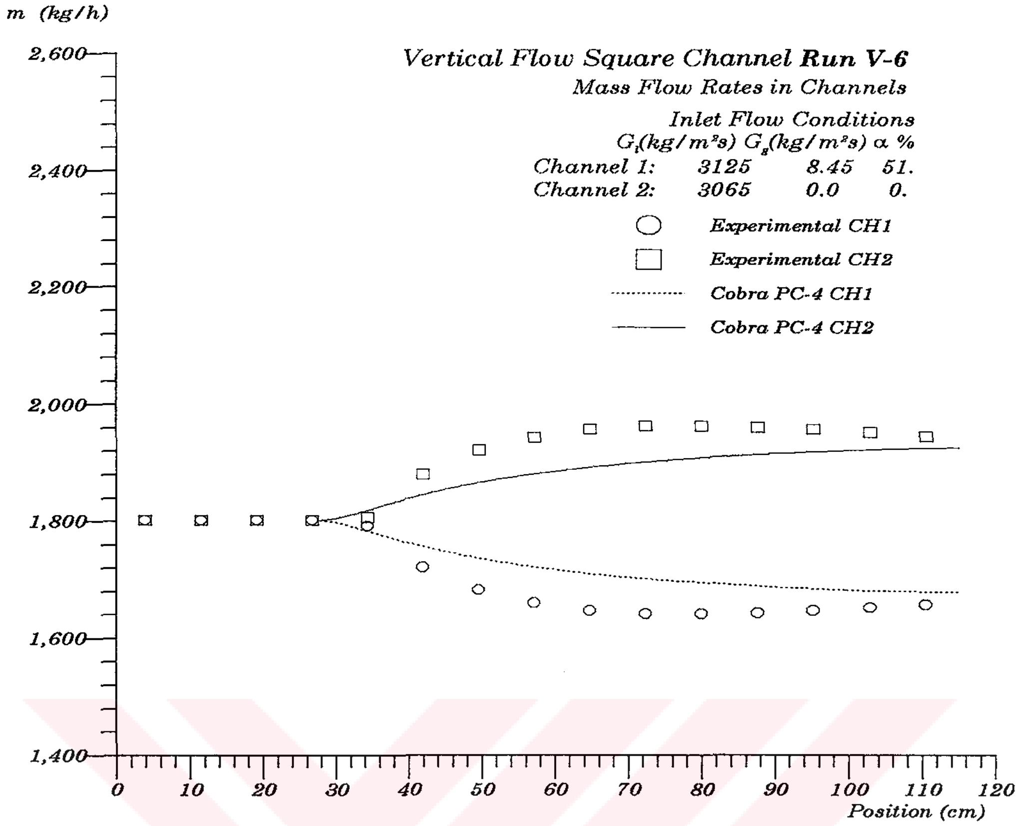

Figure 3.27 Comparison of COBRA-PC4 Predictions with Experimental Data

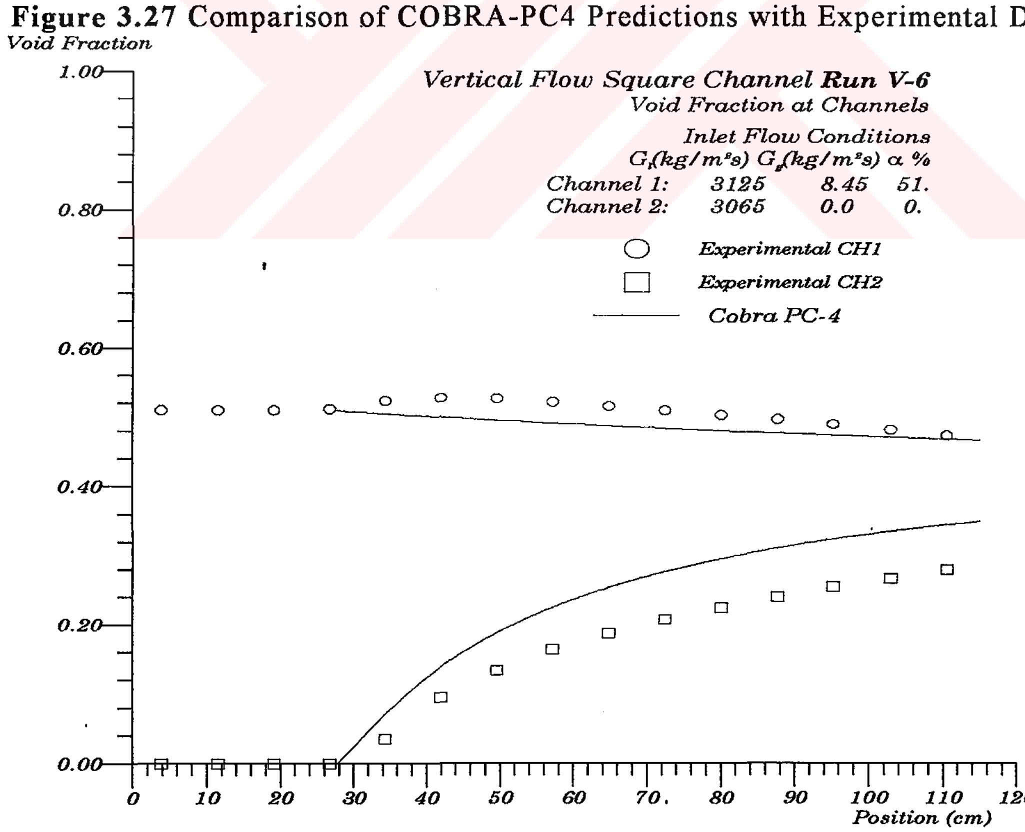

Figure 3.28 Comparison of COBRA-PC4 Predictions with Experimental Data

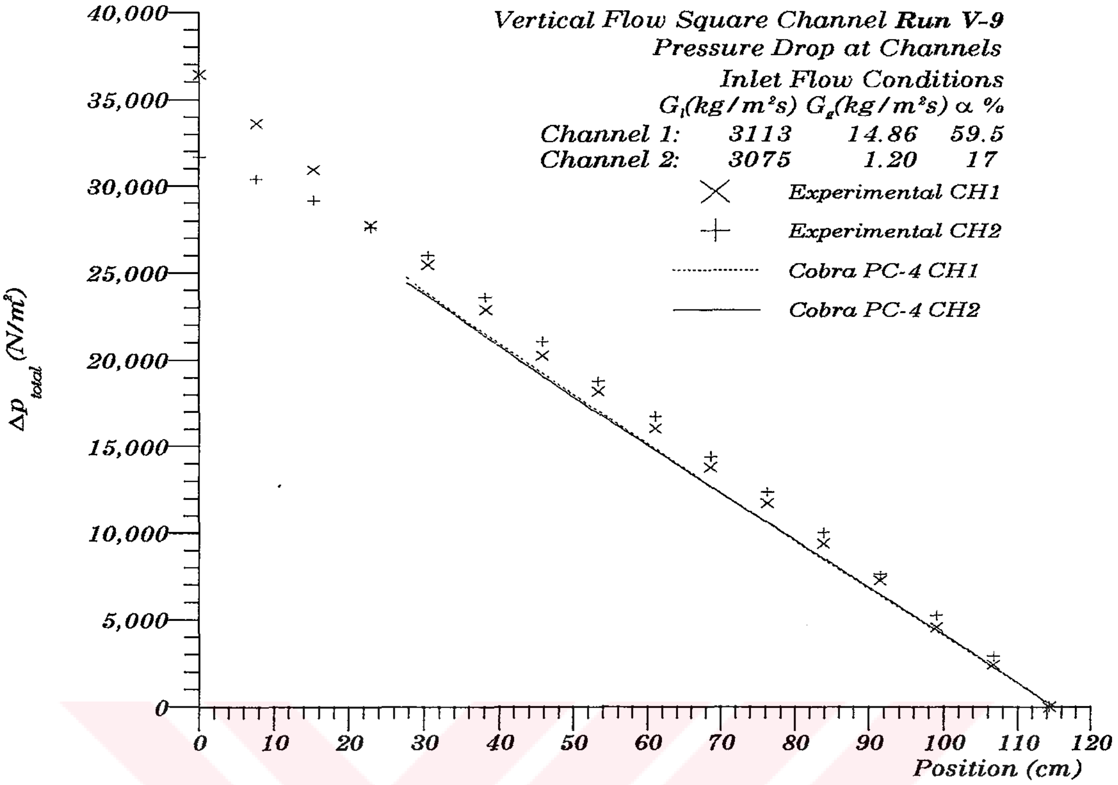

Figure 3.29 Comparison of COBRA-PC4 Predictions with Experimental Data

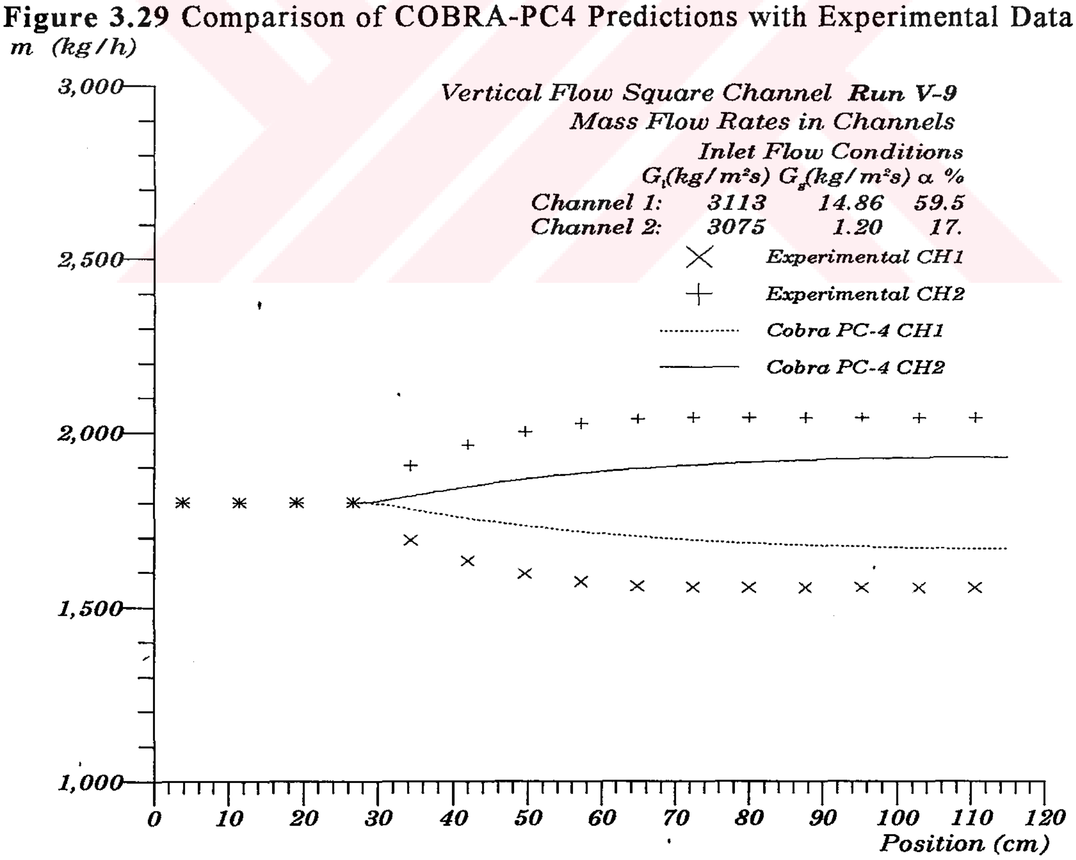

Figure 3.30 Comparison of COBRA-PC4 Predictions with Experimental Data

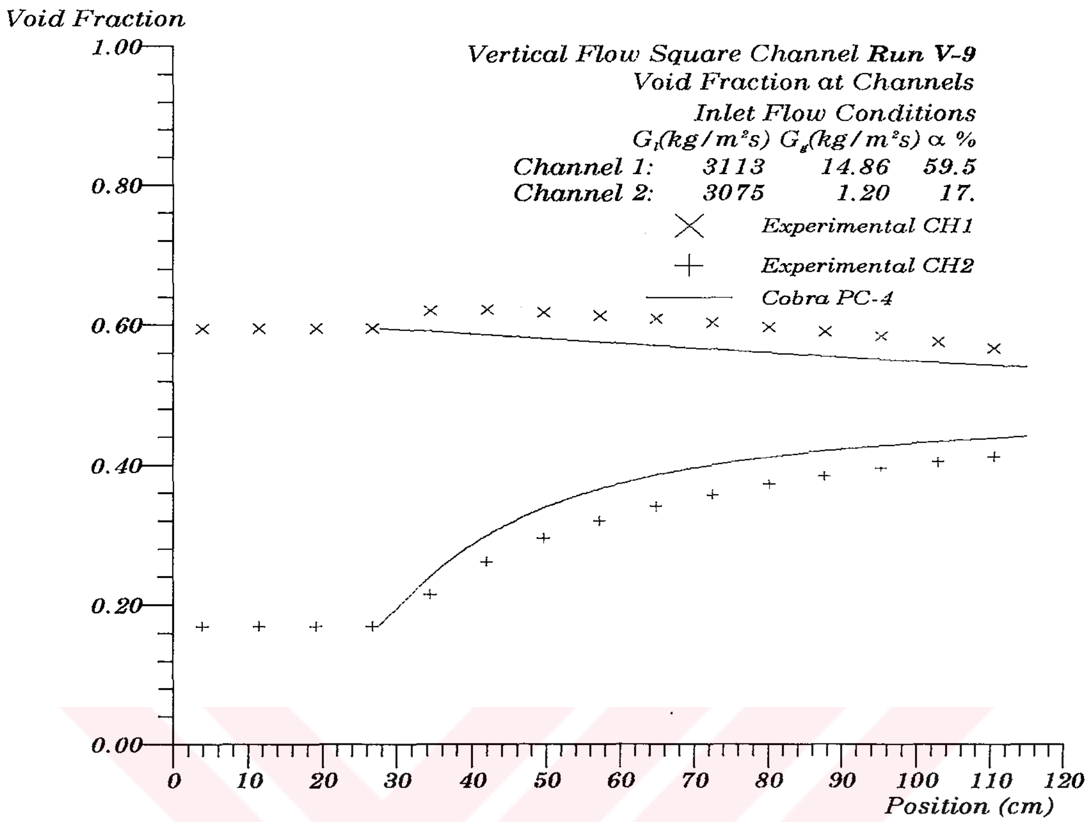

Figure 3.31 Comparison of COBRA-PC4 Predictions with Experimental Data

3.4 Two Phase Flow With Blockage

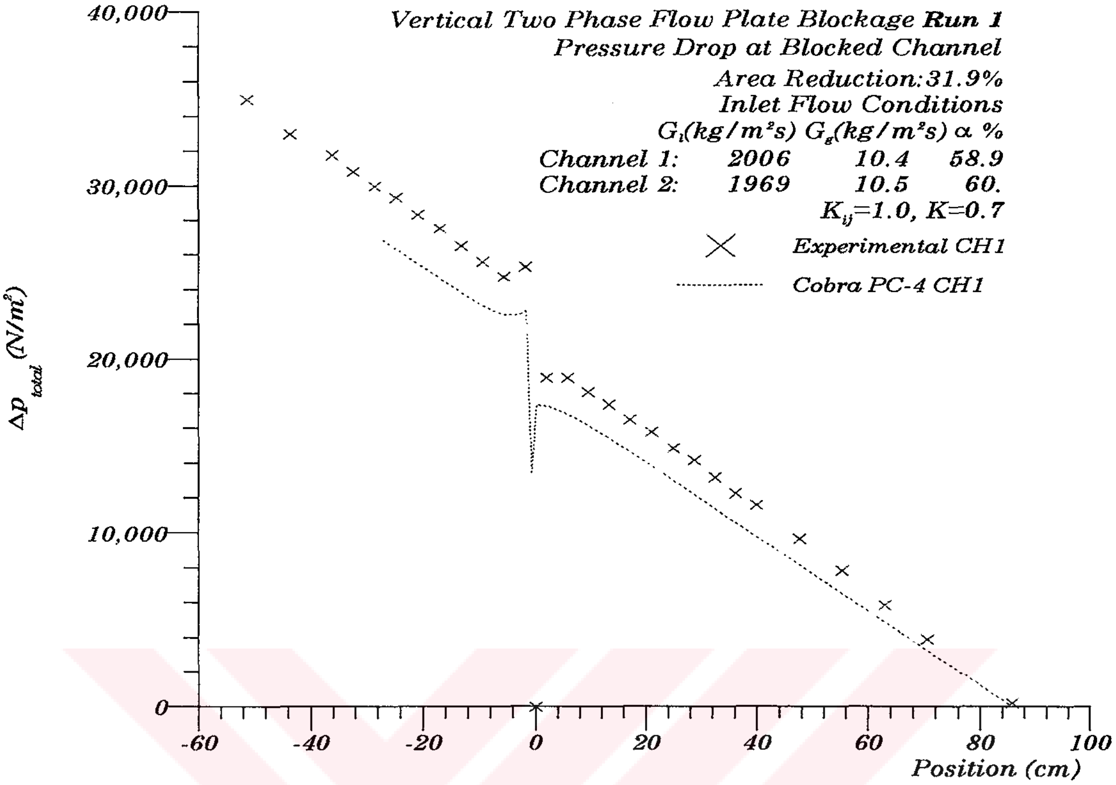

Figure 3.32 Comparison of COBRA-PC4 Predictions with Experimental Data

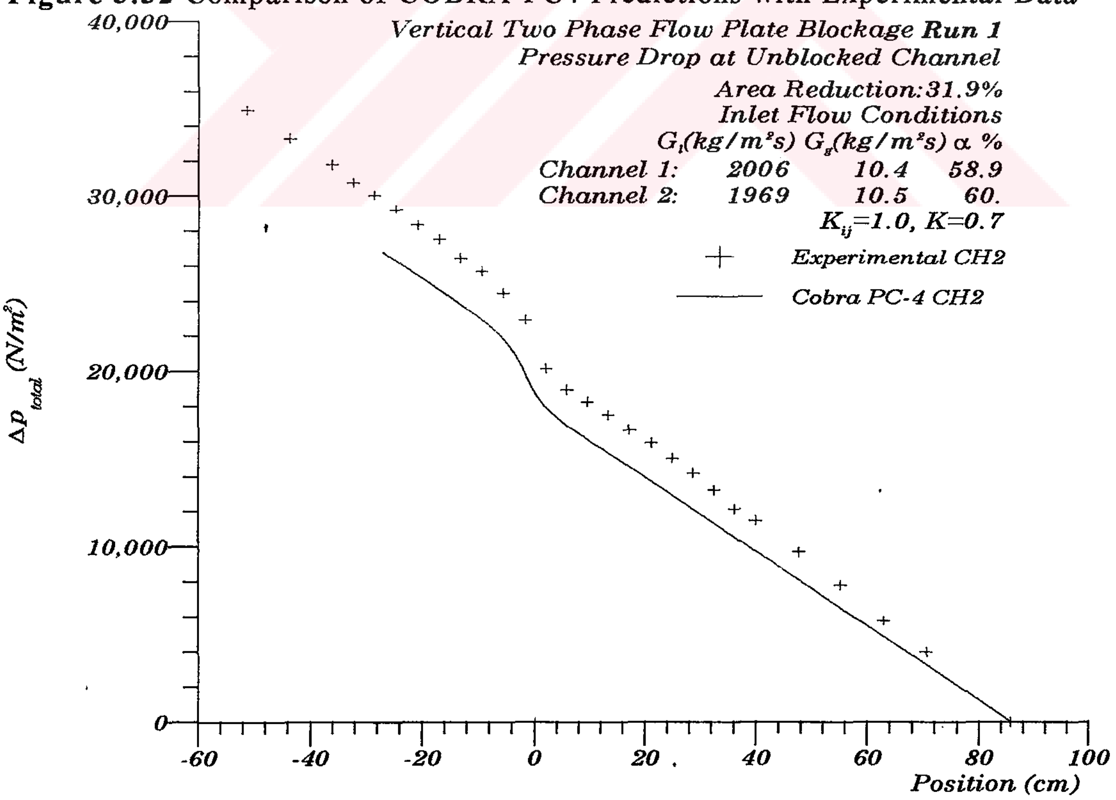

Figure 3.33 Comparison of COBRA-PC4 Predictions with Experimental Data

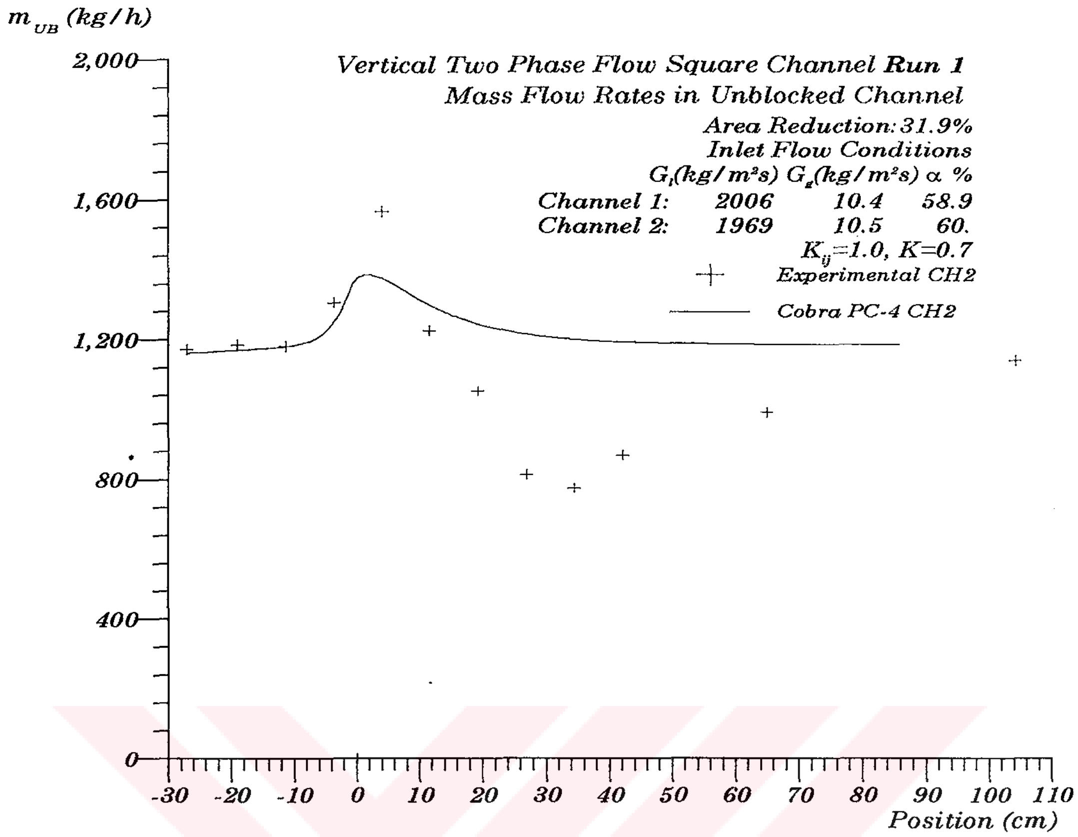

Figure 3.34 Comparison of COBRA-PC4 Predictions with Experimental Data

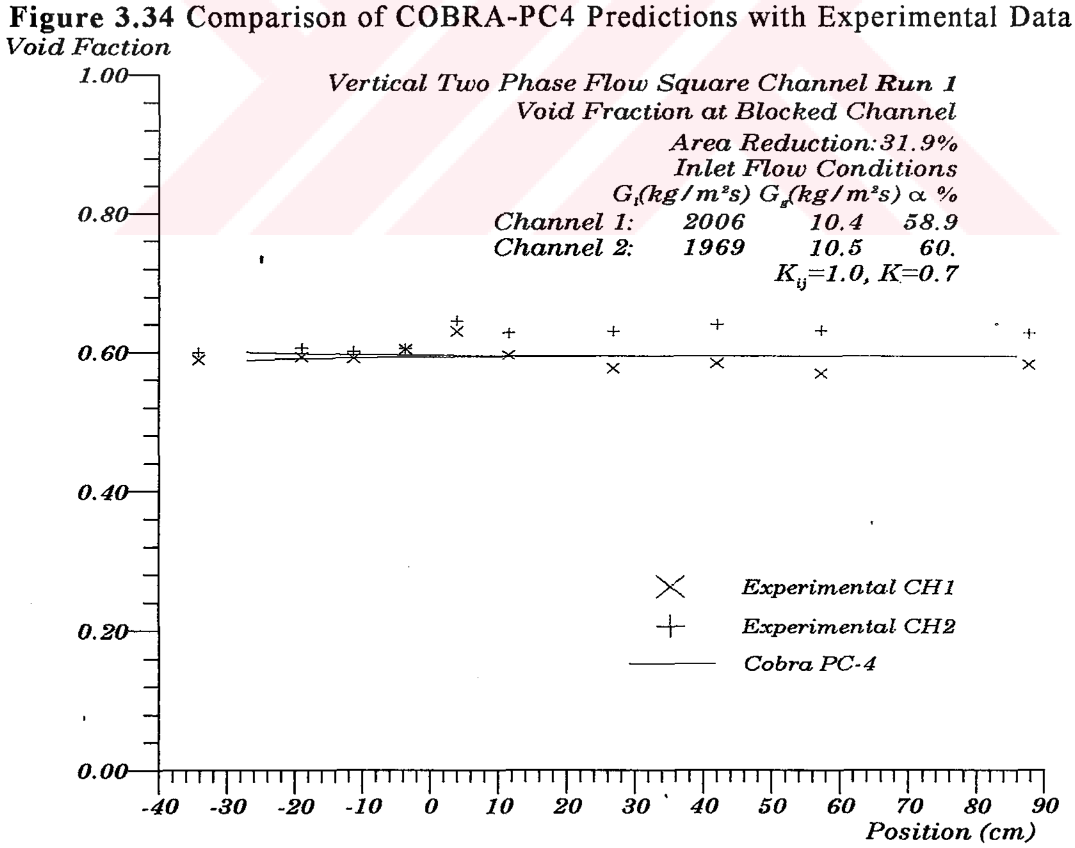

Figure 3.35 Comparison of COBRA-PC4 Predictions with Experimental Data

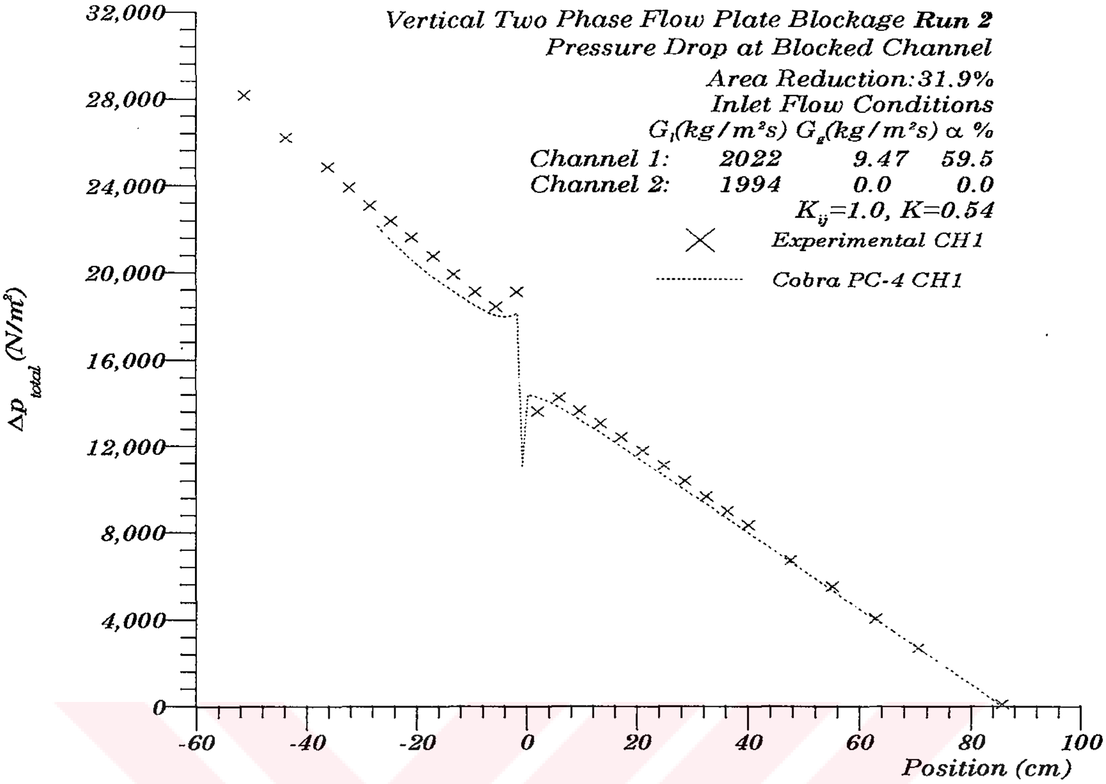

Figure 3.36 Comparison of COBRA-PC4 Predictions with Experimental Data

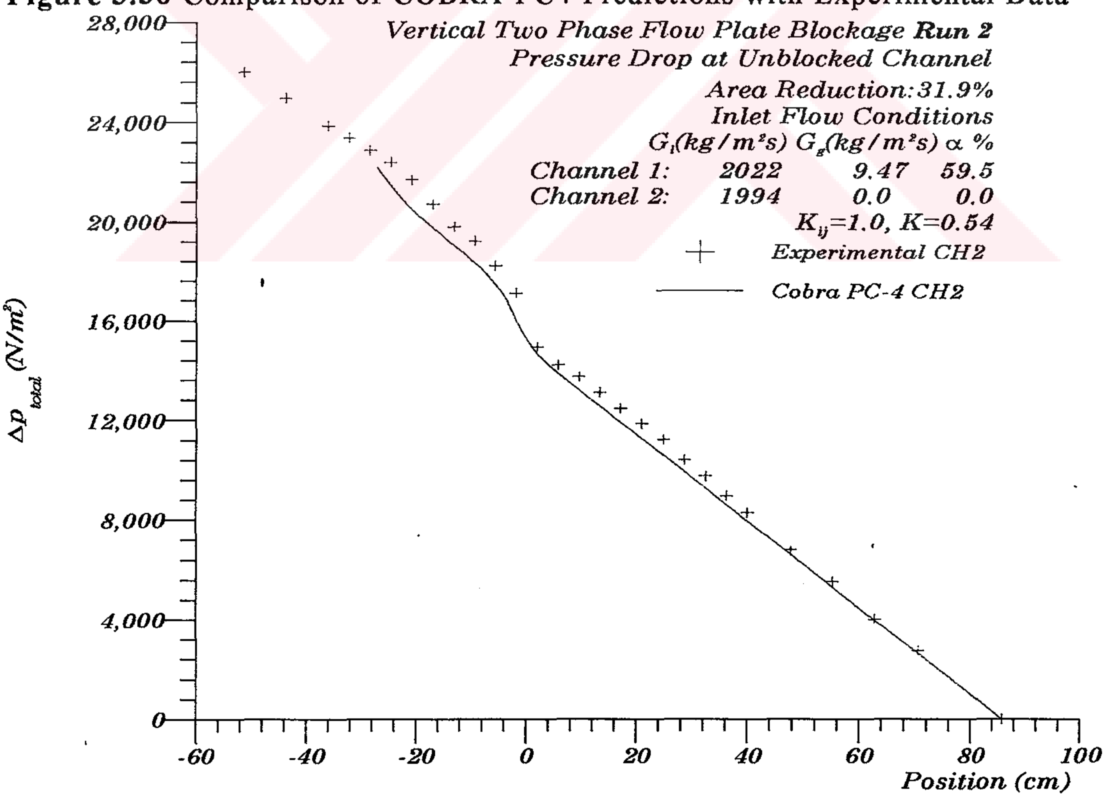

Figure 3.37 Comparison of COBRA-PC4 Predictions with Experimental Data

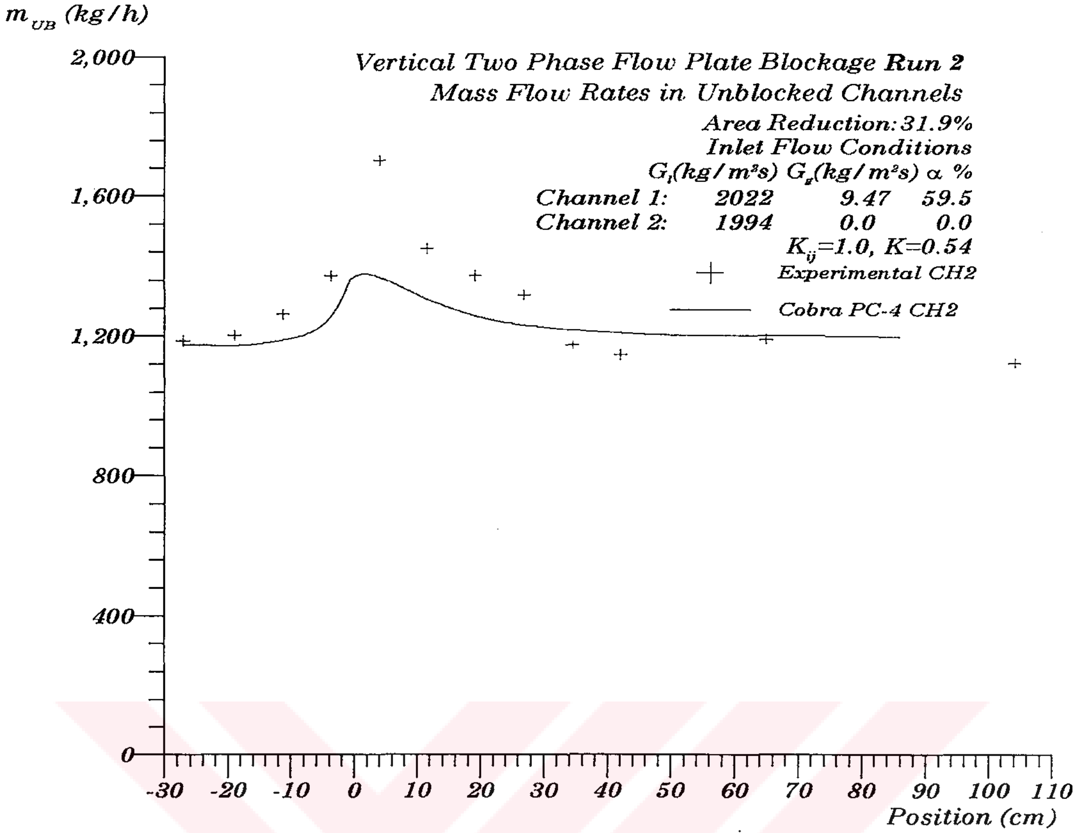

Figure 3.38 Comparison of COBRA-PC4 Predictions with Experimental Data

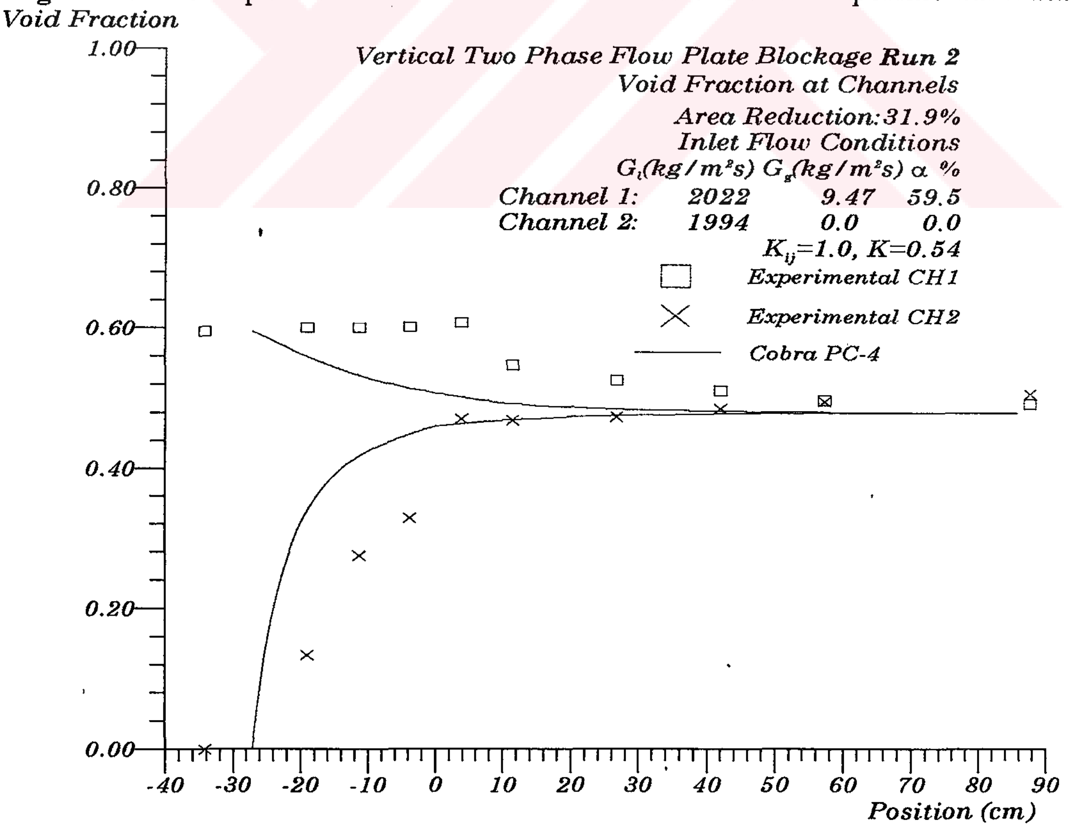

Figure 3.39 Comparison of COBRA-PC4 Predictions with Experimental Data

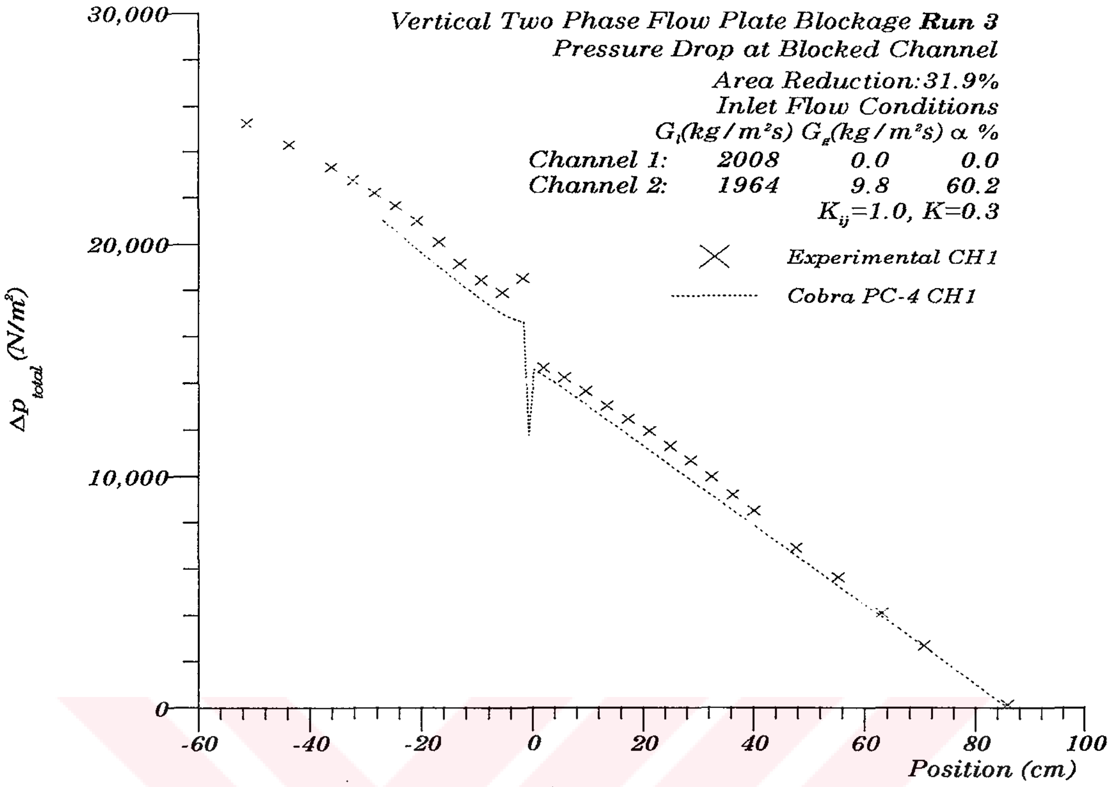

Figure 3.40 Comparison of COBRA-PC4 Predictions with Experimental Data

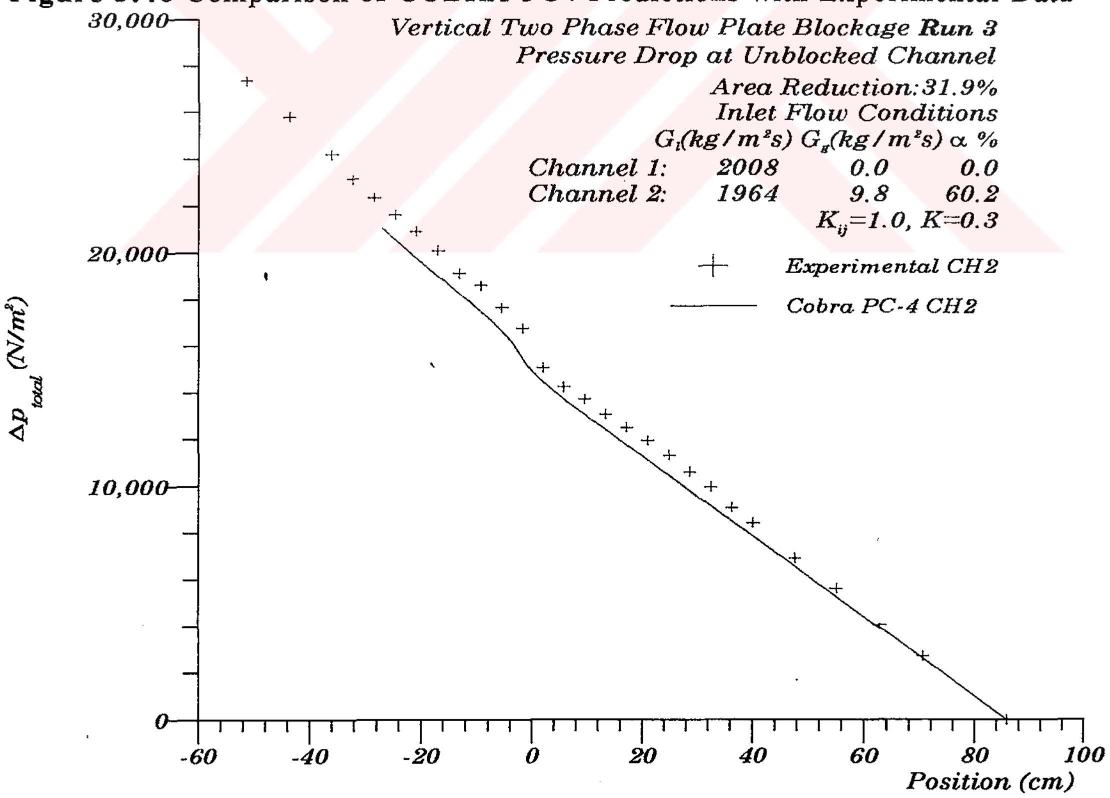

Figure 3.41 Comparison of COBRA-PC4 Predictions with Experimental Data

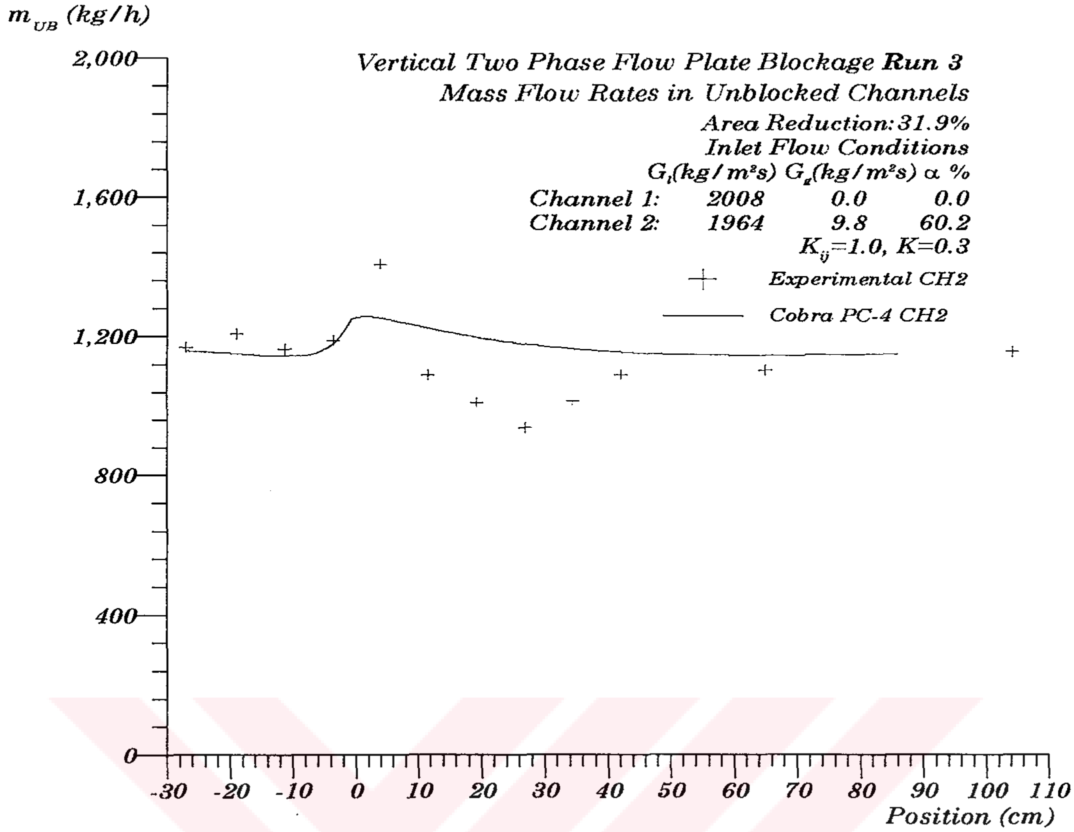

Figure 3.42 Comparison of COBRA-PC4 Predictions with Experimental Data

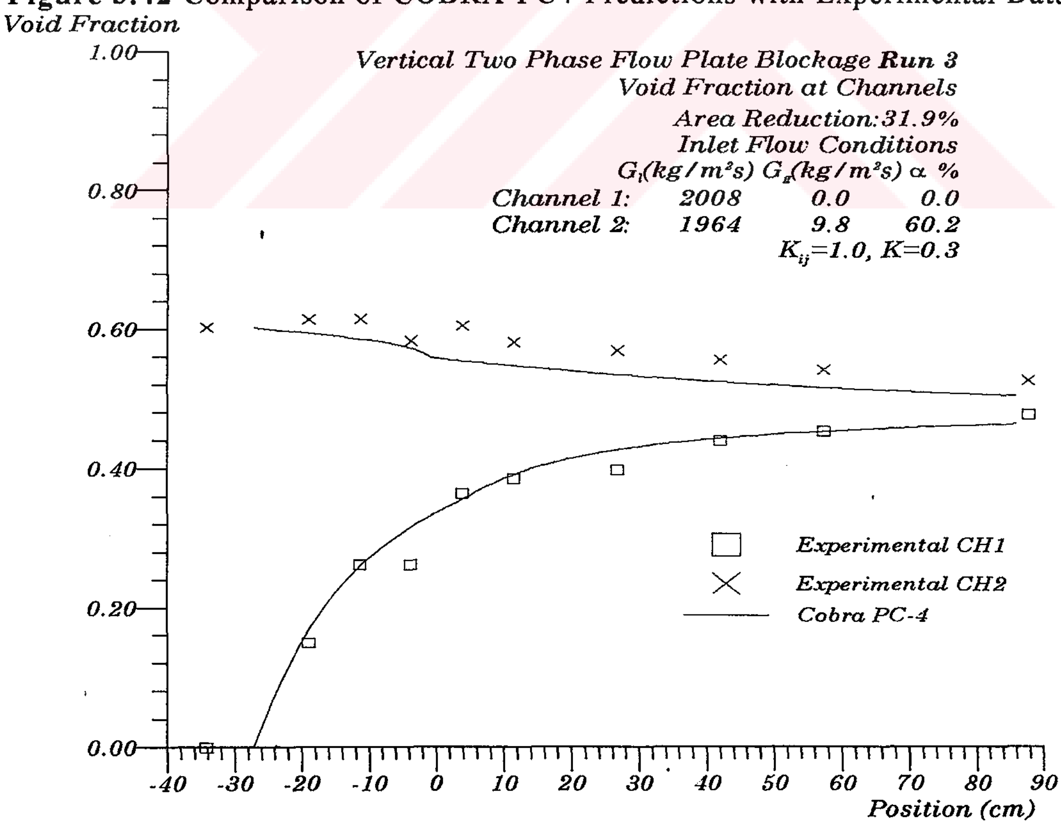

Figure 3.43 Comparison of COBRA-PC4 Predictions with Experimental Data

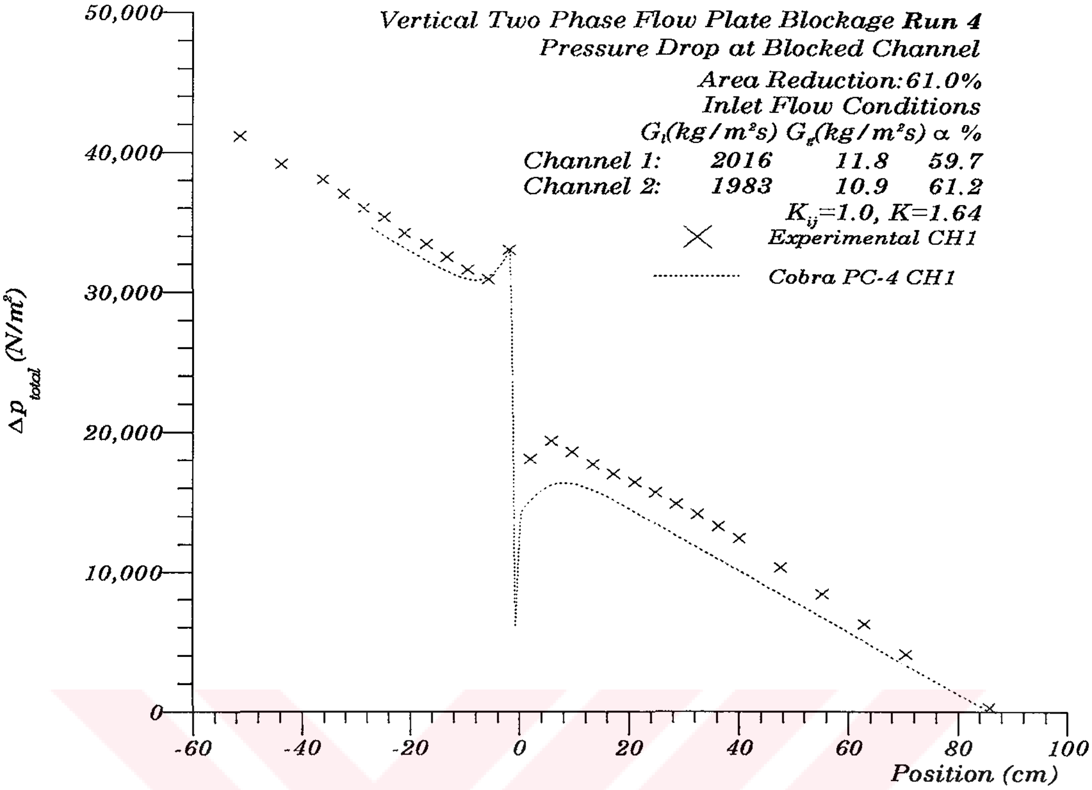

Figure 3.44 Comparison of COBRA-PC4 Predictions with Experimental Data

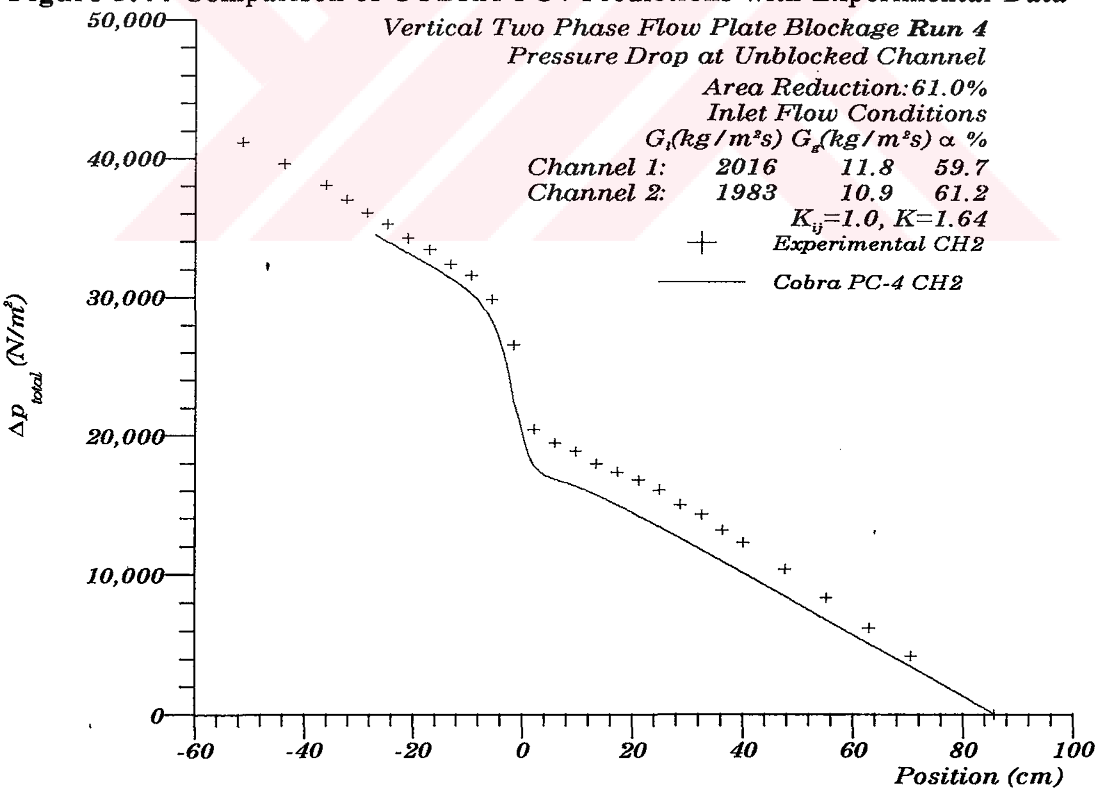

Figure 3.45 Comparison of COBRA-PC4 Predictions with Experimental Data

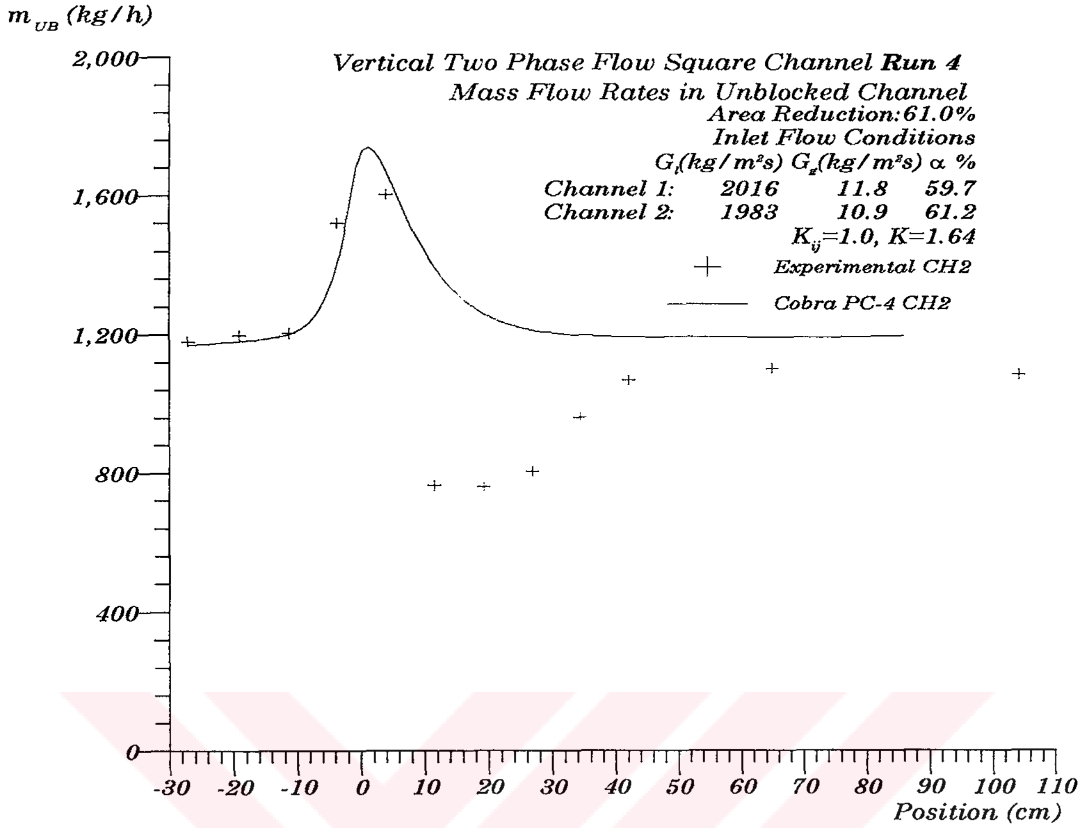

Figure 3.46 Comparison of COBRA-PC4 Predictions with Experimental Data

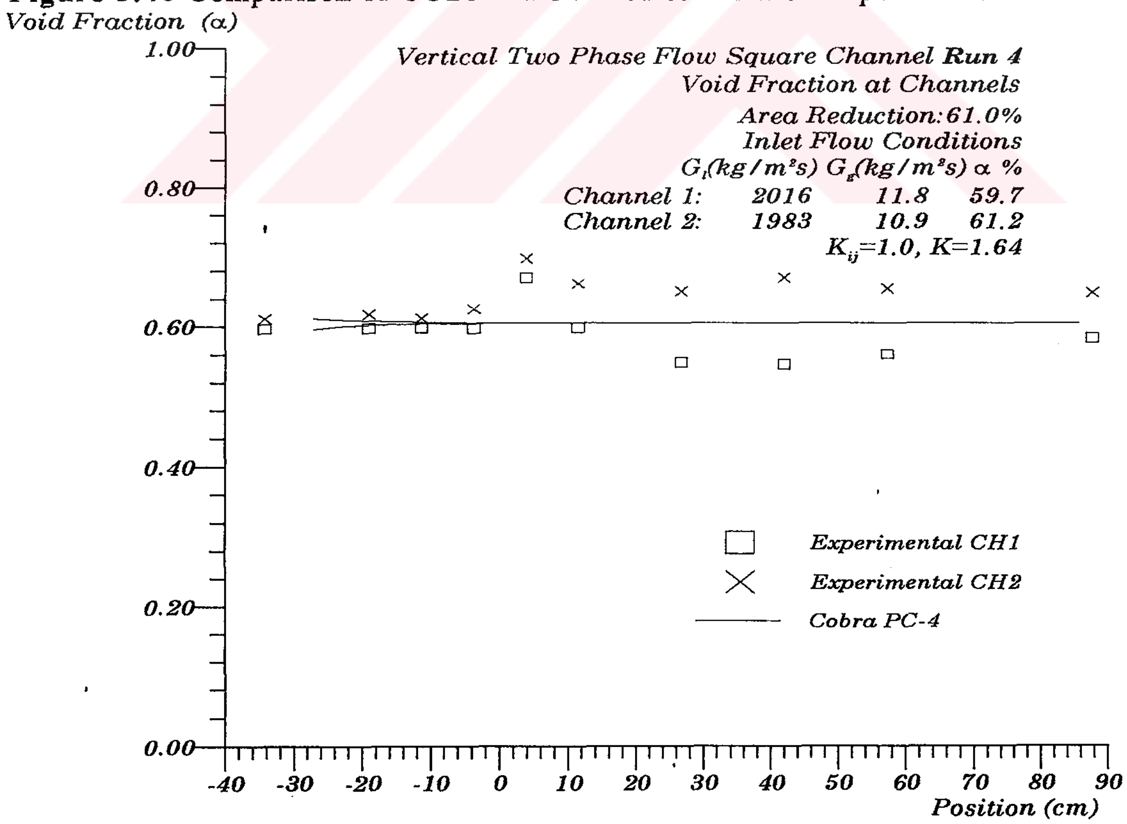

Figure 3.47 Comparison of COBRA-PC4 Predictions with Experimental Data

3.5 COBRA-IV-I Results

To show the consistency of the COBRA-PC-4 and COBRA-IV-I some of the results of COBRA-IIIC are given below [1,3]

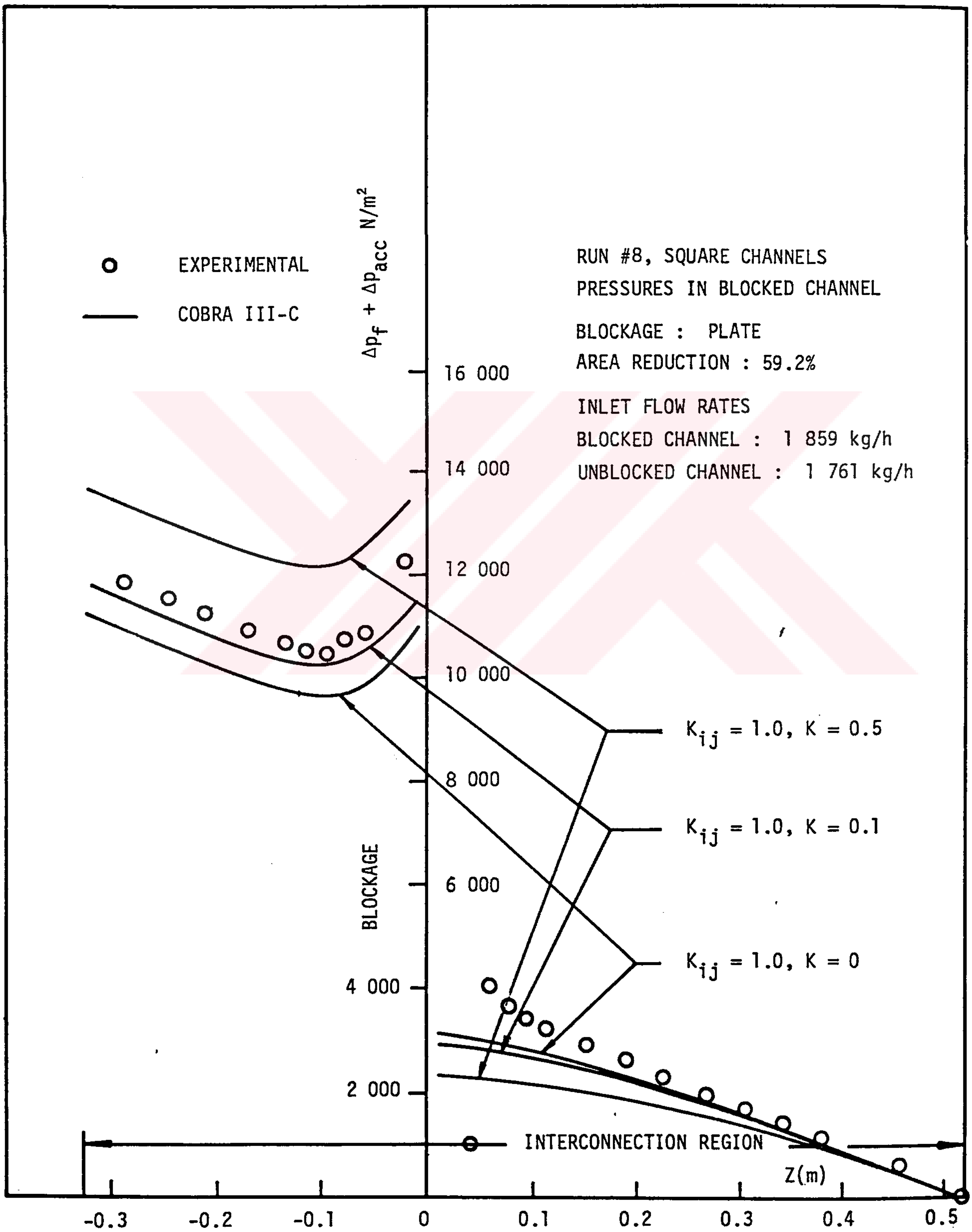

Figure 3.48 Single Phase with Plate Blockage Run#8

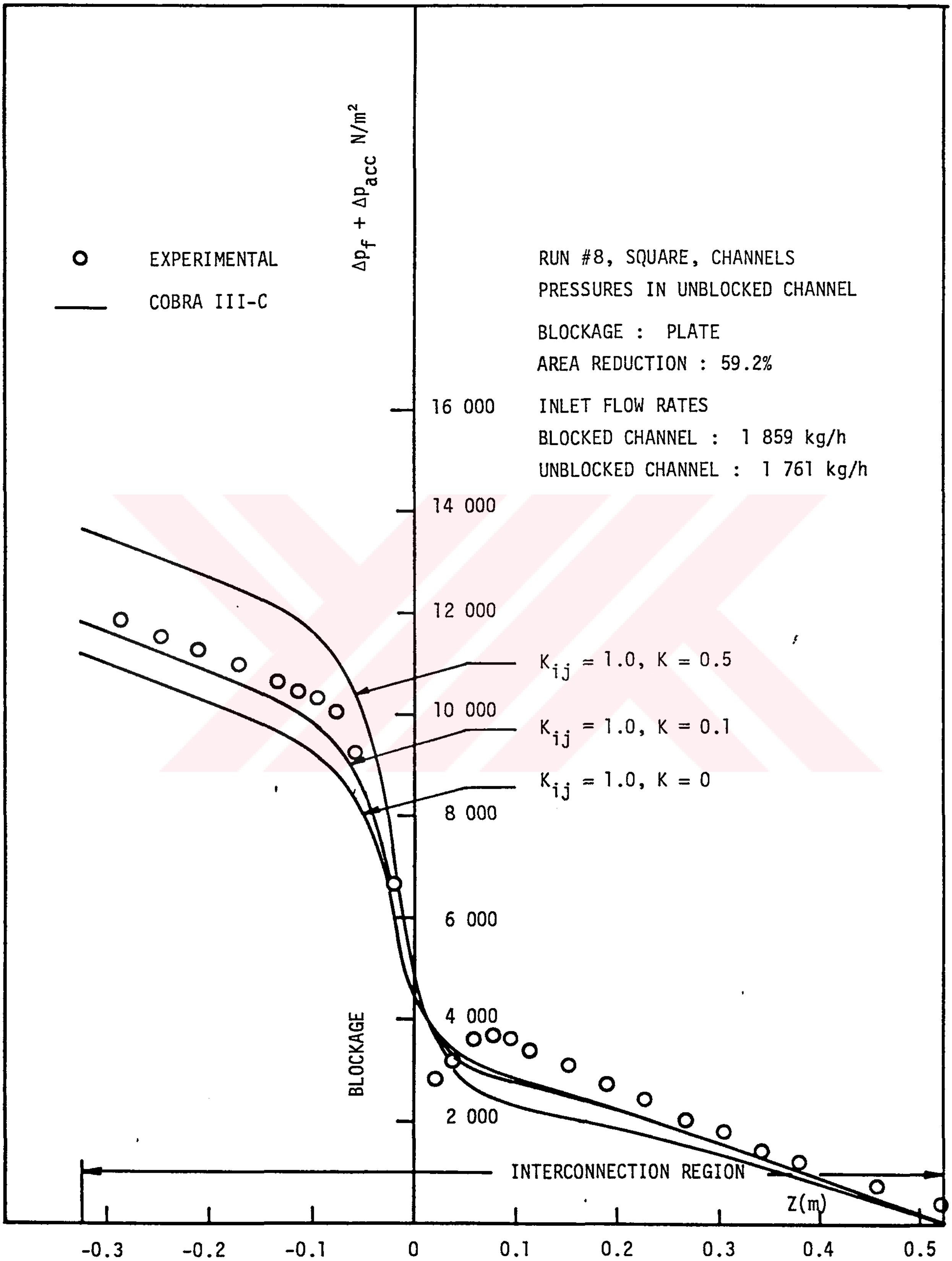

Figure 3.49 Single Phase with Plate Blockage Run#8

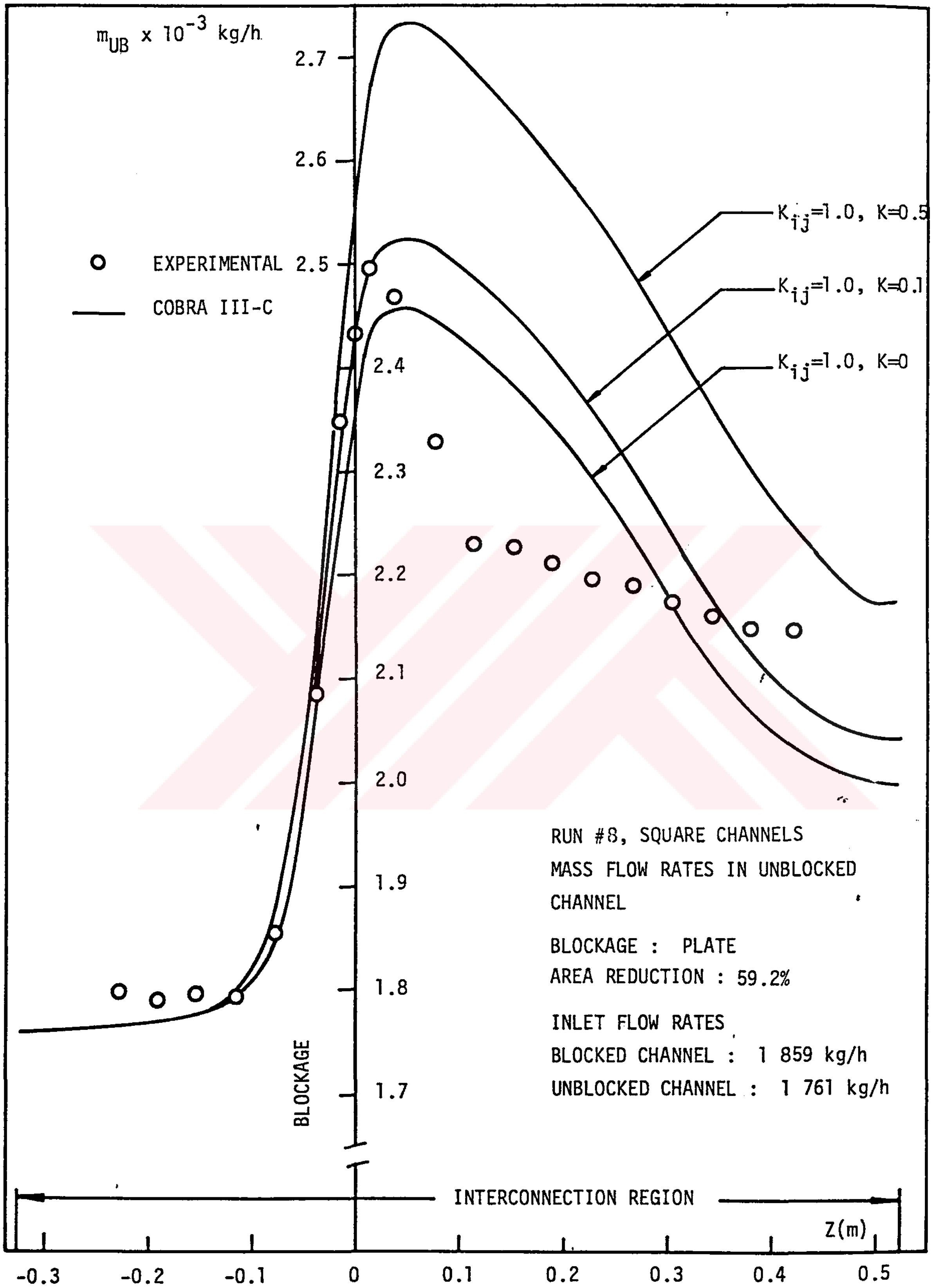

Figure 3.50 Single Phase with Plate Blockage Run#8

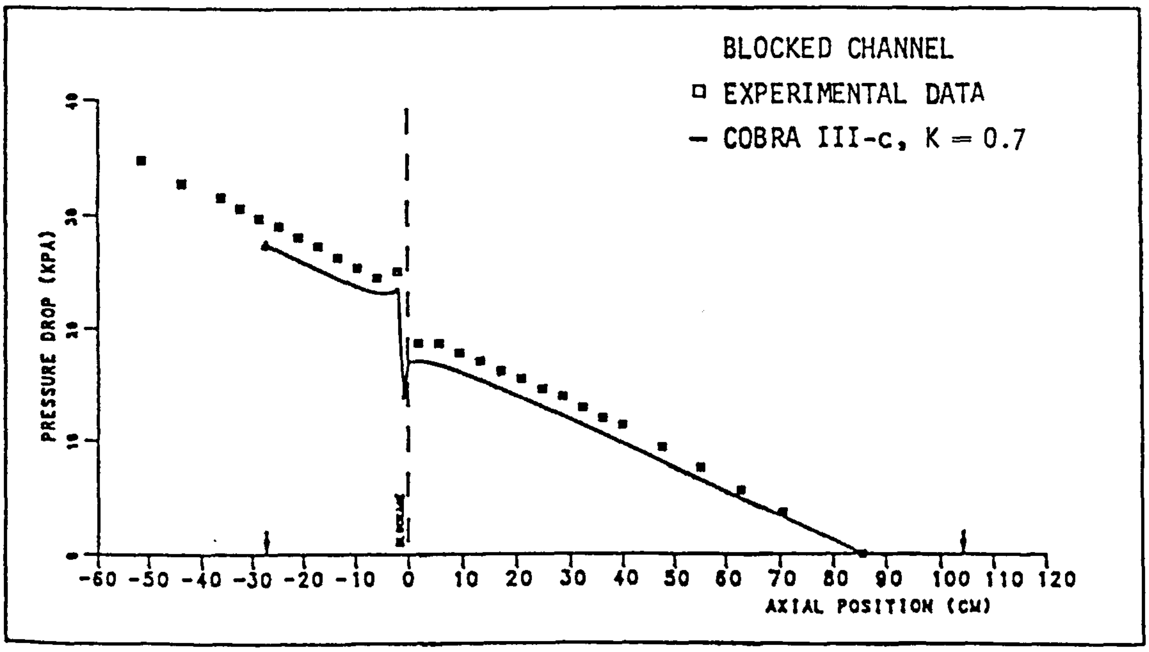

Figure 3.51 Two Phase with Plate Blockage Run#1

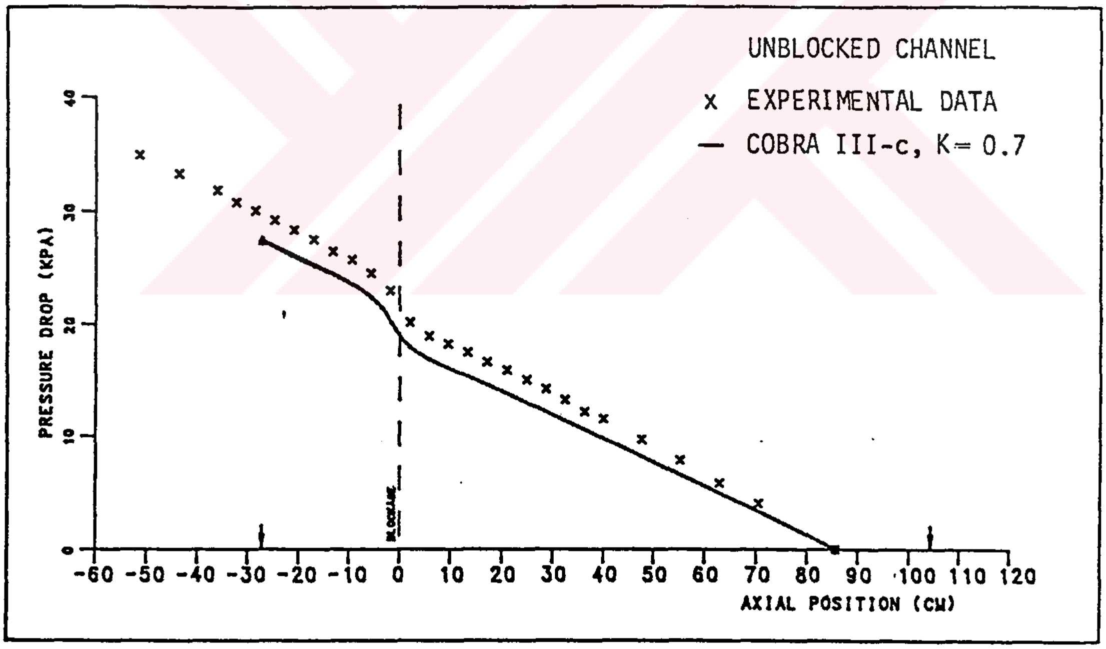

Figure 3.52 Two Phase with Plate Blockage Run#1

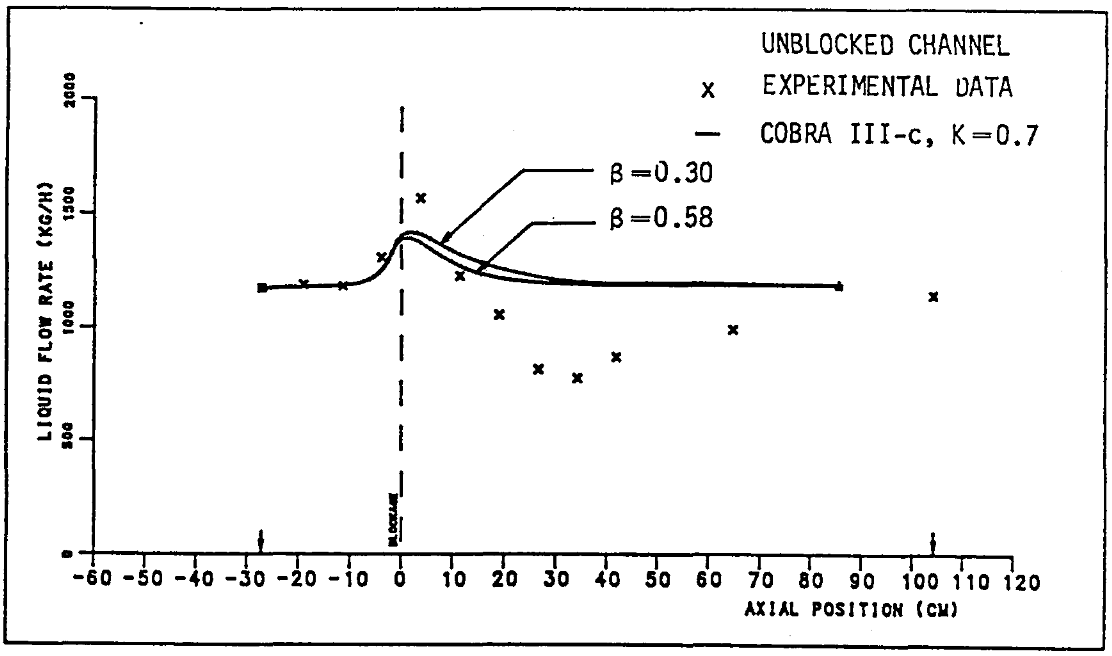

Figure 3.53 Two Phase with Plate Blockage Run#1

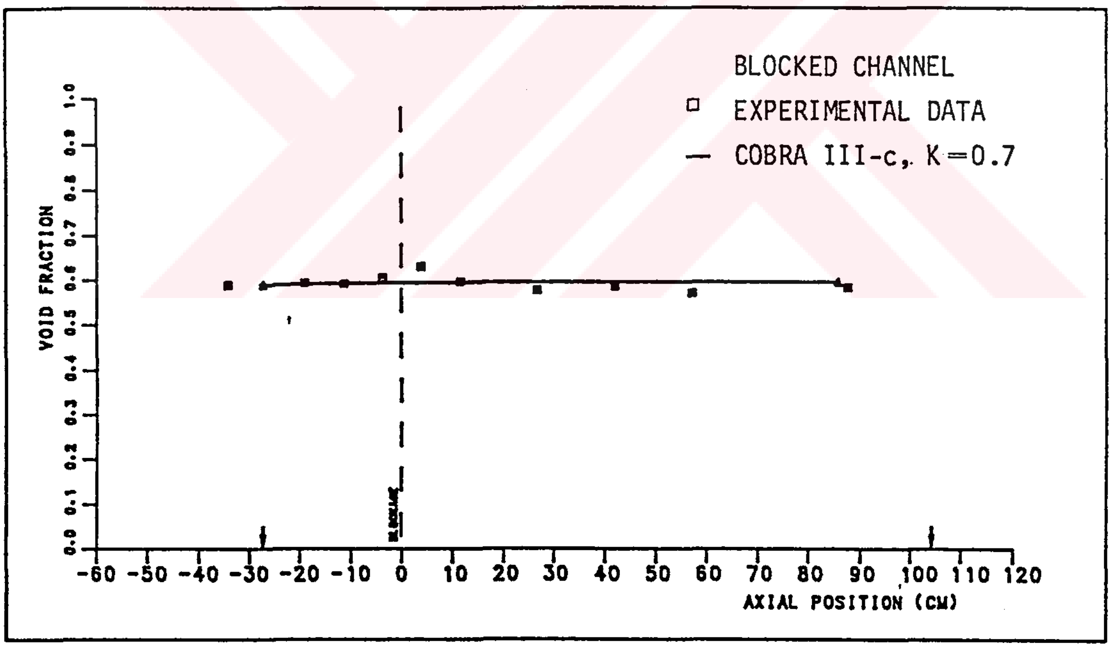

Figure 3.54 Two Phase with Plate Blockage Run#1

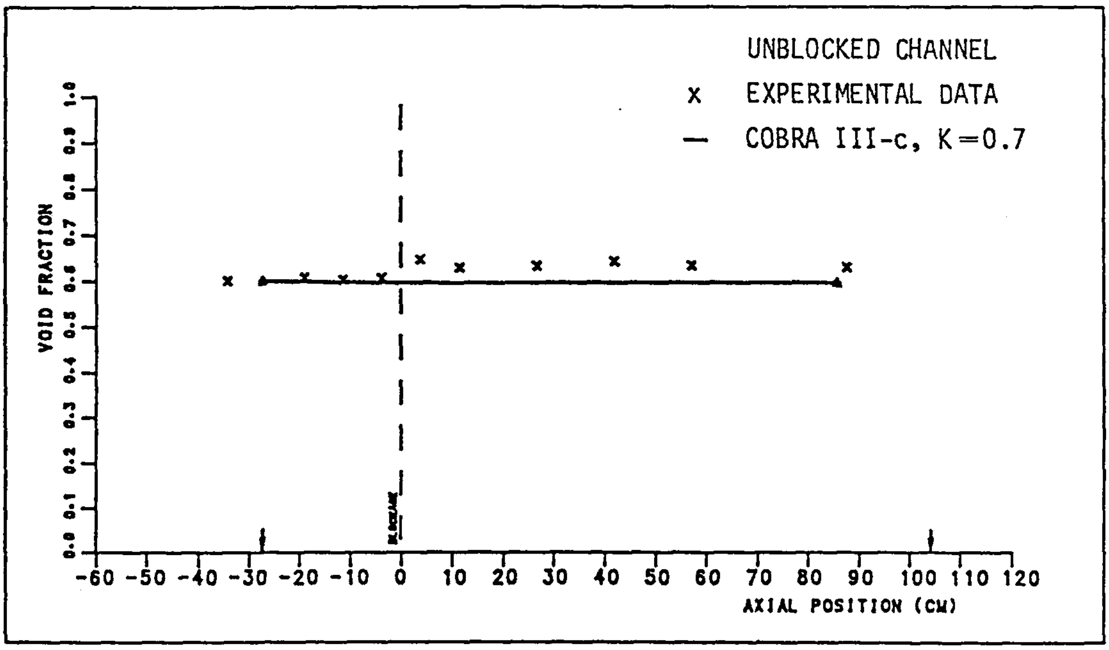

Figure 3.55 Two Phase with Plate Blockage Run#1

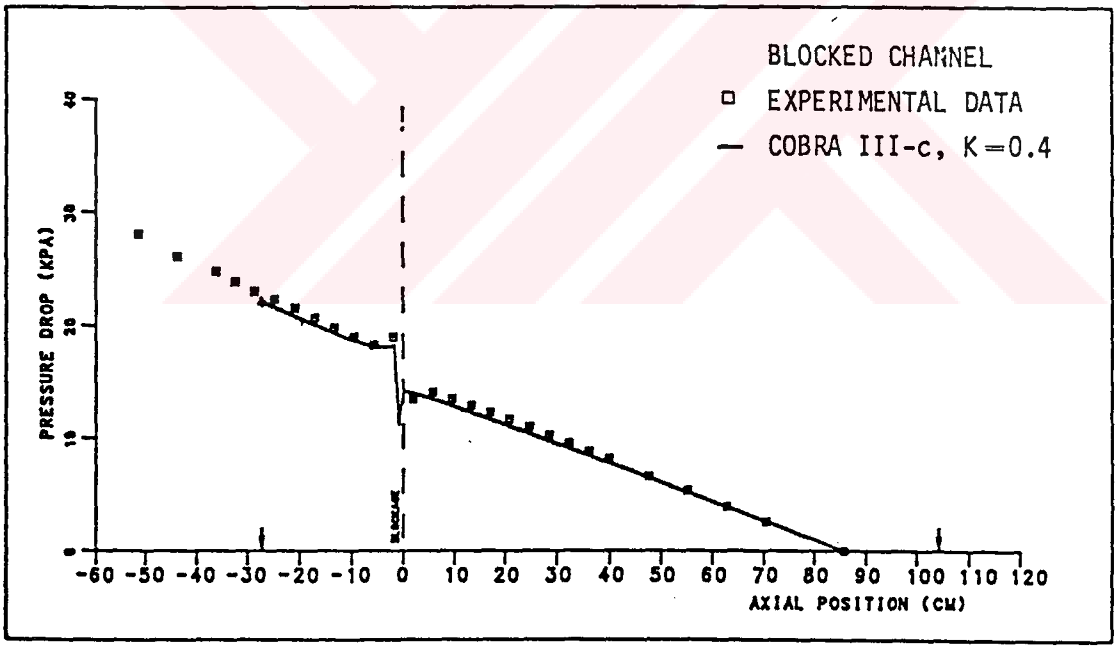

Figure 3.56 Two Phase with Plate Blockage Run#2

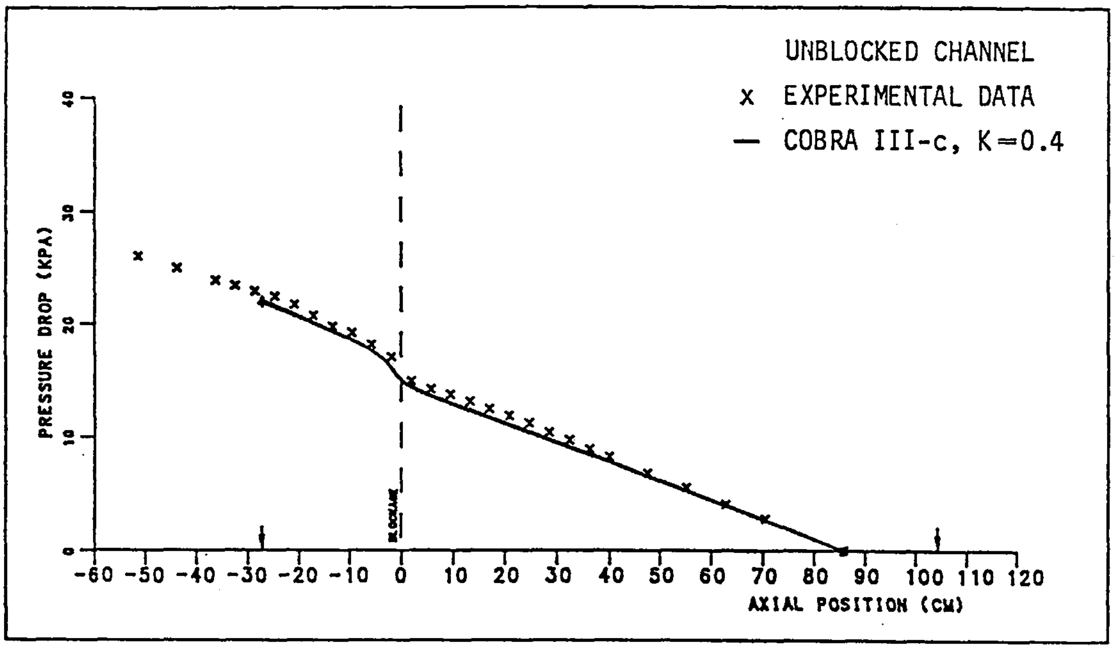

Figure 3.57 Two Phase with Plate Blockage Run#2

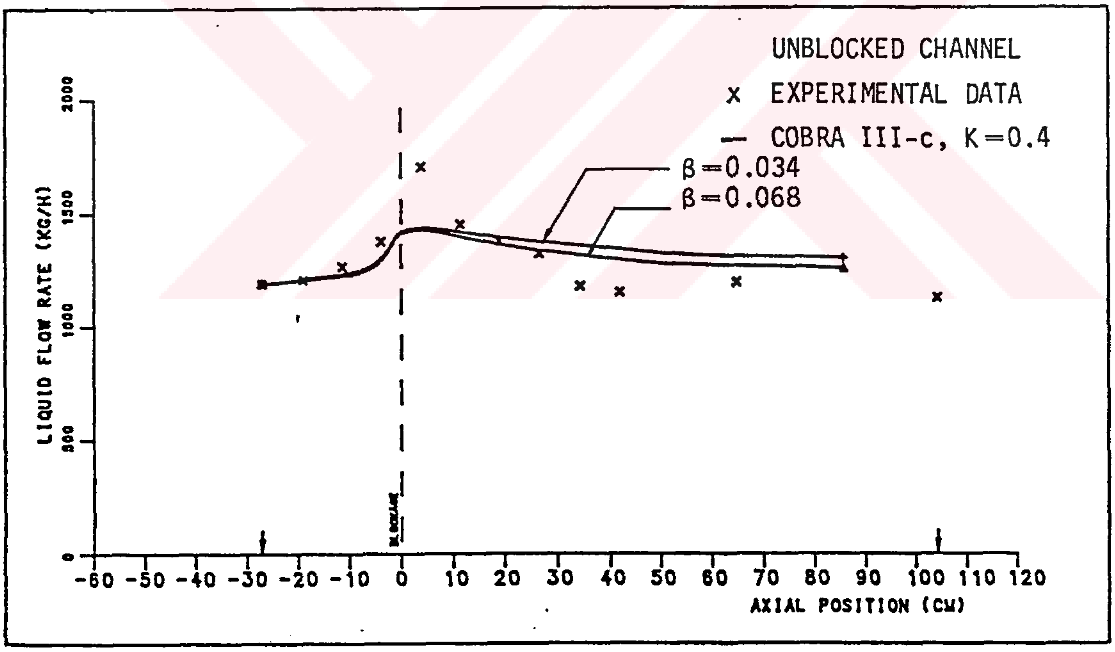

Figure 3.58 Two Phase with Plate Blockage Run#2

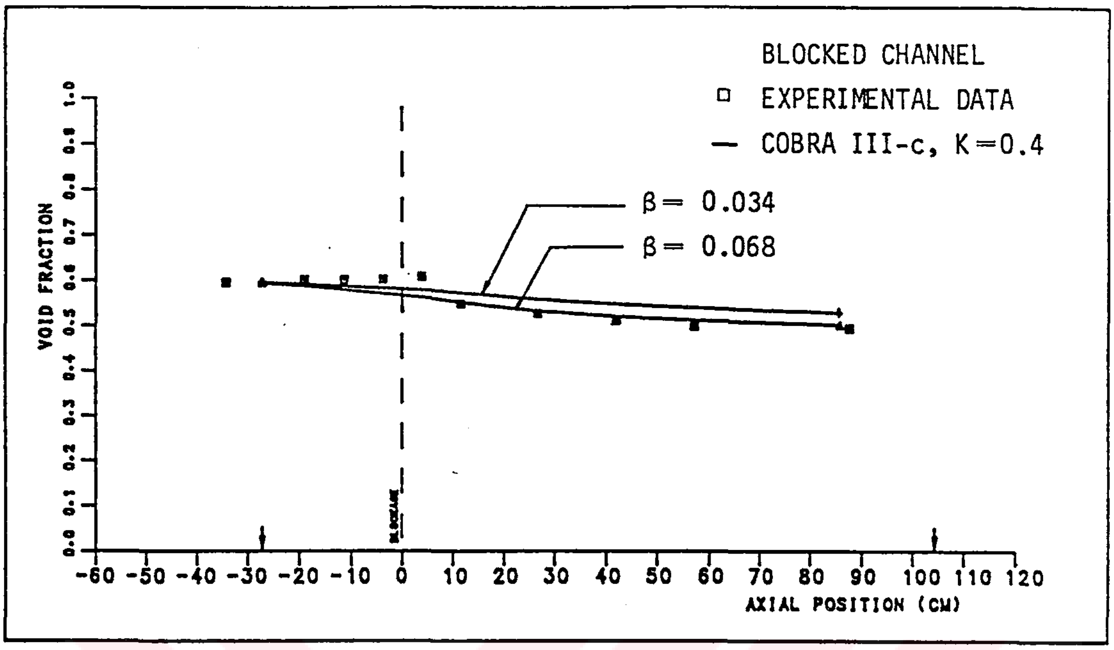

Figure 3.59 Two Phase with Plate Blockage Run#2

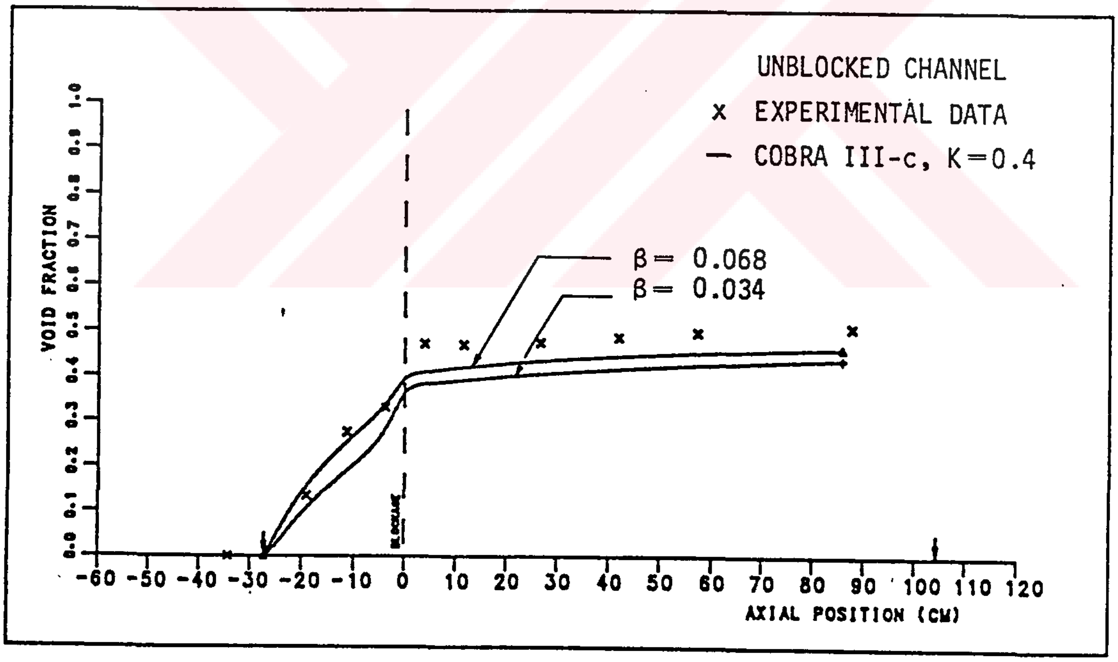

Figure 3.60 Two Phase with Plate Blockage Run#2

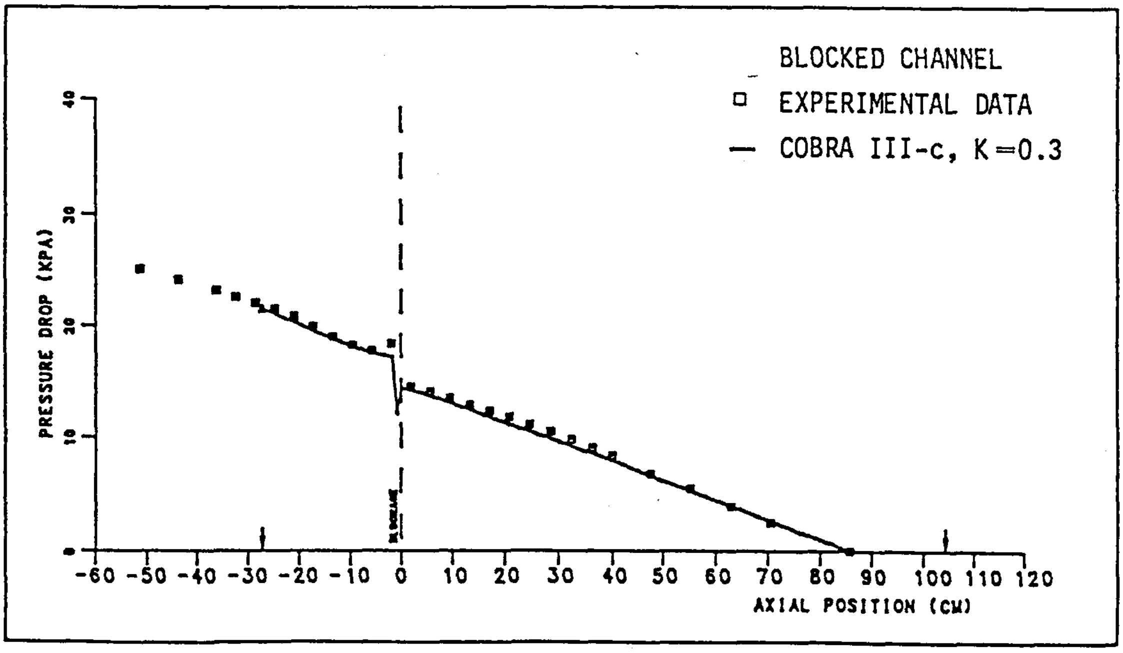

Figure 3.61 Two Phase with Plate Blockage Run#3

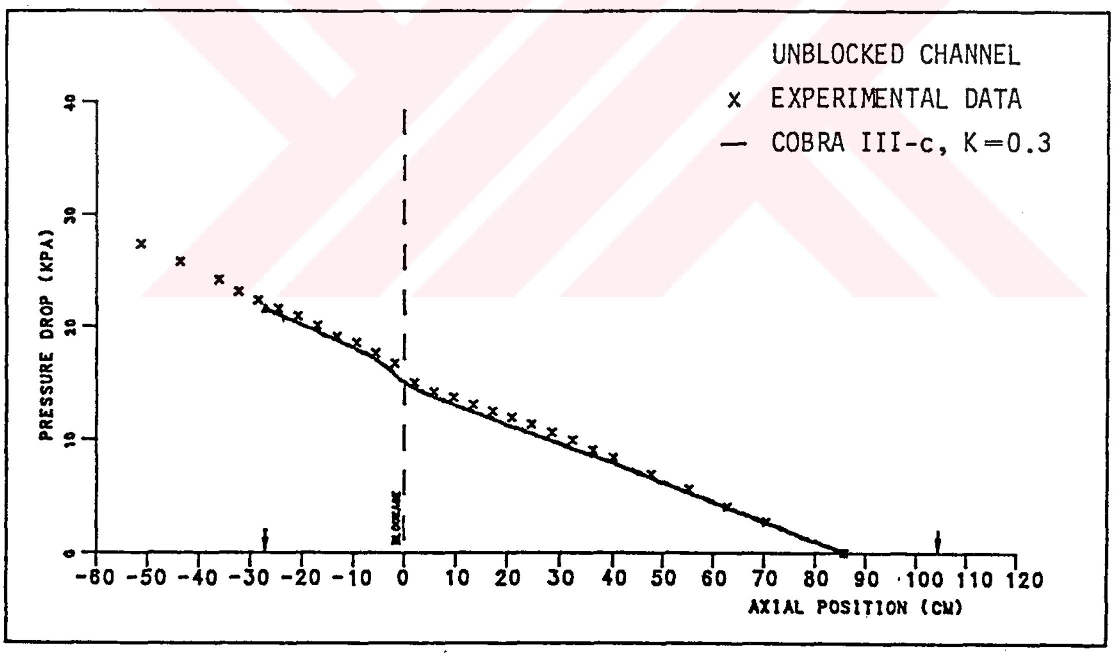

Figure 3.62 Two Phase with Plate Blockage Run#3

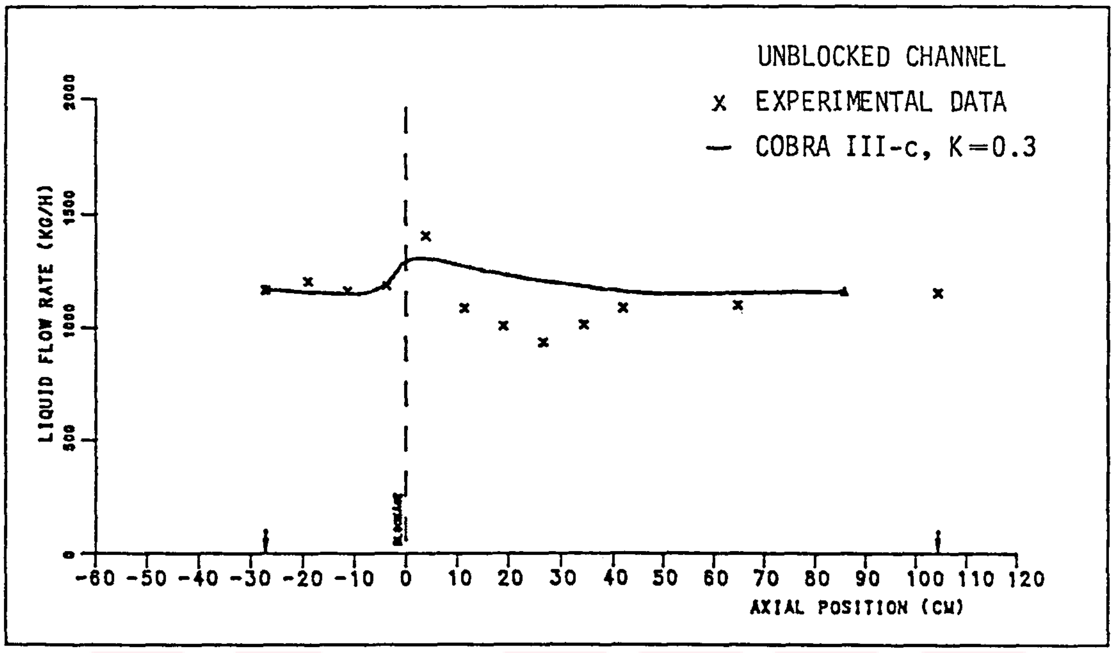

Figure 3.63 Two Phase with Plate Blockage Run#3

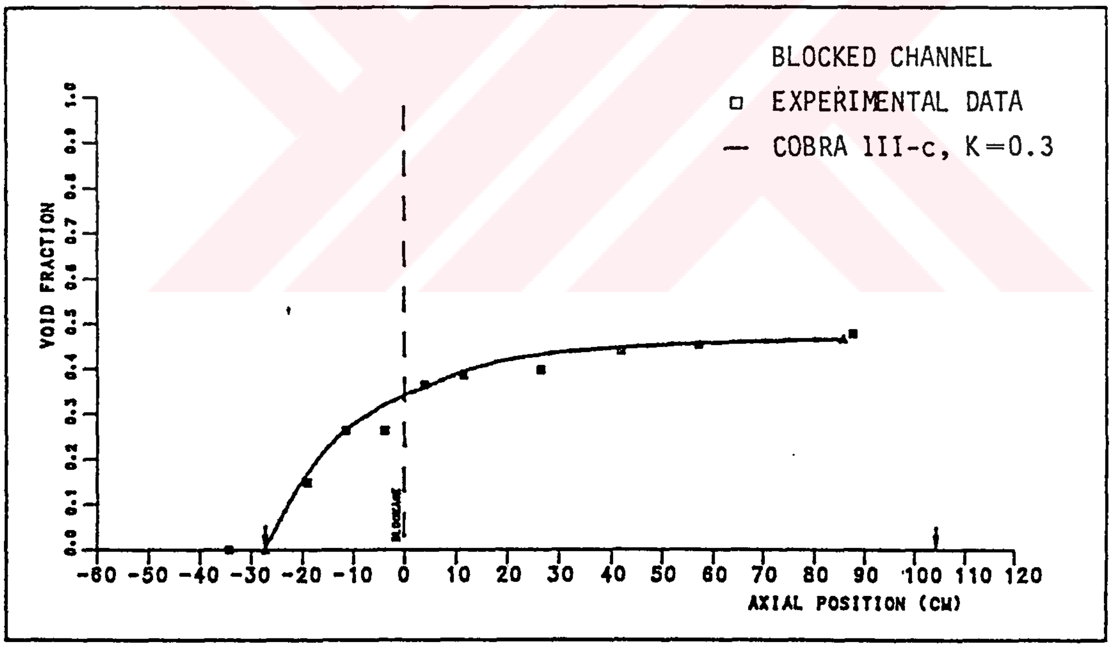

Figure 3.64 Two Phase with Plate Blockage Run#3

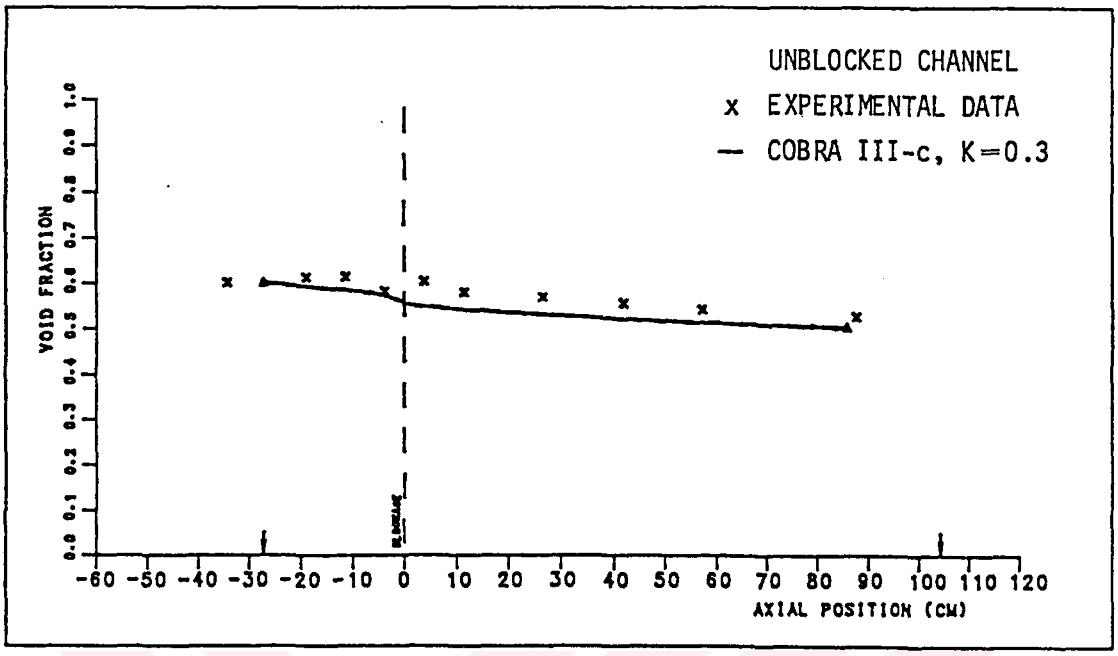

Figure 3.65 Two Phase with Plate Blockage Run#3

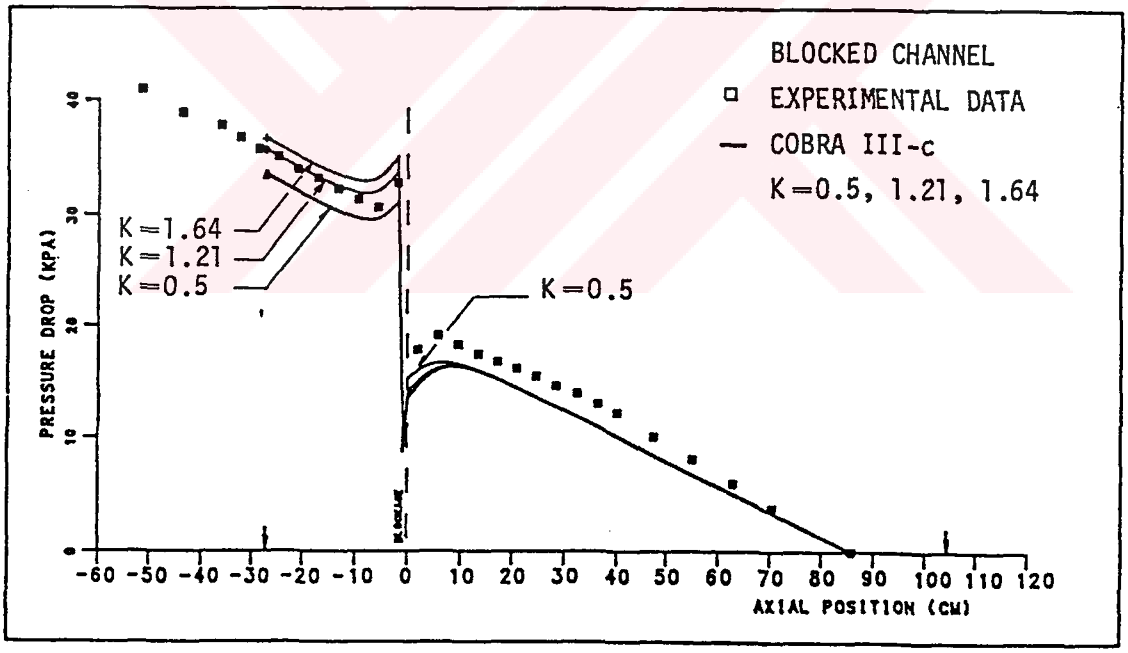

Figure 3.66 Two Phase with Plate Blockage Run#4

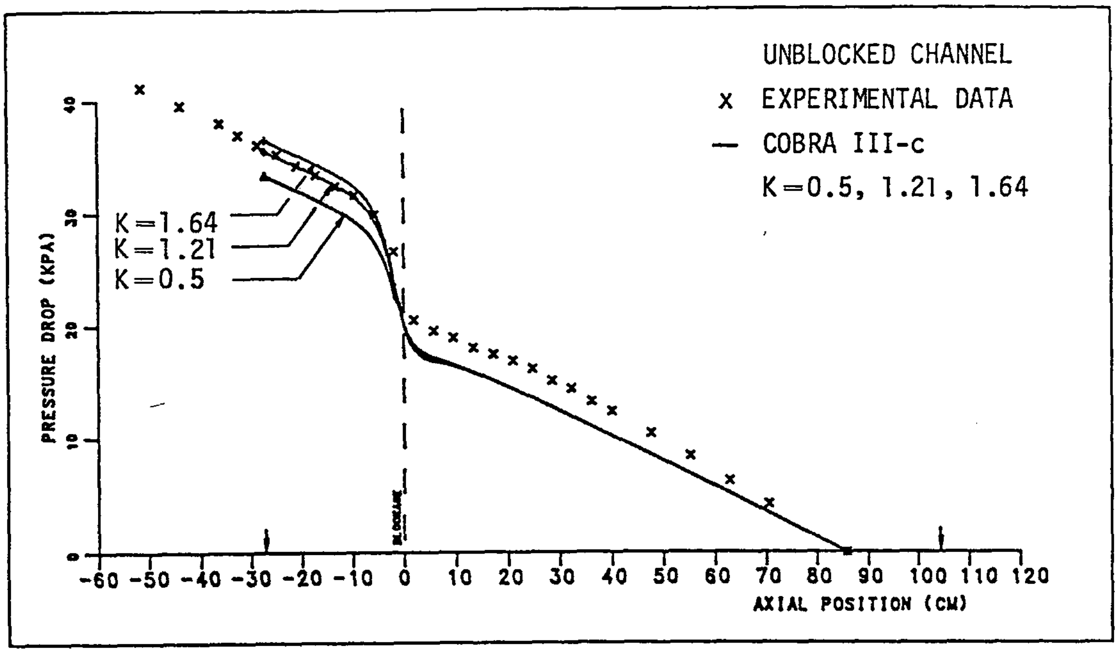

Figure 3.67 Two Phase with Plate Blockage Run#4

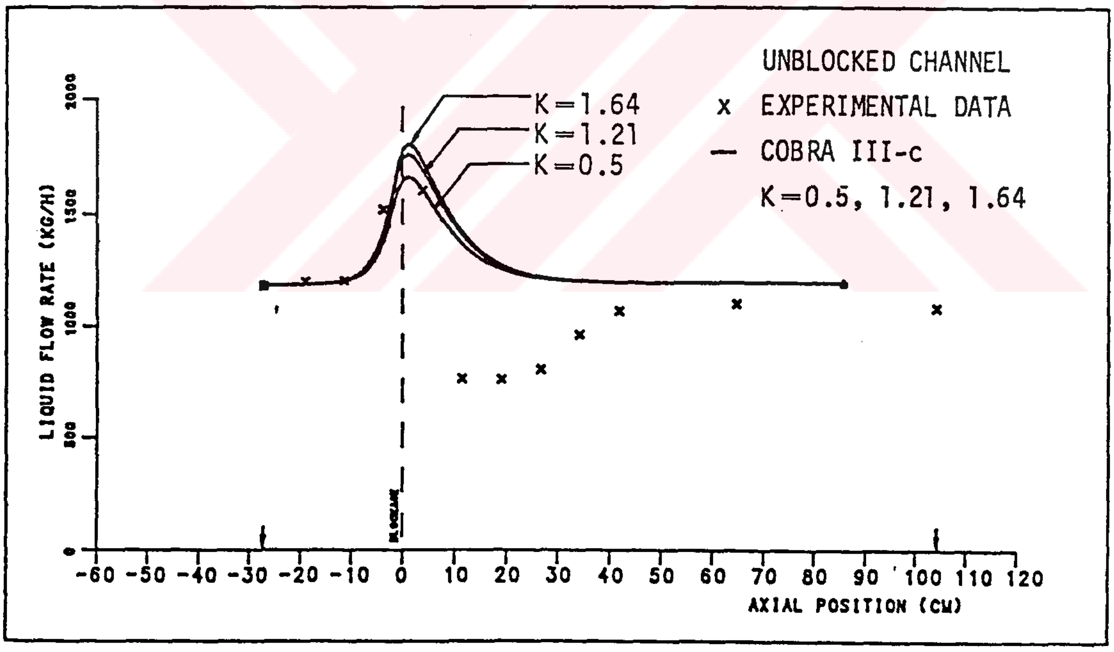

Figure 3.68 Two Phase with Plate Blockage Run#4

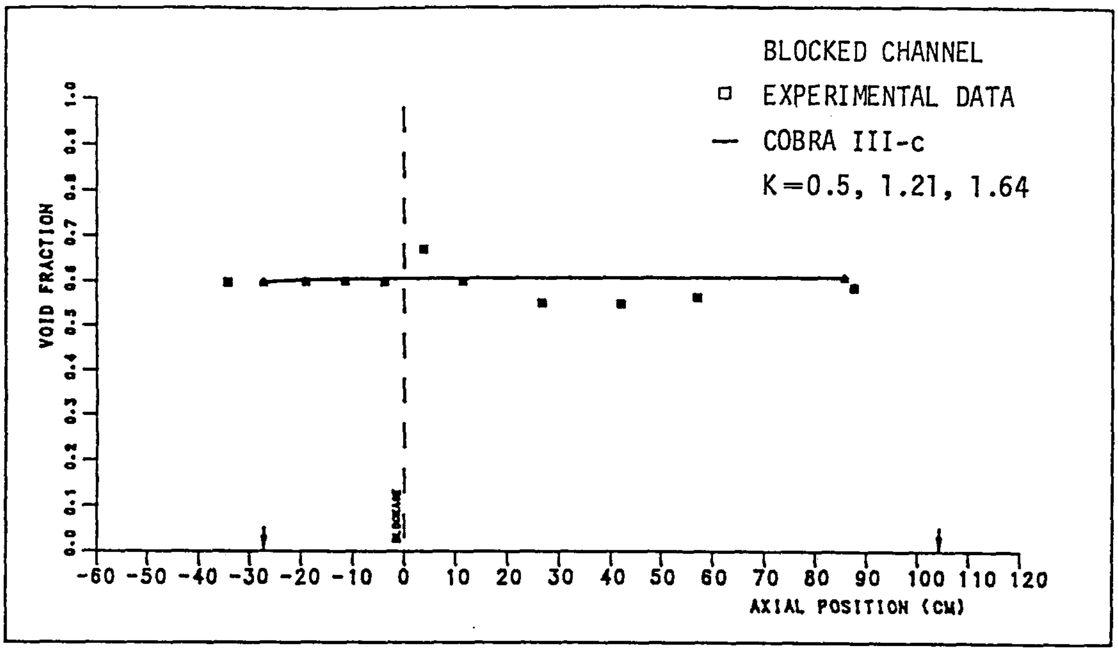

Figure 3.69 Two Phase with Plate Blockage Run#4

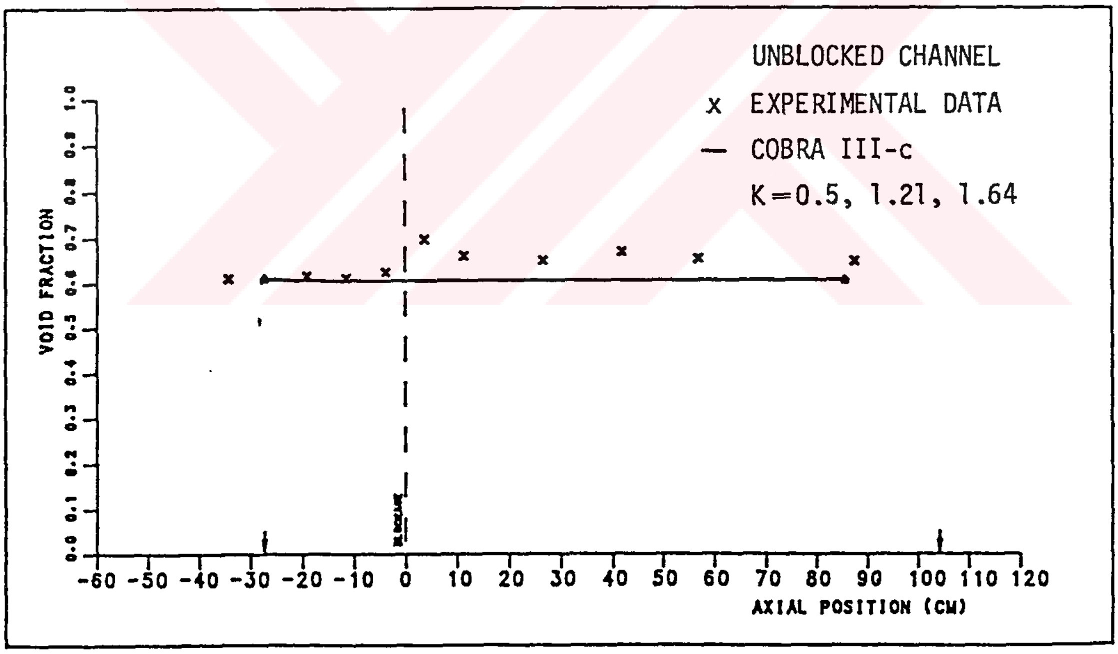

Figure 3.70 Two Phase with Plate Blockage Run#4

These are the results of the same runs which are given above.

CHAPTER 4

COBRA-PC4 PREDICTIONS ON FURTHER TEST CASES

After getting consistent results from blockage simulations with the experiments some predictive cases were performed. The results are shown in graphics.

As a further step for prediction , a model of a multi subchannel test section was simulated in COBRA-PC4. This model consists of six heater rods of three kind in an flow channel. The rods, which are made of INCONE-600 material, produce heat by conducting an electric current under certain potential difference. Since they are at different thickness, they produced different amount of heat that transferred to the coolant. The object of this case to find out whether the critical heat flux conditions are reached.

Table 4.1 Computer Experiments

1	*CH1*	*CH2*	*Explanation*
Area Reduction (%)	*31.9 (Plate)*	*No Reduction*	*Similar to Run#3*
Liquid Flow Rate (kg/h)	*1600*	*800*	*with diferrent inlet*
Void Fraction (%)	*0.0*	*60.2*	*flows*

2	*CH1*	*CH2*	*Explanation*
Area Reduction (%)	*31.9 (Plate)*	*No Reduction*	*Similar to Run#3*
Liquid Flow Rate (kg/h)	*1921*	*480*	*with diferrent inlet*
Void Fraction (%)	*0.0*	*60.2*	*flows*

3	*CH1*	*CH2*	*Explanation*
Area Reduction (%)	*31.9 (Plate)*	*No Reduction*	*Similar to Run#3*
Liquid Flow Rate (kg/h)	*2401*	*0.0*	*with diferrent inlet*
Void Fraction (%)	*0.0*	*60.2*	*flows*

Table 4.1 Continue

4	CHl	CH2	Explanation
Area Reduction (%)	No Reduction	No Reduction	Similar to Run-Vl
Liquid Flow Rate (kg/h)	2958	739	with diferrent inlet
Void Fraction (%)	60.0	0.0	flows

5	CHl	CH2	Explanation
Area Reduction (%)	No Reduction	No Reduction	Similar to Run-Vl
Liquid Flow Rate (kg/h)	2464	1232	with diferrent inlet
Void Fraction (%)	60.0	0.0	flows

6	CHl	CH2	Explanation
Area Reduction (%)	No Reduction	No Reduction	Similar to Run-Vl
Liquid Flow Rate (kg/h)	3969	0	with diferrent inlet
Void Fraction (%)	60.0	0.0	flows

7	CHl	CH2	Explanation
Area Reduction (%)	31.9 (Plate)	No Reduction	Similar to Run#3
Liquid Flow Rate (kg/h)	1500	900	with diferrent inlet
Void Fraction (%)	0.0	60.2	flows

8	CHl	CH2	Explanation
Area Reduction (%)	31.9 (Plate)	No Reduction	Similar to Run#3
Liquid Flow Rate (kg/h)	1400	1000	with diferrent inlet
Void Fraction (%)	0.0	60.2	flows

9	CHl	CH2	Explanation
Area Reduction (%)	31.9 (Plate)	No Reduction	Similar to Run#3
Liquid Flow Rate (kg/h)	1300	1100	with diferrent inlet
Void Fraction (%)	0.0	60.2	flows

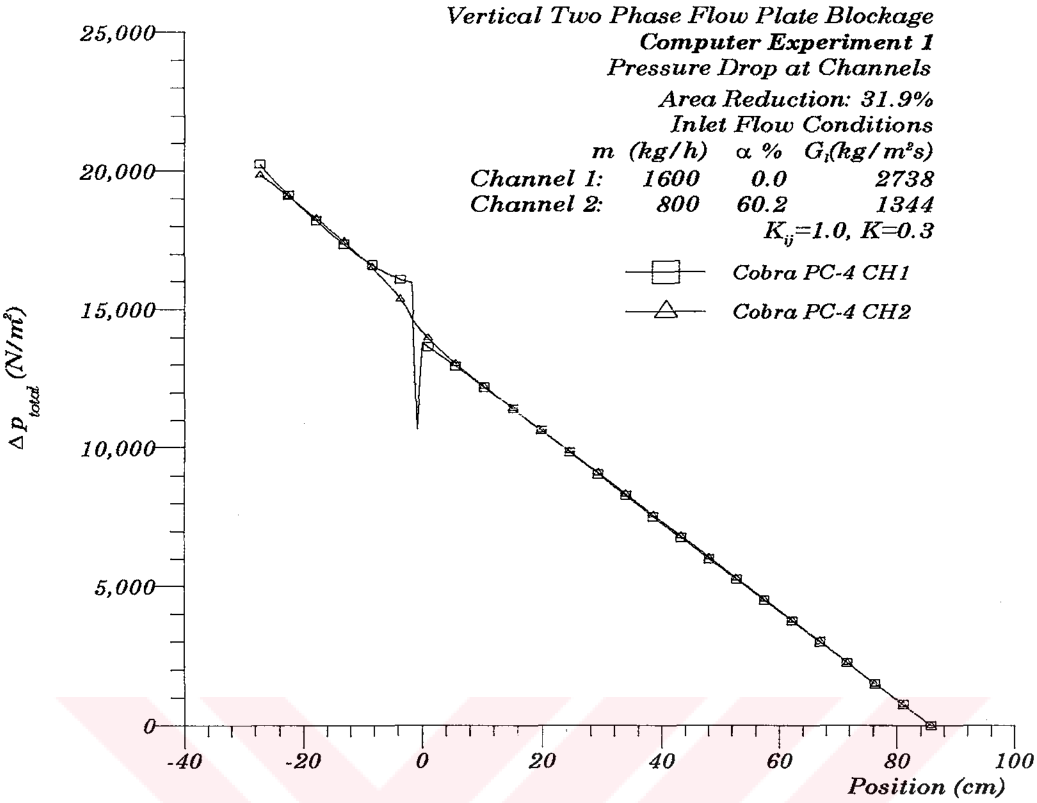

Figure 4.1 COBRA-PC4 Predictions

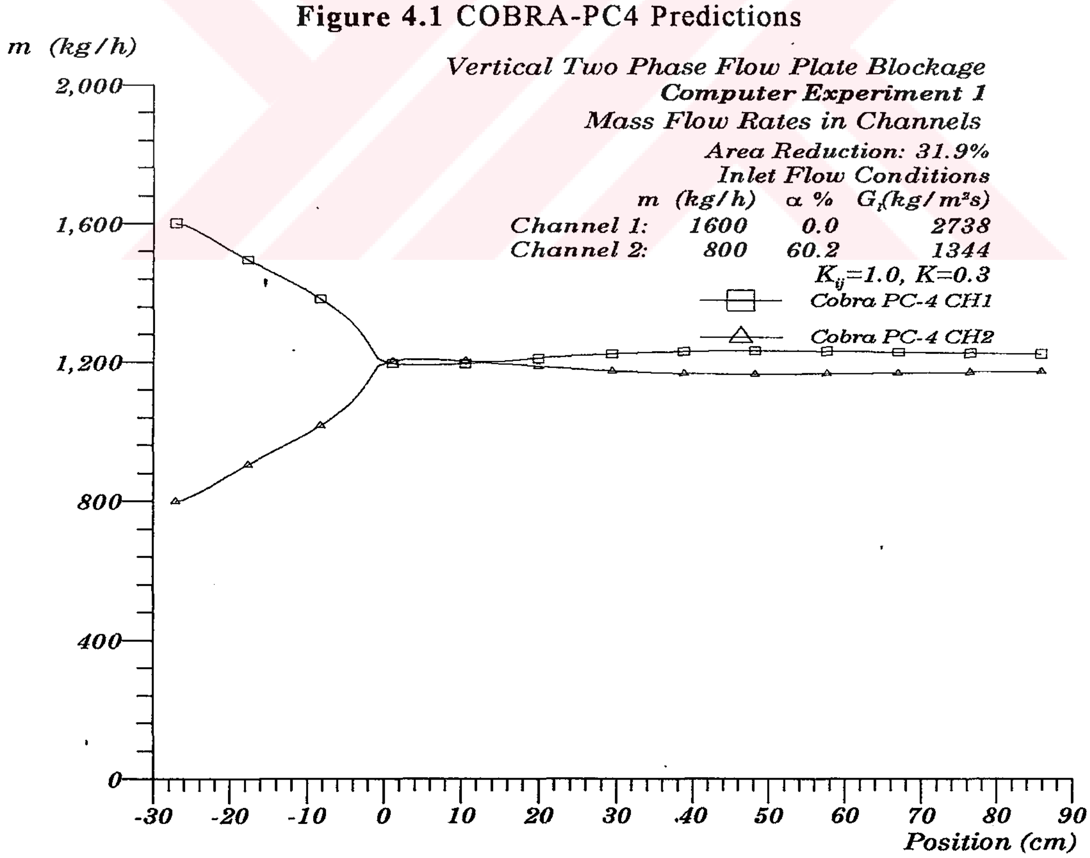

Figure 4.2 COBRA-PC4 Predictions

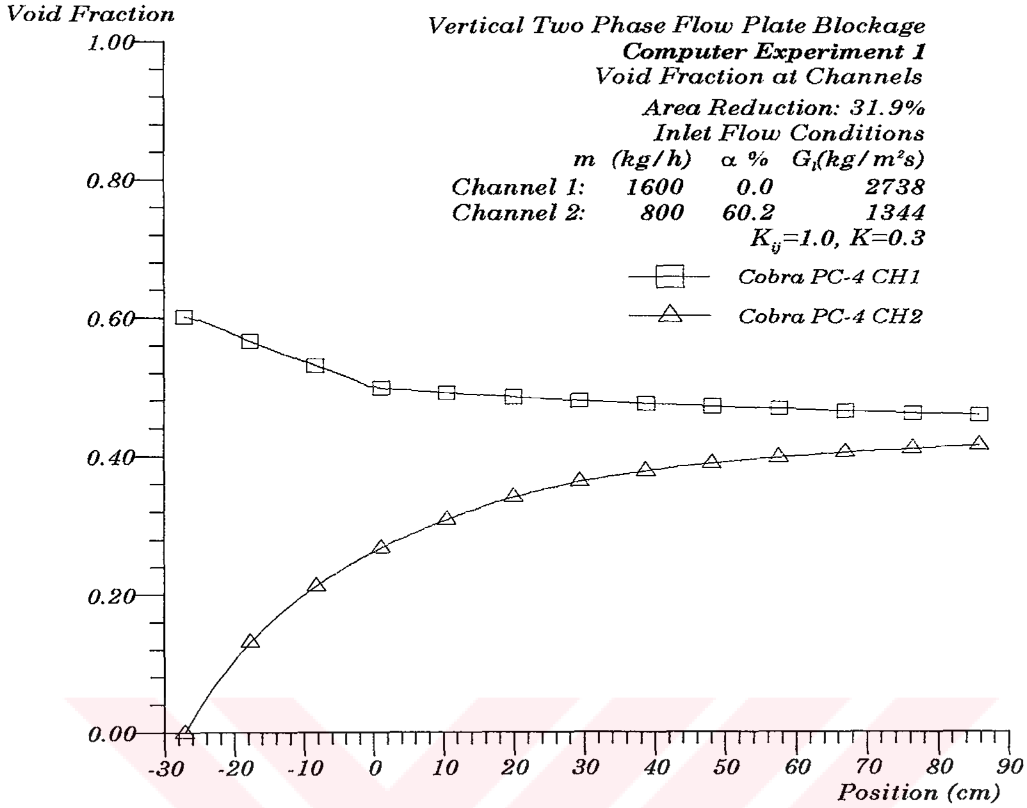

Figure 4.3 COBRA-PC4 Predictions

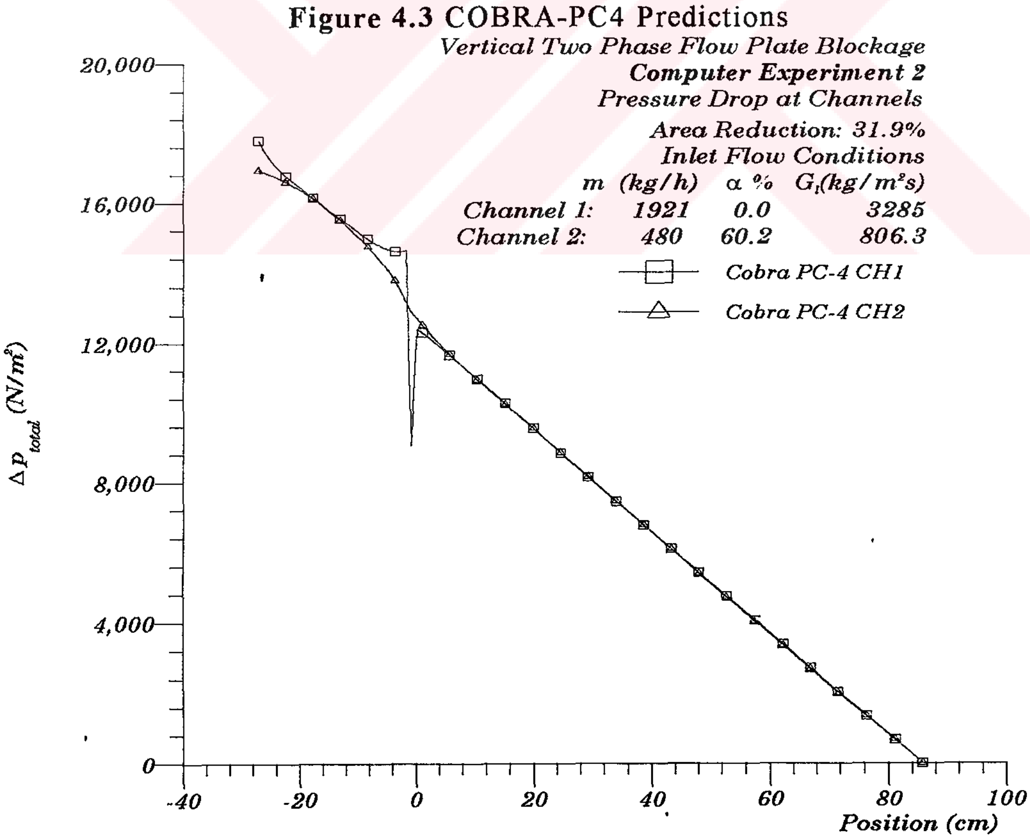

Figure 4.4 COBRA-PC4 Predictions

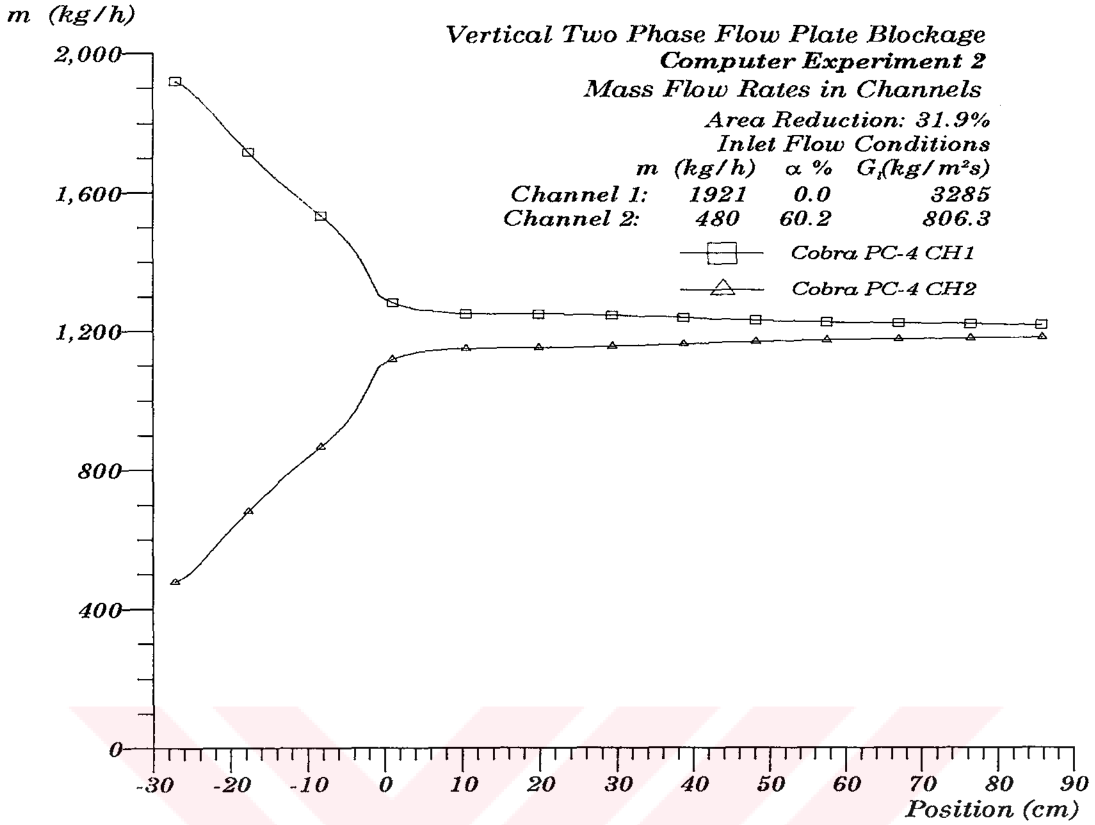

Figure 4.5 COBRA-PC4 Predictions

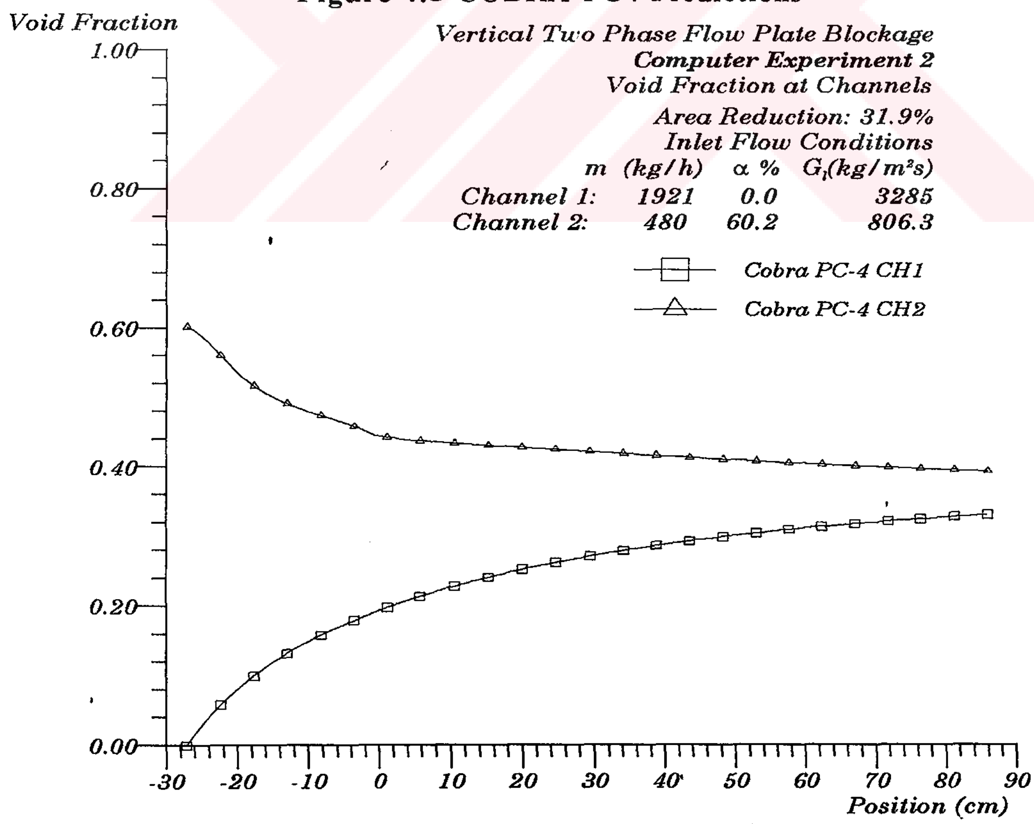

Figure 4.6 COBRA-PC4 Predictions

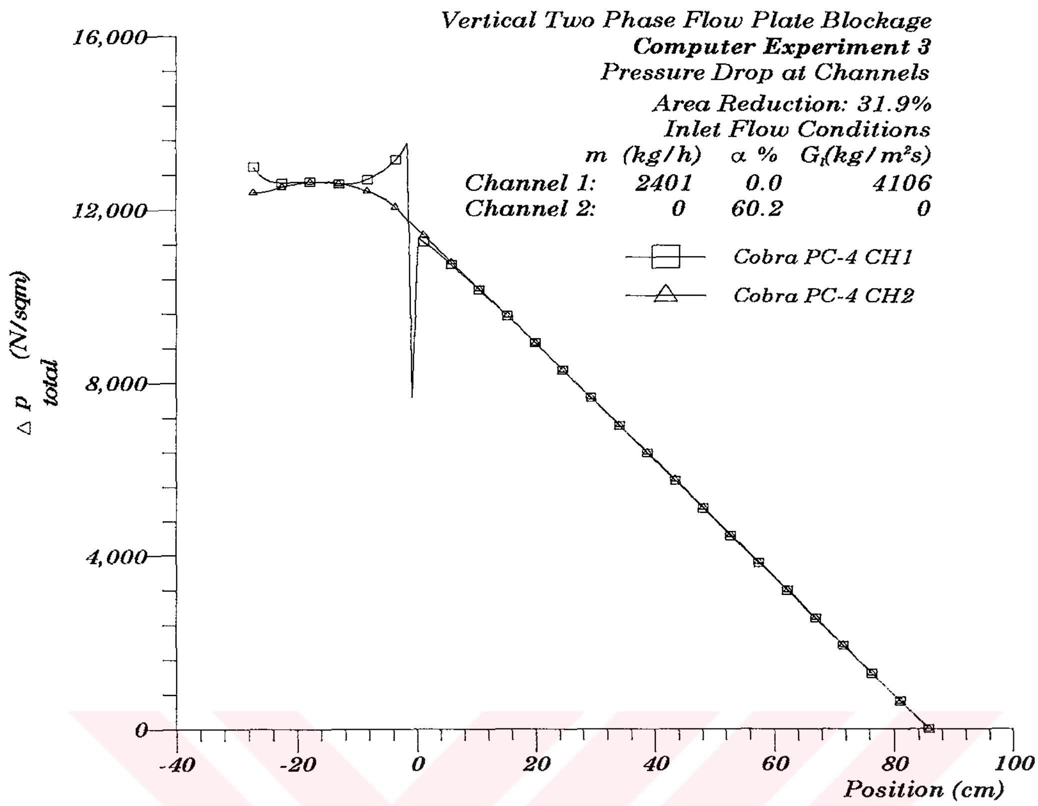

Figure 4.7 COBRA-PC4 Predictions

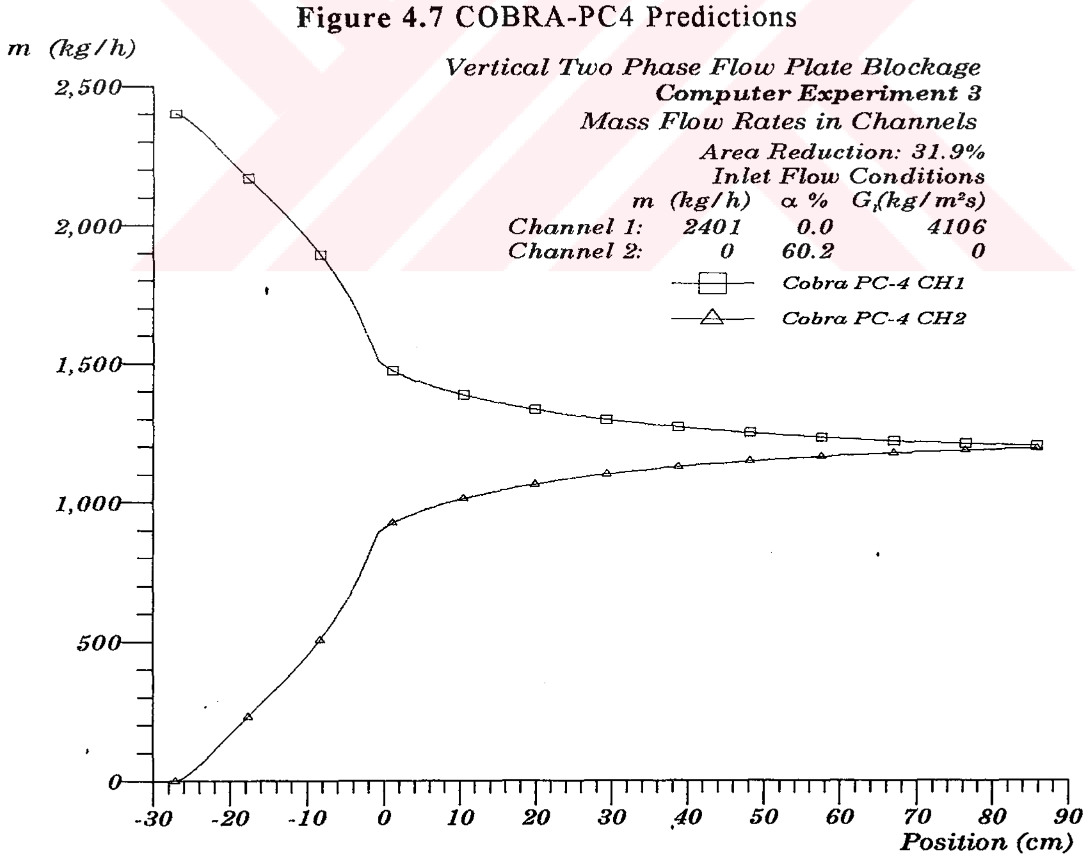

Figure 4.8 COBRA-PC4 Predictions

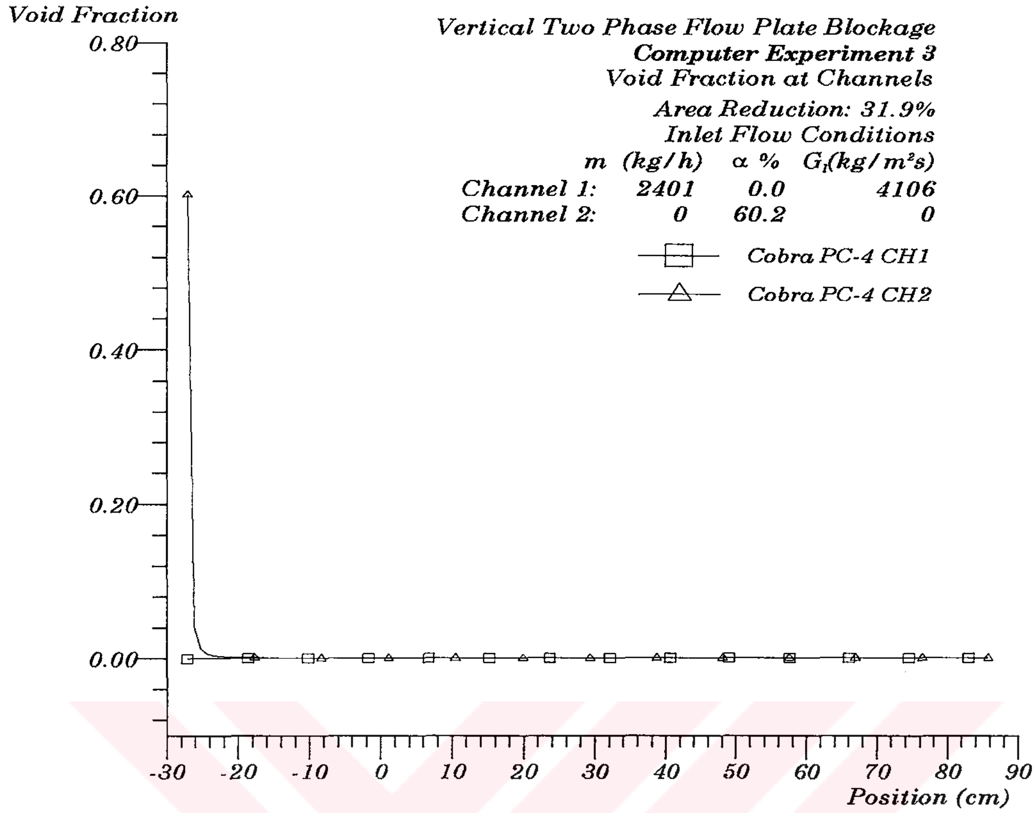

Figure 4.9 COBRA-PC4 Predictions

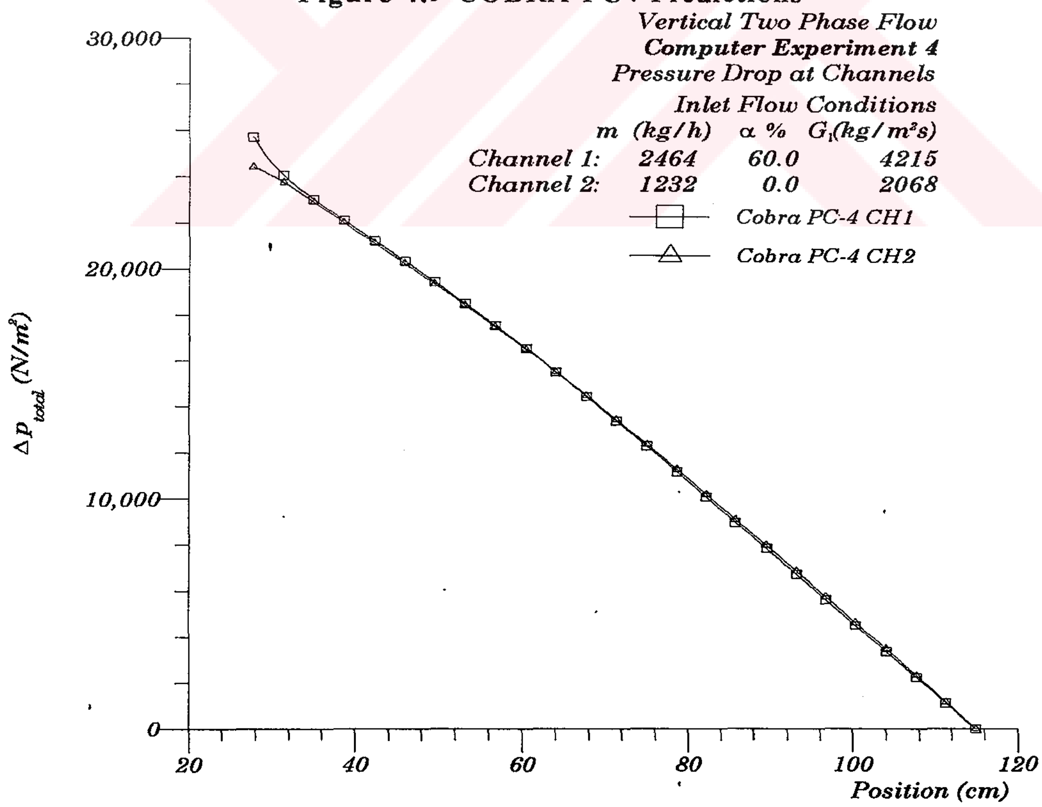

Figure 4.10 COBRA-PC4 Predictions

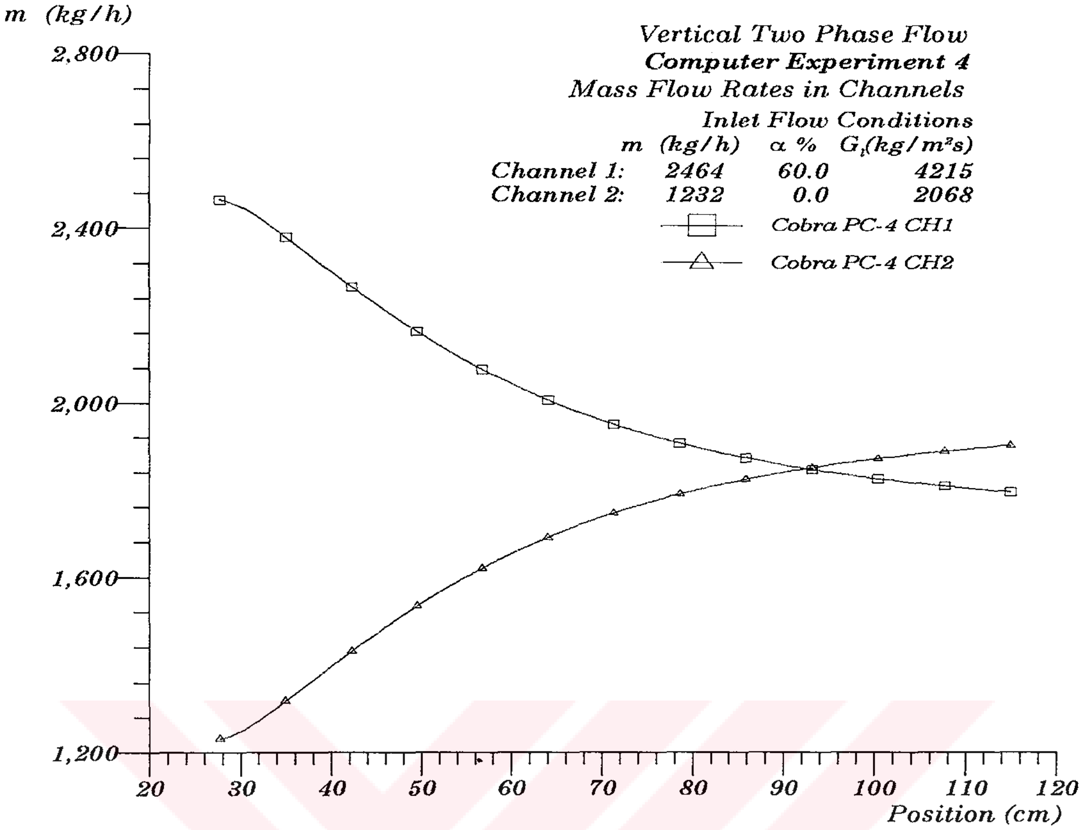

Figure 4.11 COBRA-PC4 Predictions

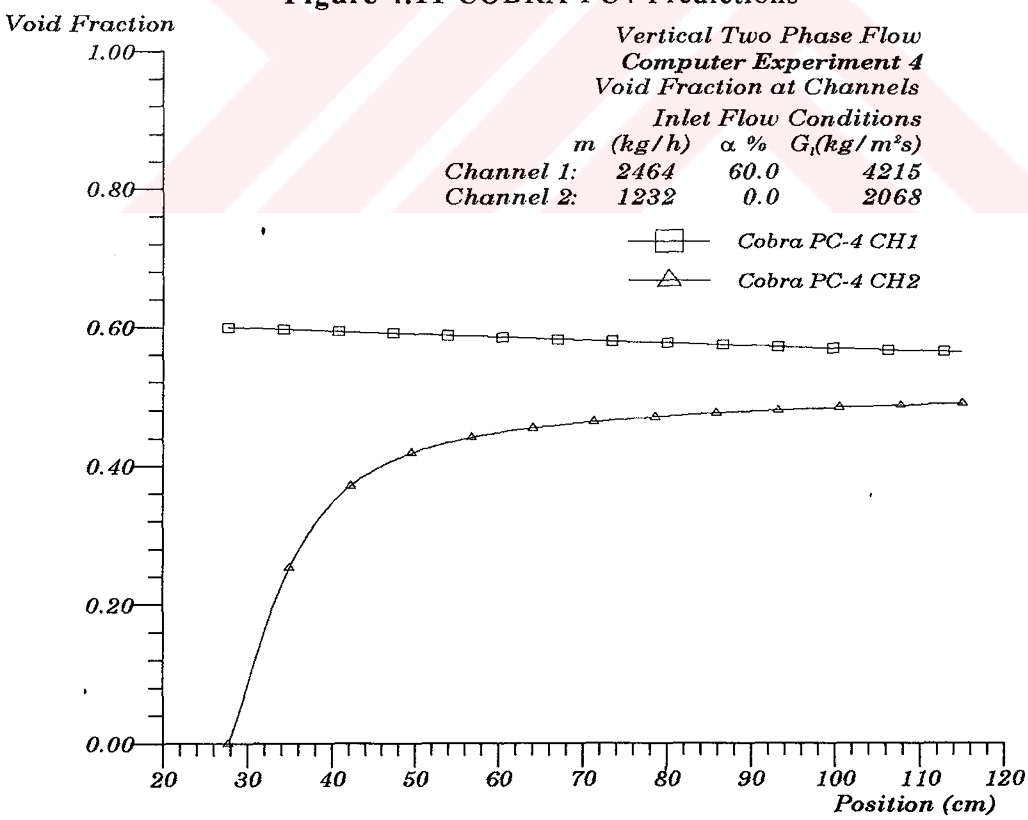

Figure 4.12 COBRA-PC4 Predictions

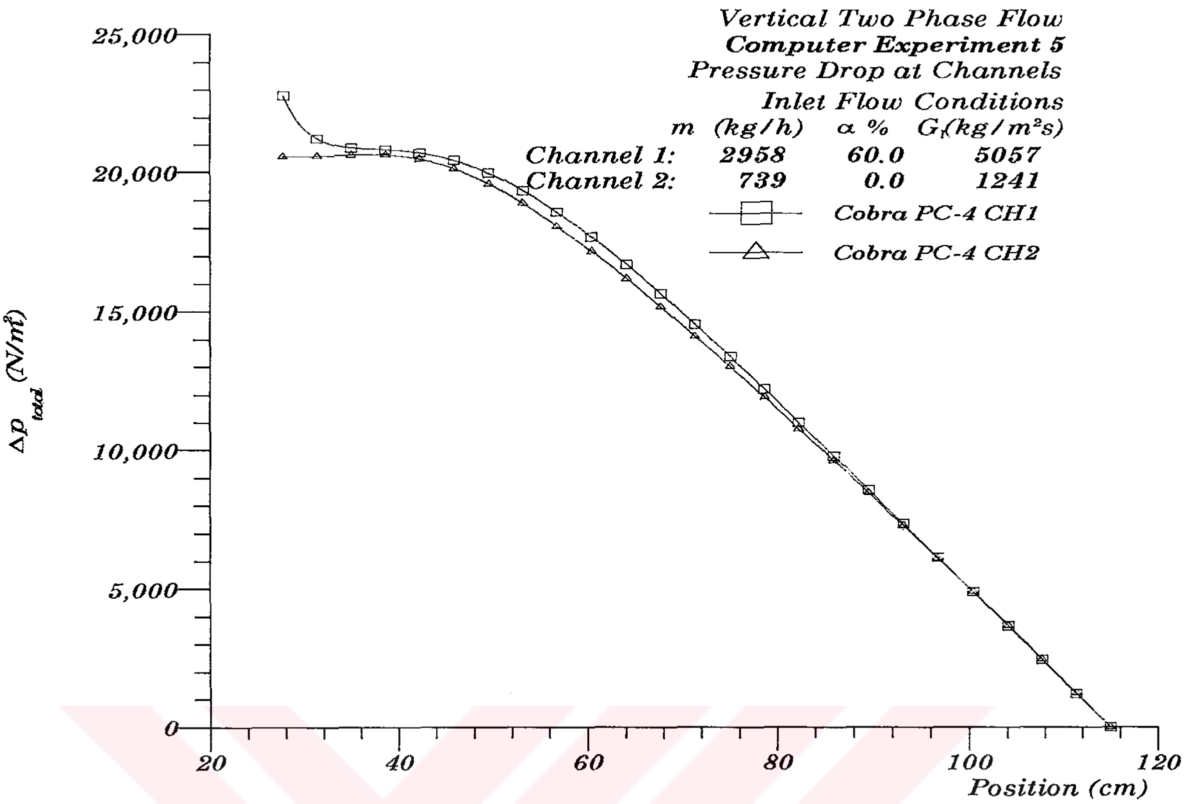

Figure 4.13 COBRA-PC4 Predictions

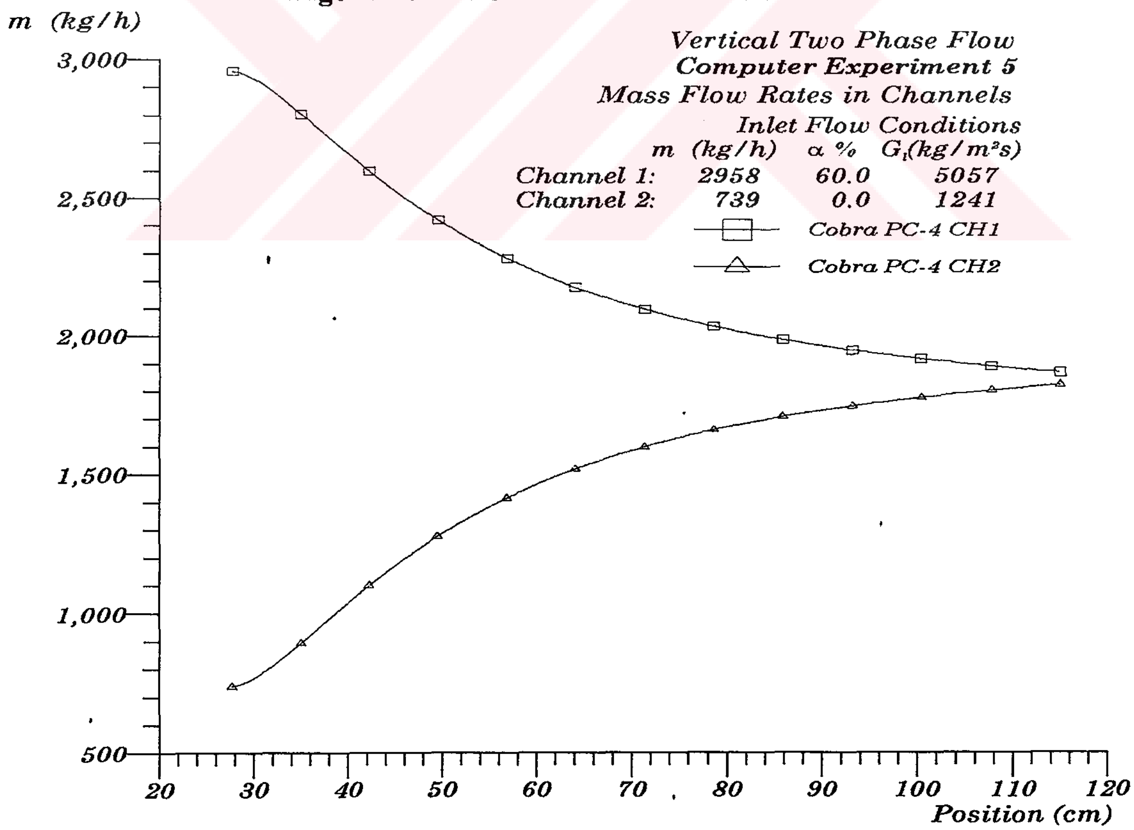

Figure 4.14 COBRA-PC4 Predictions

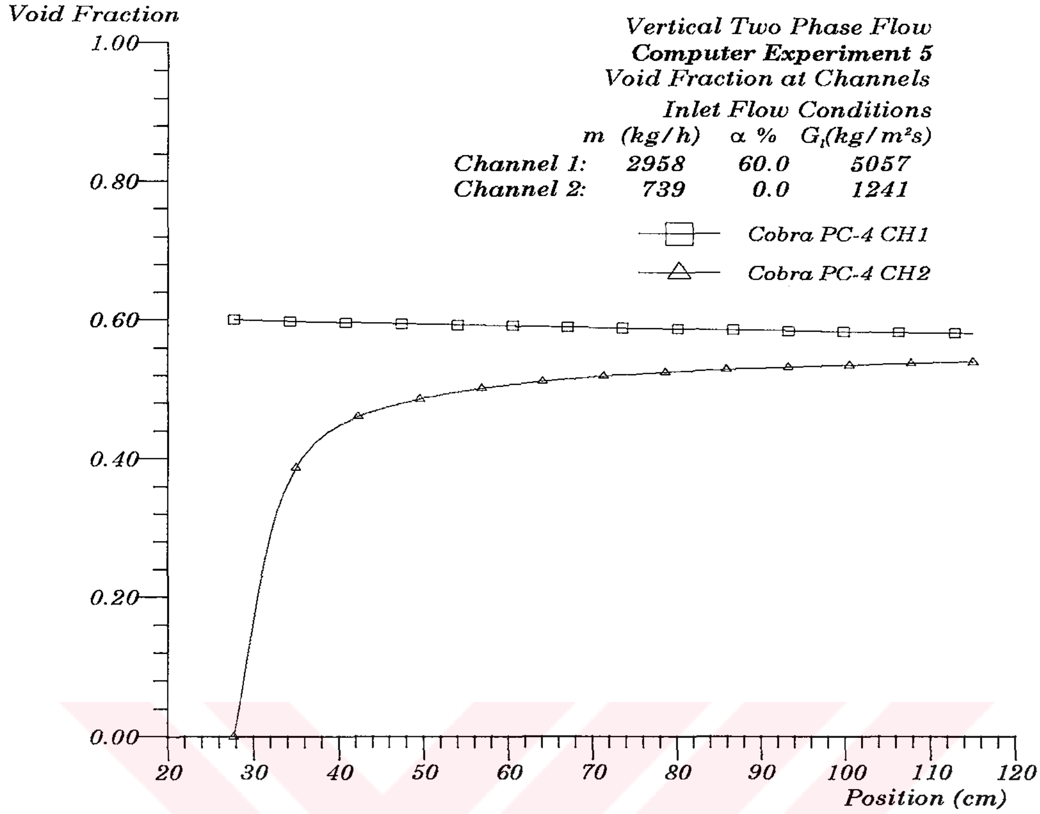

Figure 4.15 COBRA-PC4 Predictions

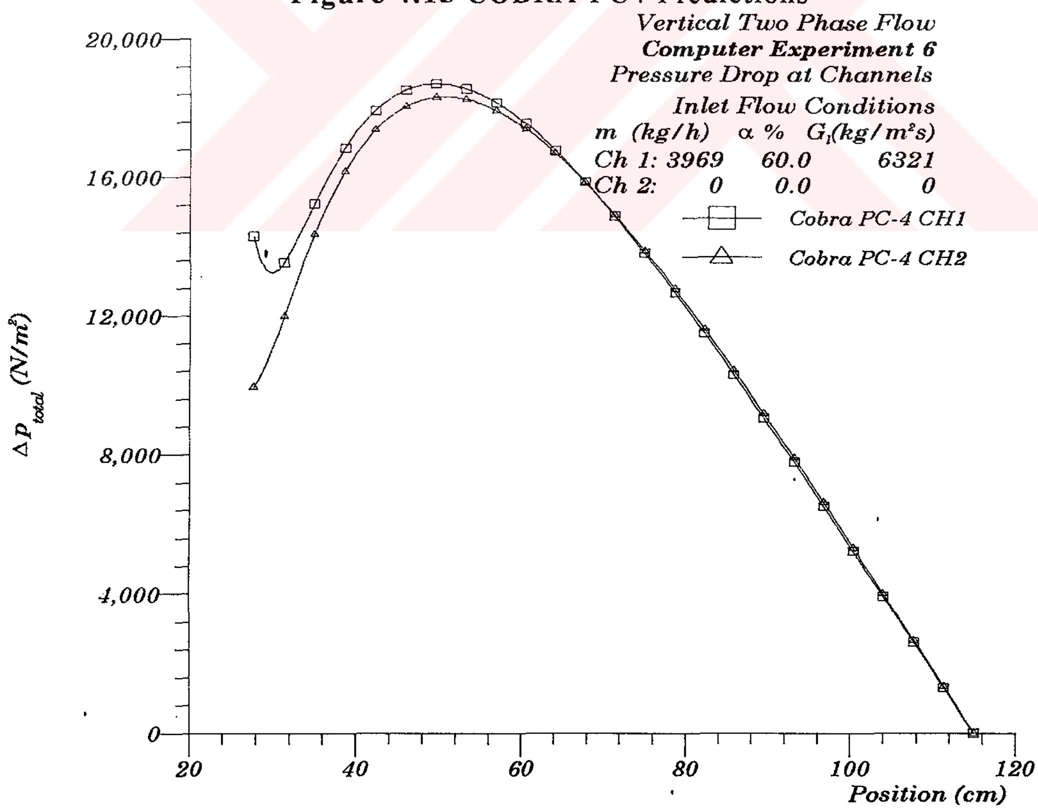

Figure 4.16 COBRA-PC4 Predictions

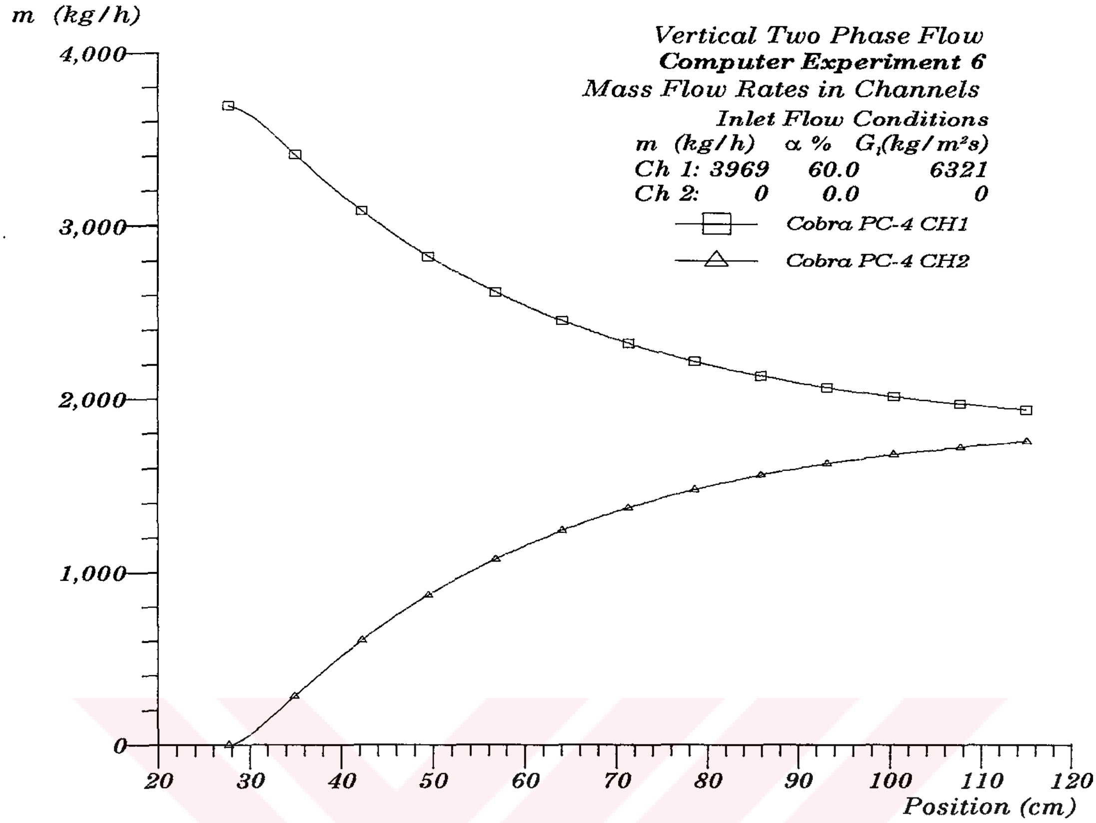

Figure 4.17 COBRA-PC4 Predictions

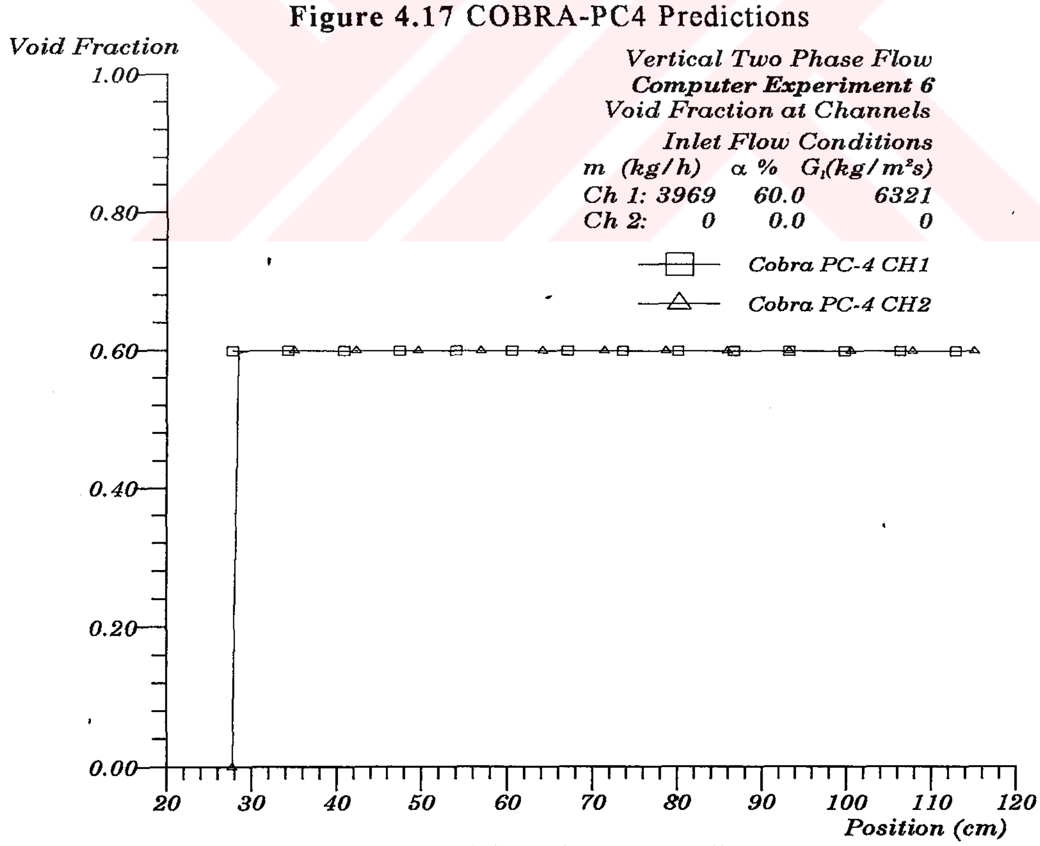

Figure 4.18 COBRA-PC4 Predictions

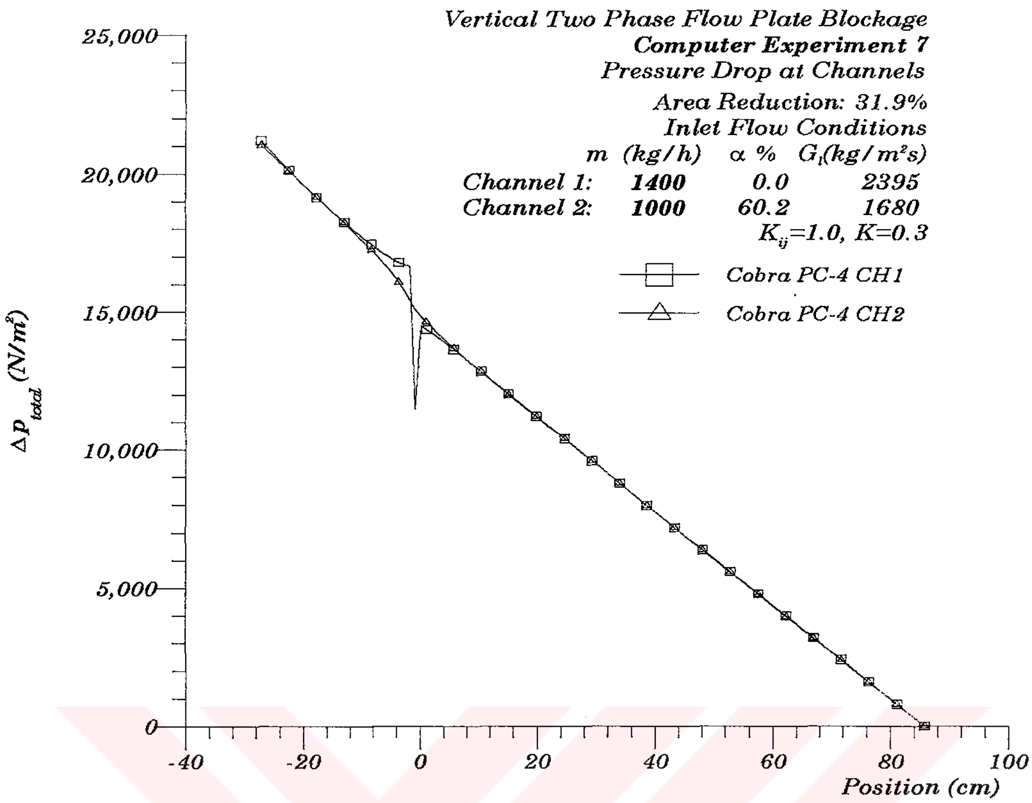

Figure 4.19 COBRA-PC4 Predictions

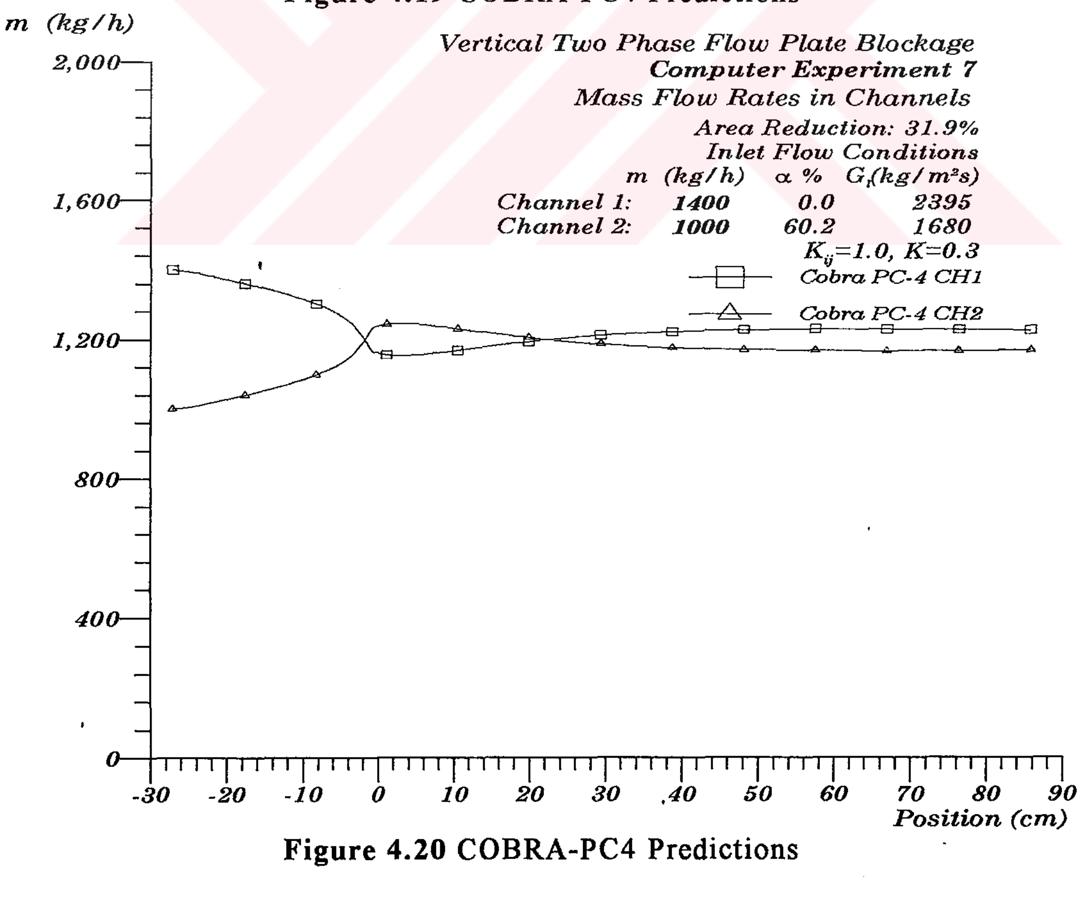

Figure 4.20 COBRA-PC4 Predictions

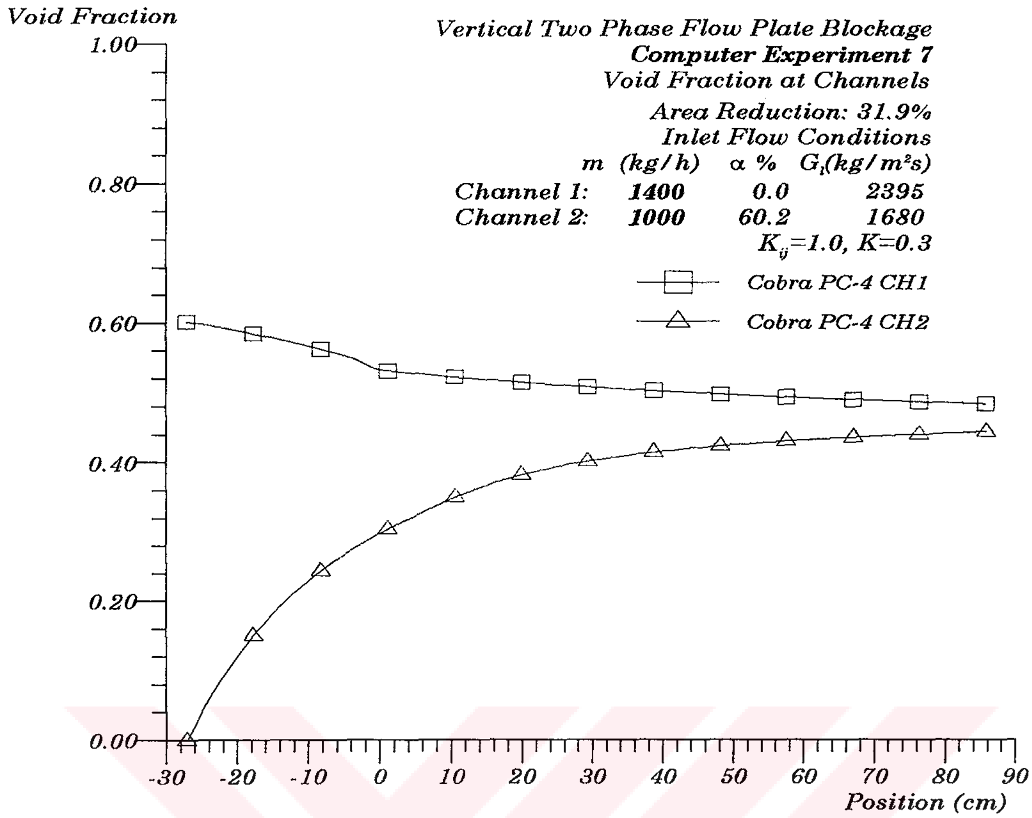

Figure 4.21 COBRA-PC4 Predictions

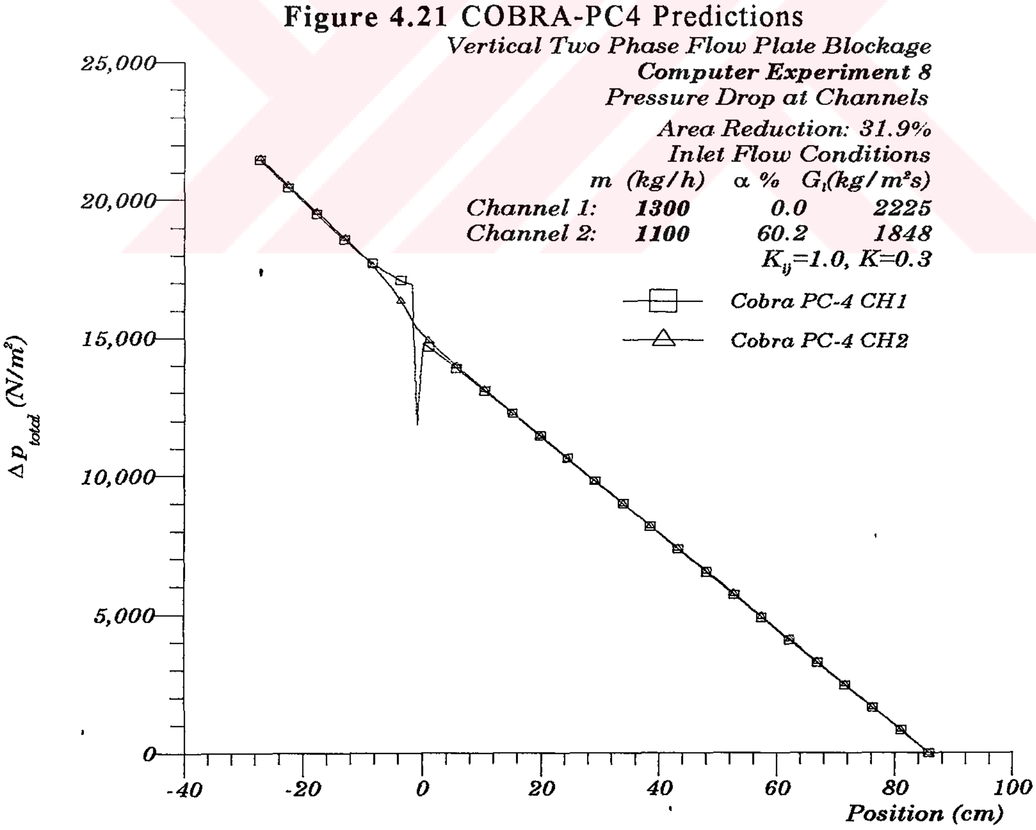

Figure 4.22 COBRA-PC4 Predictions

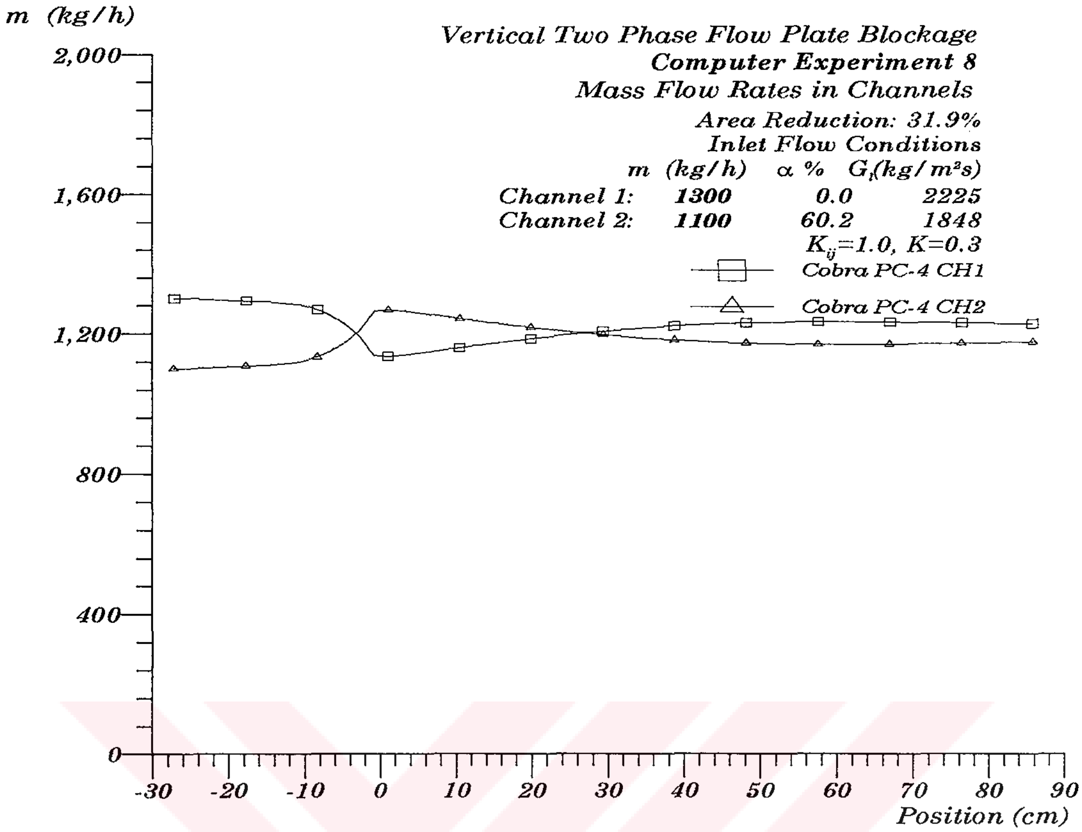

Figure 4.23 COBRA-PC4 Predictions

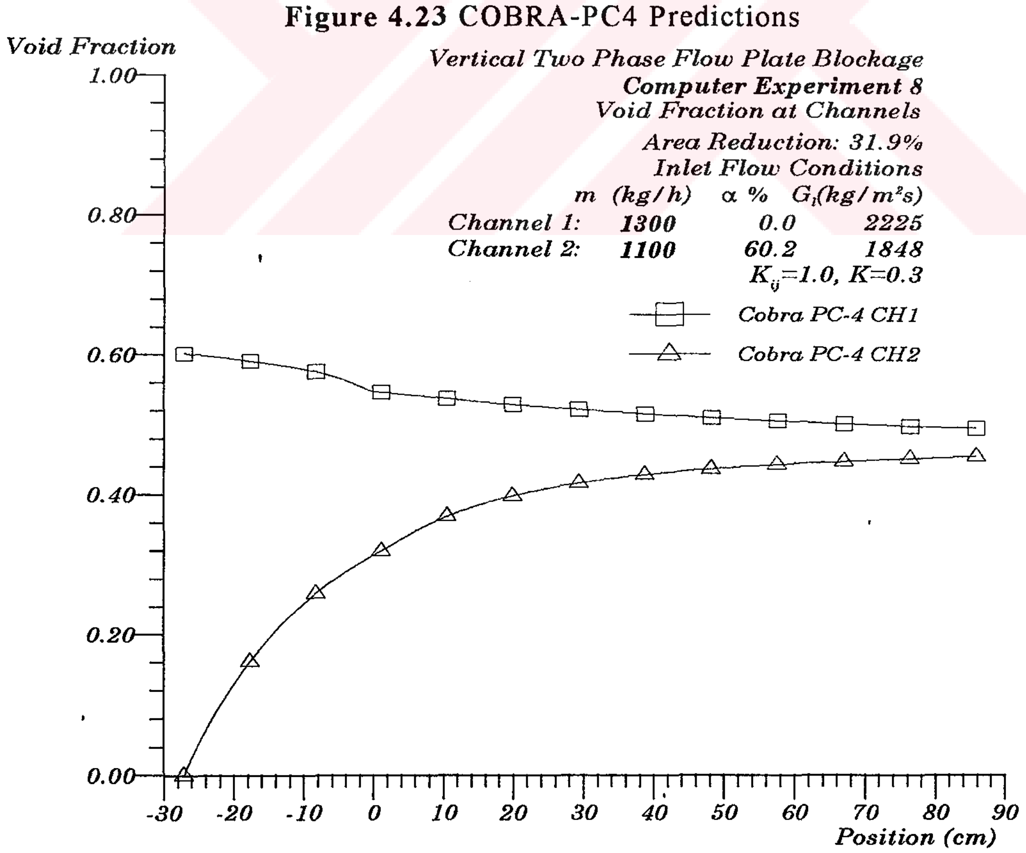

Figure 4.24 COBRA-PC4 Predictions

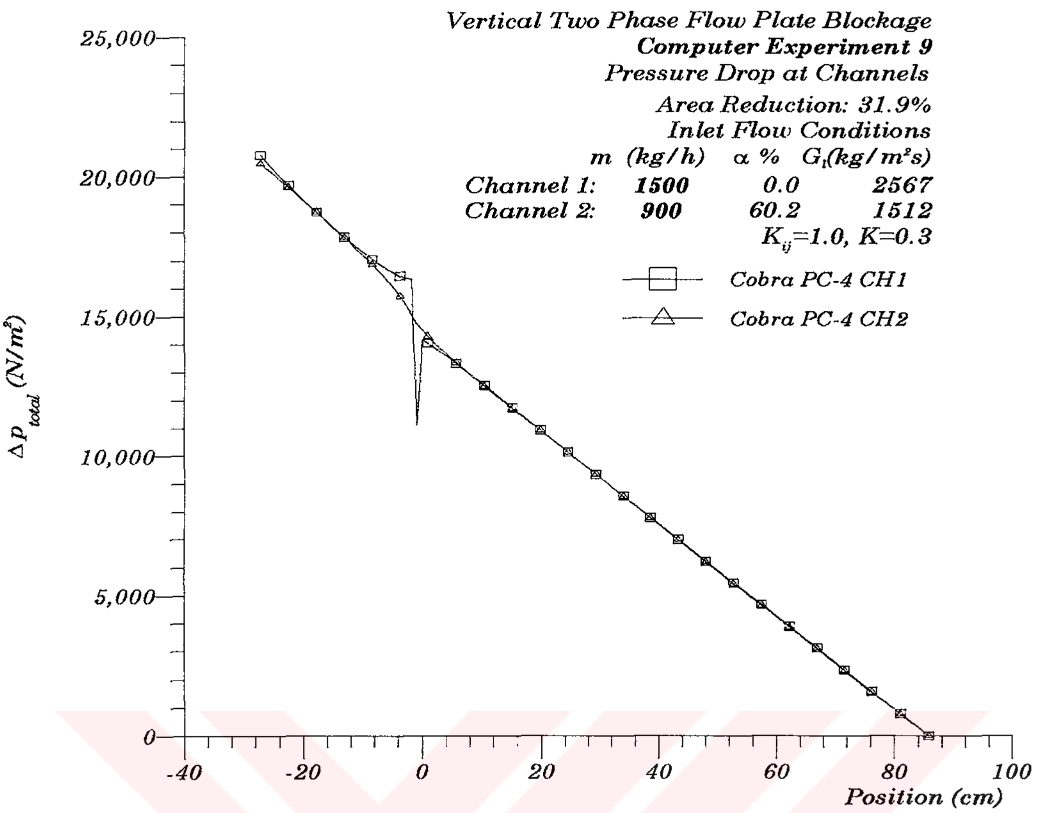

Figure 4.25 COBRA-PC4 Predictions

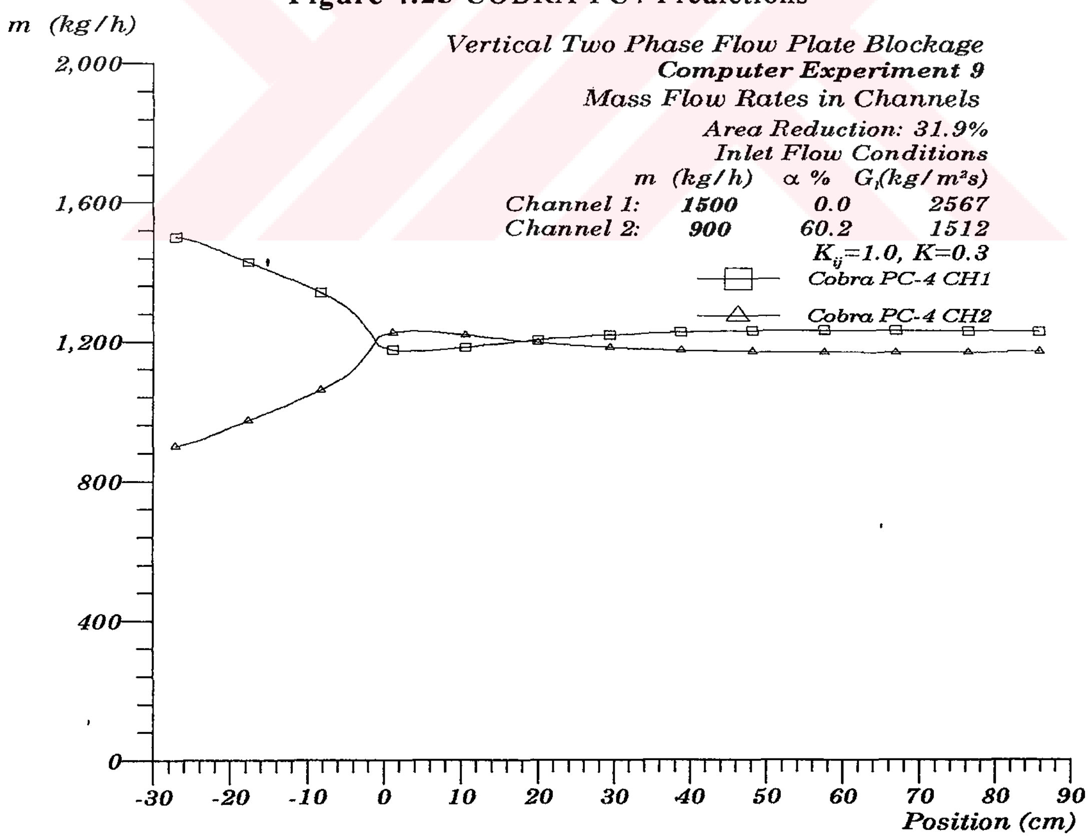

Figure 4.26 COBRA-PC4 Predictions

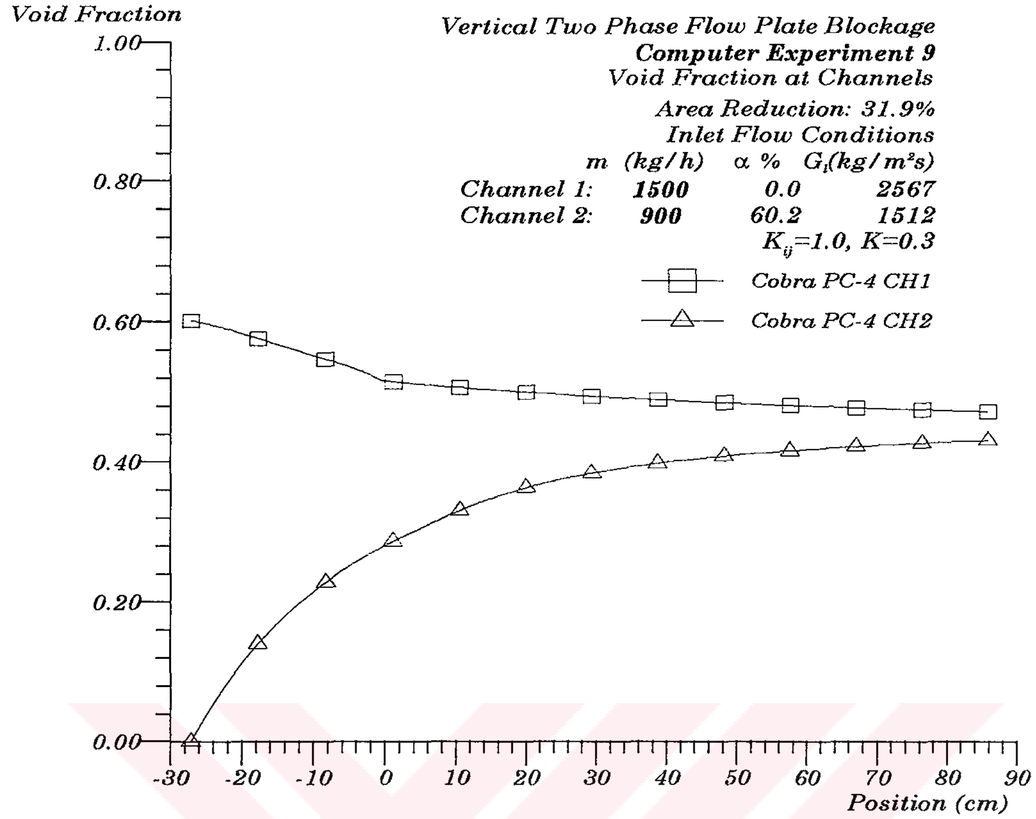

Figure 4.27 COBRA-PC4 Predictions

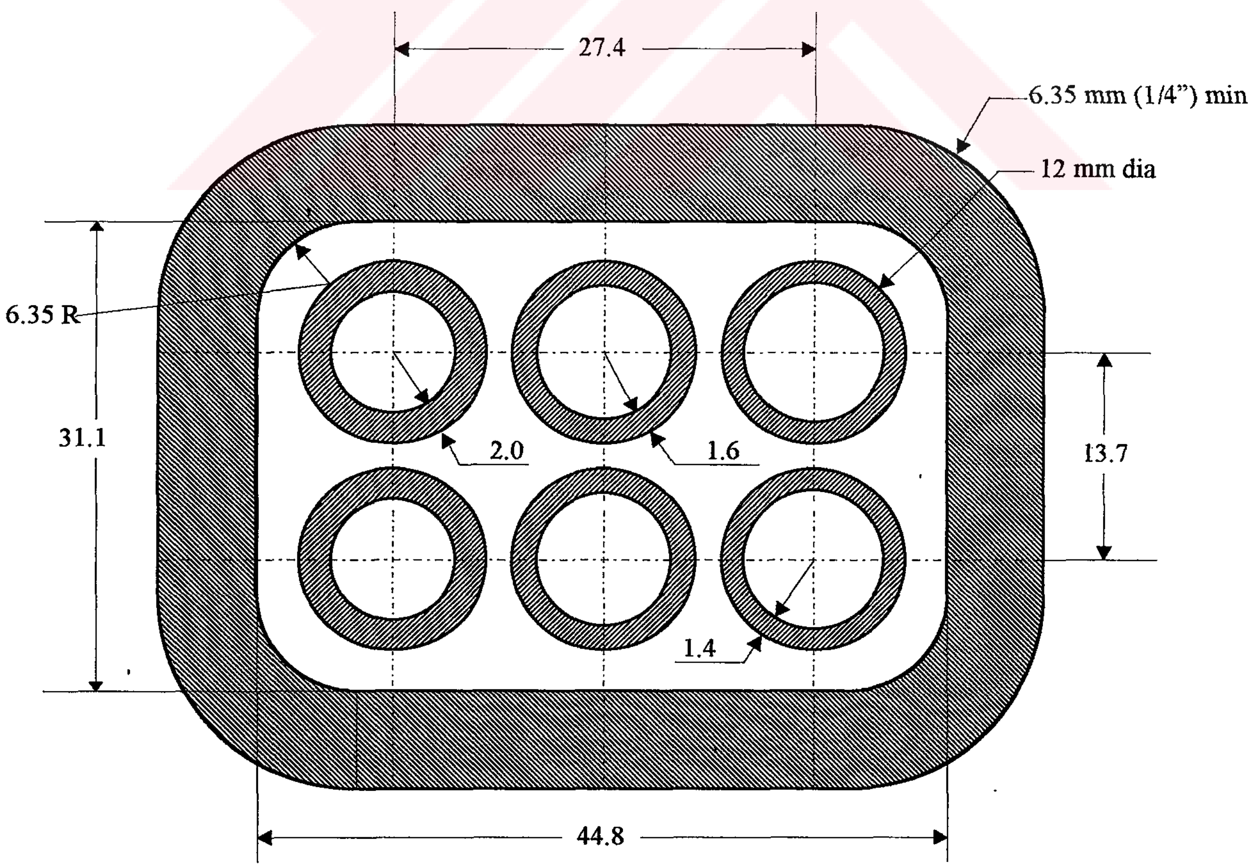

Figure 4.28 Multi Subchannel Test Section

TABLE 4.2 Comparison of the ASSERT-4 code predictions with the COBRA-PC4 predictions

ASSERT-4 Run Predictions, [10]				
Channel #	Mass Flux Mlb/hr-ft^2	Mass Flow lb/sec	Exit Quality %	Void Fraction %
1	5.6680	1.0615	9.382	44.93
2	5.3575	0.6208	7.822	40.43
3	5.2850	0.6124	8.254	42.18
4	5.5389	1.0375	10.143	47.47
5	4.7094	1.0503	17.425	63.84
6	5.6260	1.0538	9.600	45.59
7	5.2624	0.9857	11.97	52.76
8	4.3790	0.9766	21.02	69.41
9	5.3516	1.0024	11.28	50.80
10	4.8318	0.5600	11.32	51.97
11	5.1518	0.9647	12.77	54.73
12	4.9077	0.5688	10.68	50.10
COBRA-PC4 Run Predictions				
Channel #	Mass Flux Mlb/hr-ft^2	Flow lb/sec	Equil Quality %	Void Fraction %
1	5.4287	1.0168	9.135	55.554
2	4.9337	.5720	9.017	55.199
3	4.9270	.5712	9.059	55.325
4	5.3227	.9970	9.796	57.449
5	5.2331	1.1670	11.028	60.643
6	5.3374	.9997	9.705	57.196
7	5.2448	.9824	10.323	58.865
8	5.1566	1.1499	11.588	61.968
9	5.2360	.9807	10.382	59.021
10	4.7261	.5479	10.513	59.359
11	5.1434	.9634	11.046	60.689
12	4.7156	.5467	10.589	59.551

CHAPTER 5

CONCLUSIONS

The subchannel thermal-hydraulics code COBRA-IV-I is successfully adapted into PC type computers. The memory limitation originated from DOS operating system is overcome by using WINDOWS environment. Thus some memory management routines of COBRA-IV-I is eliminated while adapting.

COBRA-PC4 run with the test inputs, fuel thermal sample and U-tube sample problems produced same results as in reference outputs of these test problems.

The experimental data have been compared with the predictions of the subchannel code COBRA-PC4 to ascertain how well they can be predicted. Also some predictions are generated for the future experimental studies.

The comparison of the code predictions with experimental data taken from the literature and COBRA-IIIC results shows that;

Single phase with blockage predictions are similar to the COBRA-IIIC so that both predict 30% plate blockage fairly well, however they fail to predict the data on 60% plate blockage. For smooth blockage very reasonable agreement is obtained between COBRA-PC4 predictions and experimental data as well as COBRA-IIIC.

Predictions of the two phase experiments without blockage are in good agreement with the data. Two phase with blockage predictions also look same as COBRA-IIIC.

Using two phase results some computer experiments are performed with COBRA-PC4. Several different mass flow rate cases are predicted. The observations on these predictions are the followings.

1. For the 2:1 or higher ratio in flow rates the effect of blockage cannot be seen on mass flow rate diagram.

2. For flow rate ratios lower than 2:1, i.e. 1.4:1 the effect of the blockage is more dominant.

Another kind of comparison is performed by a multi-subchannel test section (rod bundle) simulation. Predictions compared with the results of another subchannel code, ASSERT-4. COBRA-PC4 gives reasonably compatible results with ASSERT-4.

REFERENCES

[1] GENÇAY Ş. Nükleer Reaktör Soğutma Kanallarında Tıkanma, Doçentlik Tezi, İTÜ Nükl. Ener. Enst. (Eylül 1981).

[2] TAPUCU A., GENÇAY Ş., Experimental Investigation of Mass Exchanges Between Two Laterally Interconnected Two-Phase Flow Channels, IGN-354, (1980).(Draft)

[3] TAPUCU A., TEYSSEDU A., GEÇKİNLİ M., TROCHE N., Experimental Study of Diversion Cross-flow Caused by Subchannel Blockages, EPRI NP-3459 Vol. 2, Electric Power Research Institute, California (1988).

[4] WHEELER C.L., STEWART C.W., CENA R.J., ROWE D.S., STUTEY A.M., COBRA-IV-I: An Interim Version of COBRA for Thermal-Hydraulic Analysis of Rod Bundle Nuclear Fuel Elements and Cores, BNWL-1962, Pacific Northwest Laboratory, Richland, Washington (1976).

[5] KURUL N., İki Fazlı Altkanal Analizi Yapan COBRA-IIIC Kodunun Tanıtılması, İTÜ Nükl. Ener. Enst.

[6] LAHEY R.T.Jr and MOODY F.J., The Thermal-Hydraulics of a Boiling Water Reactor, ANS, La Grande Park, 2nd ed. (1979).

[7] TODREAS N.E. and KAZIMI M.S., Nuclear Systems II, Hemisphere Publishing Co, (1990).

[8] TAPUCU A., GENÇAY Ş., TROCHE N., Experimental Study of Diversion Cross-flow Caused by Subchannel Blockages, EPRI NP-3459 Vol. 1, Electric Power Research Institute, California (1984).

[9] TAPUCU A., TEYSSEDU A.,TYE P., TROCHE N., The Effect of Turbulent Mixing Models on the Predictions of Subchannel Codes, Nucl. Eng. Des. 149 (Sep., 1994).

[10] TAPUCU A., Personal communication

CIRRICULUM VITAE

Özkan Feza BİÇER was born in Kırşehir on 11. January, 1969. He finished primary school at Ankara in 1980. Then he entered Ankara Bahçelievler Deneme Lisesi. After finishing first three years in 1983, he moved to İstanbul Kadıkoy Suadiye Lisesi and was graduated from there in 1986. The same year he entered Nuclear Energy Engineering Department of the Hacettepe University. On July, 1991 he received his BSc degree in nuclear energy engineering. He entered Institute for Nuclear Energy of the Istanbul Technical University in 1992. In 1994 he was appointed research assistant at the same institute.